Responses to Reviewer Comments

Energy Transport, Polar Amplification, and ITCZ Shifts in the GeoMIP G1 Ensemble

R. D. Russotto and T. P. Ackerman

Responses to reviewer comments in blue. Following the responses are a revised manuscript showing differences from the original version, and then a clean revised manuscript.

Reviewer 1

General Comments

In this study the authors investigate the impacts of solar geoengineering and global warming on atmospheric meridional energy fluxes by using results from an intermodel ensemble (GeoMIP) and by employing a moist energy balance model (EBM). The EBM is combined with GeoMIP output in order to attribute energy transport changes to different climate forcing agents and climate feedbacks. The study seeks to answer two separate questions related to meridional energy transport: 1. how does solar geo impact the poleward energy transport at high latitudes, and 2. how does solar geo impact the cross-equatorial energy flux. In essence, the first question asks whether solar geo would exacerbate or counteract high-latitude warming while the second question asks which aspects of GCMs contribute most to uncertainty in changes to tropical precipitation. The authors show that solar geo would counteract the poleward energy transport enhancement under global warming, which they rather elegantly attribute to changes in moisture transport. This result helps to explain the observed mid-latitude drying signal in previous solar geo studies (e.g. Tilmes et al., 2013) and is a very useful inference. It also helps to explain why solar geo effectively (though not completely) offsets high-latitude warming. In an attribution study with an EBM, the authors attribute the largest source of uncertainty in poleward energy transport changes to cloud feedbacks, in agreement with previous studies looking at energy transport under global warming. They also show that cloud feedbacks contribute most to uncertainties in cross equatorial energy transfer (and hence tropical rainfall migration) under solar geo.

The paper is a very useful contribution to the solar geoengineering literature and helps to shed light on important results of previous studies such as residual high-latitude warming. The background information (section 1) is comprehensive and the methodology is sound. The use of an EBM is appropriate, although I think the disparities between the results of the EBM and GCMs (e.g. Fig. 5) should be elucidated more carefully in the text. My primary concern with the paper is the lack of consideration for oceanic energy transport changes – in particular for cross-equatorial energy fluxes where oceanic energy transport is important. The manuscript would benefit from looking at oceanic energy transport changes explicitly (a methodology for calculating meridional oceanic energy transport is provided by Hawcroft et al, 2016). This may elucidate why the ITCZ shifts in abrupt4xco2 are not correlated with atmospheric cross-equatorial energy transport changes. If the authors are unable or unwilling to investigate oceanic energy fluxes, then I would suggest altering the title of the manscript to "*Atmospheric* energy transport, polar amplification, and ITCZ shifts in the GeoMIP G1 ensemble" to better reflect the paper's contribution. Once these changes (and various minor changes listed below) are made, I'd be happy to recommend publication.

Thank you for the detailed suggestions in this review. The differences between the EBM and GCM results are smaller now that a major bug has been fixed in our implementation of the EBM (see response to Reviewer 2's Major Point 2). We add more discussion of the EBM-GCM differences in this version.

As for ocean transport, we have added some discussion of this to the introduction, However, we still think our focus on atmospheric energy transport makes sense. As Reviewer 2 points out, any changes in oceanic heat transport or storage are already taken into account in the atmospheric energy budget via the surface fluxes.

The *poleward* ocean heat transport is important to another aspect of this study: the explanation for the residual polar amplification in G1. We originally did not adequately discuss the possibility of an increase in ocean heat transport as a possible reason for this, but Hong et al. (2017) found that poleward heat transport by the ocean (northward across 30 degrees N in the Atlantic) decreases in G1, like that by the atmosphere. We now discuss this in the paper.

Specific Comments

P1 L5: First instance of CO2 – define as carbon dioxide

Done.

P1 L8: Mention explicitly that it is the *radiative forcing* from enhanced GHGs that is being offset by solar reduction in G1

Done.

P1 L8: Sentence beginning "In G1,..." - consider starting with "We show that ..." to distinguish your results from prior results

Done. Also added clarification about sign of net forcing.

P1 L19: Consider replacing "compensated for" with "counteracted". Also add a suitable reference at the end of this sentence

Done.

P1 L23: Sentence beginning "since reflecting sunlight would affect ..." is ambiguous. Explain why solar geoengineering leaves residual warming at high latitudes – at least give the primary theories – e.g. more sunlight in the tropics on average – with a suitable reference (e.g. Kravitz et al., 2013)

This sentence has been rewritten, and a reference has been added. The rest of the paragraph has also been revised, to maintain a logical flow.

P2 L12: Replace "subtropical" with "tropical" - Haywood et al identified Sahelian drought as a concern of hemispheric geoengineering and did not look at the subtropics

Done.

P2 L14: Add a suitable reference to the last sentence of this paragraph – which study explicitly identifies an ITCZ shift following a symmetric SAI application?

We now refer to Smyth et al., 2017, which studied ITCZ shifts in G1 (like this study does). A solar constant reduction is an example of a symmetric solar geoengineering deployment. Space mirrors would effectively cause a solar constant reduction.

P2 L15: You say "ITCZ shifts are closely related to the meridional transport of energy by the atmosphere". This is irrefutable, although you should add an appropriate reference, but only tells half the story. Add more discussion about the relative importance of ocean heat transport here, and its ability to control ITCZ position. The following references may be useful: Green and Marshall (2017), Hawcroft et al (2016), Haywood et al (2016), Hwang et al (2017), Marshall et al (2014)

We have added a paragraph discussing the relationships of the ITCZ to the atmosphere and ocean energy transport to the introduction, citing some of these and some other references.

P2 L30: The aim of G1 is not to "keep global mean temperature at approximately preindustrial levels" as you say – be more explicit about the simulation design

We now clarify that the experiment is designed to maintain energy balance at the top of atmosphere.

P4 L5: Define $\nabla.F_L$ at first use (i.e. latent energy transport)

We now define F_L, and also clarify F_L and F_M as horizontal fluxes to distinguish from the surface fluxes.

Figs 1 and 2: Consider also changing the y-units to 'poleward energy transport' rather then 'northward energy transport' to assist comparisons. Lastly, I'd suggest putting 'Latitude (N)' as the x-title rather than 'Latitude'

These suggested changes to the figures have been made.

P7 L2: Add a suitable reference for the DSE response to high-latitude warming

We have added reference to Hwang et al. (2011) here, and we also now refer back to Figures 1 and 2.

Eqn 3: This equation is valid for temperature in units in Kelvin, whereas your plots give temperature in units of ^{o}C – pick one for consistency and use throughout the manuscript – I'd personally go with the SI unit K

We now use K consistently throughout the paper.

P8 L14: Sentence "This leaves the differing spatial patterns of forcings as the only possible explanation" should have a caveat that meridional ocean heat transfer is negligible at high-latitudes (e.g. Fig. 6 in Hawcroft et al 2016)

We have now cited this figure as well as the reduction in Atlantic Meridional Overturning Circulation strength found by Hong et al. (2017) and a lack of increased energy input to the tropical ocean as reasons not to expect an increase in oceanic heat transport to the poles.

P8 L30: I recommend that the authors explicitly look at changes to meridional ocean heat transfer in the G1 and abrupt4XCO2 simulations using the methodology of Hawcroft et al (2016). Whilst the caveat about ocean heat transport in P8 L30 is appreciated, explicity looking at changes to ocean heat content / transport would significantly improve the manuscript whilst not altering the primary results

We have expanded on the possible reasons for the poor correlation between the ITCZ shift and cross-equatorial energy flux in abrupt4xCO2 in the revised manuscript. See response to Reviewer 2 major comment 1, which had some suggested reasons for this.

Fig. 4: Consider adding the correlation coefficients to the the respective figures

They are already in this figure, in the titles. We have reduced the number of decimal places from 3 to 2, following Reviewer 2's suggestion.

P9 L2: Reference the Haywood et al (2013) study at the end of "shifts toward the warmed hemisphere"

We decided to delete this sentence, since it lacked clarity. We now reference the Haywood et al. (2013) study at the beginning of the next sentence.

P9 L2: Change “It implies” to “The ITCZ shifts in Fig 4b imply”

Done.

P10 L10: Change “40 ^{o}N” to “40 ^{o}N/S”

Done.

P10 L11: Add a space between piControl and (Figure 5c)

Done.

P10 L12: Yes there are strong correlations, but that doesn't mean the EBM is doing a good job! For instance, for abrupt4XCO2 the EBM predicts a negative poleward energy transport anomaly at 40 ^{o}N for 6 out of the 8 models where the GCMs give a positive anomaly. This issue should be discussed and not glossed over.

The EBM simulations have all been redone (see response to Reviewer 2 major comment 2). Now that humidity is being correctly simulated in the EBM, the EBM does a somewhat better job of reproducing the GCM energy transport changes. For example, the EBM now gives positive energy transport anomalies at 40 ^{o}N/S for all models in Figure 5c. The discussion of Figure 5 has been updated to address the recent changes.

Fig. 5: A minor suggestion - put “40 ^{o}S/N” into the plot titles for b) and c)

Done.

Fig. 6: In the caption and the titles note that it is the *northward* energy transport that you are plotting

Done.

P13 L5: Again – I urge you to explicitly assess oceanic heat uptake in these simulations – you say that the results of the EBM imply that oceanic heat uptake differs between the GCMs – it would not be difficult to assess this hypothesis and would add value to your results

This entire paragraph has been rewritten because of the redone EBM simulations; while the conclusion that clouds are the largest source of inter-model spread has not changed, the spread in the other experiments is somewhat different from before. We now mention here that the spread in this term could represent an atmospheric response to cross-equatorial ocean energy transport. We did not mean that the results of the EBM are the best way to make inferences about oceanic heat uptake—in fact we calculated the net energy flux into the ocean (really into the surface, but over land it is negligible) in order to run this experiment.

Explicitly calculating the ocean energy storage and transport would not be trivial, because it would require obtaining and analyzing output from the ocean component of the models, which we have not done before. In any case, Hong et al. (2017) have already done a lot of analysis in this direction.

P13 L7: Sentence beginning "The impact of the solar forcing term ..." is very wordy and does not read well – rephrase

This sentence was eliminated in the rewrite of this paragraph.

P13 L25: "has" → "have"

Done.

P13 L27: Sentence beginning "Models with a greater negative change..." - include an example

Added MPI-ESM-LR as an example.

P13 L30: I would also use Fig. 6 in Hawcroft et al (2016) to argue your point that poleward energy transport changes in are likely not due to oceanic heat transport changes – i.e. more background meridional heat transport in the atmosphere than the ocean

We have cited the Hawcroft figure (and the Hong et al. 2017 paper) at the earlier place you suggested it, but we have deleted this sentence. The argument we originally made here was incorrect, because the surfaceFlux experiment is about the response of the atmospheric heat transport to the ocean heat transport and doesn't necessarily tell us anything about what the ocean heat transport itself is doing.

P14 L8: You should add caveats that the EBM does not get the sign of the energy transport right in the Northern Hemisphere (Fig. 5c). I would seriously consider removing Fig. 8A and associated analysis due to this issue as it indicates the EBM is missing the point and any analysis is compromised

Again, the fixed EBM now does get the sign of the energy transport right in the Northern Hemisphere. The discussion of Figure 8A has been revised to account for the redone EBM simulations.

P16 L18: Following "poleward atmospheric energy transport decreases" refer to Figs 1a,d

Done.

Reviewer 2

Overview

Overall, this manuscript makes an interesting contribution to the physical climate's response to solar radiation management geoengineering. The analysis framework is centered on moist static energy transport, which has been a valuable way of understanding other climate perturbation (e.g., from carbon dioxide and other anthropogenic radiative forcing). Bringing this perspective to the geoengineering simulations is helpful to understand the ways in which the reduced solar constant is not perfectly offsetting the regional climate changes from increased carbon dioxide, even if the global-mean surface temperature is near zero. The conclusions concerning the critical role of the spatial pattern of the forcing (vs. the possibility that radiative feedbacks differ between solar and greenhouse gas forcing) is nice to broadcast clearly, as the abstract does.

I think the manuscript is suitable for publication, but there are some important caveats about the analysis that need to be added and the authors need to alter how they perturb the moist EBM to be more consistent with what we know about the radiative forcing of carbon dioxide (at least the global mean part).

This review, particularly the scrutiny of our methods for imposing the CO_2 radiative forcing in the EBM, was extremely helpful to us as it helped us to find a bug in our implementation of the Hwang and Frierson (2010) EBM and to finally find out why we could not originally reproduce one aspect of their results. The bug has been fixed and the EBM experiments have all been re-run and the associated figures replaced. Details of the bug are described below. Thank you also for pointing out interesting papers in the literature that help to better contextualize our analysis and understand its limitations.

Major Points

1) ITCZ shifts: recent literature

There are a few relevant new publications that the authors should engage with. Seo et al. (2017) showed that the cross-equatorial energy flux does not always account for ITCZ shifts in GCM simulations of carbon dioxide warming. It's fine to continue to use this as a first cut toward understanding the simulations' behavior, but its limitations need to be acknowledged. It may be that the non-zero intercept in Fig. 4a comes about for a reason discussed there: the gross moist stability (energetic stratification) can also change.

We now discuss possible reasons for discrepancies between the cross-equatorial energy flux and ITCZ shifts when discussing Fig. 4a.

Viale and Merlis (2017) analyzed simulations with solar forcing and carbon dioxide forcing and found the ITCZ shifted a different amount. They interpreted this result through the refined energy flux equator argument described by Bischoff and Schneider (2014). The result in Viale and Merlis (2017) is in line with the typical GCM results here: more sensitivity to carbon dioxide than solar forcing in ITCZ shifts, so a poleward shift in geoengineered climate. This comes about by a different spatial pattern in the radiative forcing (not differences in radiative feedbacks).

We now mention the results of the Viale and Merlis (2017) paper when discussing the multi-model mean ITCZ shift in Section 2.1.

Last, the TRACMIP simulations (Voigt et al., 2016) have examples of radiatively forced warming where the ITCZ shift does not follow the energy flux equator. I've seen this shown in conference talks, though it may not have been published yet.

This is still not published (personal communication from Michela Biasutti). We will add a citation if it is published before the final deadline for changes to our paper.

I think this literature needs to be invoked rather than ocean heat storage (p. 8 L30) for the breakdown in abrupt 4x simulations: the ocean heat storage is already taken into account through the surface fluxes. That cannot explain the why the cross equatorial energy fluxes in the atmosphere are uncorrelated to the ITCZ shift.

We now mention the Seo et al. and Bischoff and Schneider papers when discussing this breakdown, as part of a broader discussion of the limitations of the cross-equatorial energy transport/energy flux equator proxies for the ITCZ position.

2) Moist EBM analysis

First, I appreciate that the methodological details are described in a greater detail than in previous papers that use this approach and the authors have made their codes available.

* Eqn. B1 has a mistake (see North 1975 and subsequent diffusive EBM papers). There is a missing (1 - x^2):

$$\frac{\partial}{\partial x}\left[(1-x^2)\frac{\partial MSE}{\partial x}\right]$$

I hope this is a typesetting mistake and not a problem with the implementation of the EBM used for the analysis.

Thank you for pointing this out. The factor of (1-x^2) has in fact always been (implicitly) in the EBM code; the error in the manuscript came from us misinterpreting the code from Yen-Ting Hwang that was written in θ rather than x coordinates. There is also a factor of the square of the radius of the earth that was left out of the equation (absorbed into D in the North papers). In the revised manuscript, for clarity, we have written this equation in both θ and x coordinates, to help alleviate any confusion about where the (1-x^2) comes from.

* The convention of OLR = aT_s - *b* is confusing when other EBM literature has the opposite use of *a* and *b* (e.g., OLR = *a* + bT_s), but I understand the desire for continuity with Hwang and Frierson (2010).

We have chosen to retain the aT_s - *b* convention in the revised version.

* I think it's valuable to try to set the record straight concerning how Hwang and Frierson (2010) described the change they made to do the warming EBM simulations. I thought they made a terminology mistake, saying that they re-fit *b* “to capture the change in climate sensitivity”, which would be a change in *a*. Changing just *b* is reasonable as you can think of that as a change in radiative forcing (e.g., Rose et al., 2014). This manuscript, however, suggests both *a* and *b* must be changed to simulate altered climates. I don't follow that, as Rose et al. (2014) and others have done moist EBM simulations that are just changing *b* and have changes in energy transport. The values of a don't seem to change too much, generally near 2 $W/m^2/K$ as expected from the sum of temperature and water vapor feedbacks, so I'm confused.

See response to next comment.

* Again, I want to praise the authors for disclosing the methodological details. I have not seen the parameter values for a and b when using linear fits to GCMs before (Table 4). However, the results are troubling and perhaps earlier work would have attracted scrutiny if this had been disclosed. If we think of *b* as representing the carbon dioxide radiative forcing (change in OLR with unchanged surface temperature), the fits imply carbon dioxide radiative forcing that varies across models from 0 to 16 W/m^2 (just considering the abrupt 4x column vs. the control). This is a problem! It also affects the G1 simulations.

Thank you for bringing up this issue, as it resulted in us finding and fixing a bug in our implementation of the EBM that affected all the EBM simulations. Hwang and Frierson (2010) did in fact re-fit only *b* instead of *a* and *b* (Dargan Frierson confirmed this). The reason we assumed that they didn’t was that we could not get much of a response of energy transport to the “greenhouse” experiment when changing only *b*. It turned out that when re-implementing the EBM in Python, we neglected to convert saturation vapor pressure from hPa to Pa, resulting in specific humidity being too low by a factor of 100. So, we were effectively running a dry EBM instead of a moist EBM. Now that this problem has been fixed, we get changes in MSE transport when changing only *b* that are of similar magnitude to those in the Hwang *et al.* papers. Before the moisture bug was fixed, changing only *b* amounts to a uniform reduction in OLR everywhere, which has no effect on the energy transport (so this methodology won’t work in a dry EBM). But when humidity can adjust to temperature, it goes up much more in the tropics than the poles responding to a uniform initial OLR perturbation, leading to an increase in meridional energy transport as a result of the stronger greenhouse effect.

We re-ran all of the EBM simulations with the corrected moisture issue, also having fixed a more minor bug where it had been assumed the GCM latitudes are evenly spaced (in fact most GCMs use non-even Gaussian grids), and re-fitting only *b* instead of *a* and *b* in the all-perturbation and greenhouse experiments. The results are qualitatively similar in most respects to those in the previous version of the manuscript, and our overall conclusions have not changed. The agreement between the EBM and GCMs in Figure 5 has improved somewhat. The plot axes in Figures 5 through 8 had to be expanded because the EBM moves more energy now, and the text has been changed to reflect the changes in methodology and results where necessary.

Regarding the value of the CO_2 forcing, the values of *b'* where *a* has been fixed when re-fitting are now included in Table 4 (and the old values of *a'* and *b'* deleted). Comparing *b'* to *b* in this table shows that the radiative forcing values are now all around 7-9 W/m^2 for G1; for abrupt4xCO2 they are a little higher in some models (as much as 13 W/m^2 for CESM) but this doesn't seem entirely unreasonable because clear-sky LW feedbacks such as water vapor and lapse rate feedbacks are included. (Also, *b'* is greater than *b*, as it should be with the OLR = aT_s - *b* convention; when re-fitting *a* and *b*, not only were the values of radiative forcing wildly divergent, as you pointed out, but they were all *negative*.)

* The last important thing that should be noted is that the approach of prescribing TOA perturbations (e.g., from cloud radiative effect changes) in the moist EBM does not capture the fact that feedbacks are interacting with each other (Feldl et al., 2017) and with the changing energy transport (Rose et al., 2014; Merlis, 2014; Rose and Rayborn, 2016). There's still value in this way of diagnosing things (partially interactive), but it's not the full story and may help explain why EBM is changes less than the GCM.

We now note these limitations, as well as the fact that the EBM does not capture the spatial structure of CO_2 forcing, in the 2nd paragraph of Section 3. Note that the poleward energy transport change in the EBM is now greater than that for the GCMs in G1 and for the northern hemisphere in abrupt4xCO2 in the redone EBM experiments (see Figures 5b,c).

3) Forcing estimates

The authors describe in conclusions that the radiative forcing for carbon dioxide is not uniform, but this seems important enough to come earlier when describing the EBM set up (p. 10 L1).

* The authors cite only Zelinka and Hartmann (2012) (p. 15) when discussing the extratropical response to carbon dioxide. Those authors neglected the structure of carbon dioxide, which was subsequently included in Huang and Zhang (2014). They also looked at the same CMIP5 abrupt 4x simulations, so it's important to confirm consistency.

Thank you for pointing out the role of the non-uniform CO_2 forcing in the response of energy transport to CO_2 increases. The non-uniform forcing not captured by the EBM when re-fitting only *b*. We now cite the Huang and Zhang paper and mention the non-uniform forcing in the discussion of the "greenhouse" EBM experiment in Section 3.3.1.

* Other authors (e.g., Feldl and Bordoni, 2016) have taken the approach of diagnosing the forcing, including its spatial structure, from fixed SST simulations (“troposphere adjusted forcing”). Given my concern about the linear fit estimate of *b* values above, I think this is a superior way to drive the moist EBM. Another alternative would be to take previously published global-mean adjusted forcing estimates and use those—at least all the carbon dioxide forcing would be near 7 W/m^2.

Having re-run all the EBM simulations with corrected moisture transport and re-fitting only *b* and not *a*, we think we have adequately addressed the concerns about accuracy of the CO_2 forcing. It is true that this does not capture the spatial structure of the CO_2 forcing, but there are no obvious, workable alternatives. Using forcing estimates from fixed-SST simulations would include rapid adjustments from clouds and other variables in the “greenhouse” experiment. This experiment was intended to simulate the effects of the enhanced greenhouse effect, including water vapor, lapse rate and Planck feedbacks, but not cloud feedbacks. If cloud feedbacks were included in the greenhouse experiment, they would be double-counted when the SW and LW cloud effects were also included (as in the “all_G1” and “all_4xCO2” experiments), and it would be hard to distinguish between the effects of CO_2 forcing and changes in clouds. We also considered re-fitting *b* in individual latitude bands instead of globally, but since we can only use clear-sky OLR for the fit, this would miss the portion of the spatial structure of radiative forcing that is caused by pre-existing clouds (thanks to Dargan Frierson for pointing this out).

Minor Points

p. 3 L19: “moisture fluxes" terminology is not ideal for the latent surface fluxes, given that meridional energy and moisture fluxes are discussed later.

“Moisture” here has been changed to “latent heat”.

Fig. 3: how close is the global-mean surface temperature change to zero in these simulations? I understand this is discussed in other papers using G1, but it would be helpful to at least state a representative number (e.g., within 0.2 K).

Global mean temperature changes have been added to Table 1.

Fig. 3 caption: presumably these are zonal *and annual* mean *surface air* temperature changes? I didn't see this in the main text either. Likewise for saturation vapor pressure.

It has now been clarified that these are surface air temperature and surface specific humidity. A clarification that all months are included has been added to the description of the averaging procedure in the first paragraph of Section 2.

p. 8 L27, and elsewhere: a big excessive on the number of digits for *r*.

The number of digits for *r* has been reduced from 3 to 2 throughout the paper.

Fig. 5: plot 1-to-1 lines here

Done. Also, the plot aspect ratio has been changed to 1:1.

p. 16 L6: the ocean heat uptake is weighted toward subpolar oceans (vs. a uniform uptake which wouldn't affect extratropical atmospheric energy transport)

We now make this clarification in the text.

Specific Comment 1

P4 L10-13: The "unphysical result" problem stated in your manuscript is due to a postprocessing (CMORizing) error in the first G1 realization (r1i1p1) from BNU-ESM, there is no such problem in the second G1 realization (r2i1p1). You could download all BNUESM CMIP5/GeoMIP results at http://esg.bnu.edu.cn/thredds/esgcet/catalog.html. If you have problems please let us know.

The r2i1p1 realization of G1 in BNU-ESM still has the problem that the global mean temperature is not adequately maintained at preindustrial levels, which is important to our analysis. After this comment was posted, the BNU modeling group provided us with the output from a new G1 realization, r3i1p1, which did a good job of maintaining global mean temperature. However, there was not enough time to incorporate this model into our analysis for this revision. We have removed the reference to the "unphysical result" in the text.

Energy transport, polar amplification, and ITCZ shifts in the GeoMIP G1 ensemble

Rick D. Russotto[1] and Thomas P. Ackerman[1,2]

[1]Department of Atmospheric Sciences, University of Washington, Seattle, Washington, USA
[2]Joint Institute for the Study of the Atmosphere and Ocean, University of Washington, Seattle, Washington, USA

Correspondence to: Rick D. Russotto (russotto@uw.edu)

Abstract.

The polar amplification of warming and the ability of the inter-tropical convergence zone (ITCZ) to shift to the north or south are two very important problems in climate science. Examining these behaviors in global climate models (GCMs) running solar geoengineering experiments is helpful not only for predicting the effects of solar geoengineering, but also for understanding how these processes work under increased carbon dioxide (CO_2). Both polar amplification and ITCZ shifts are closely related to the meridional transport of moist static energy (MSE) by the atmosphere. This study examines changes in MSE transport in 10 fully coupled GCMs in Experiment G1 of the Geoengineering Model Intercomparison Project, in which the solar constant is reduced to compensate for the radiative forcing from abruptly quadrupled CO_2 concentrations. In G1, poleward MSE transport decreases relative to preindustrial conditions in all models, in contrast to the CMIP5 abrupt4xCO2 experiment, in which poleward MSE transport increases. Since We show that since poleward energy transport decreases rather than increasing, and local feedbacks cannot change the sign of an initial temperature change, the residual polar amplification in the G1 experiment must be due to the net positive forcing in the polar regions and net negative forcing in the tropics, which arises from the different spatial patterns of the simultaneously imposed solar and CO_2 forcings. However, the reduction in poleward energy transport likely plays a role in limiting the polar warming in G1. An attribution study with a moist energy balance model shows that cloud feedbacks are the largest source of uncertainty regarding changes in poleward energy transport in mid-latitudes in G1, as well as for changes in cross-equatorial energy transport, which are anticorrelated with ITCZ shifts.

1 Introduction

As solar geoengineering, or the artificial cooling of earth by reflecting sunlight, increasingly gains attention as part of a possible strategy to deal with the effects of climate change, two important issues are whether the polar amplification of CO_2-induced warming can be fully compensated forcounteracted, and whether regional precipitation patterns will shift, exacerbating flooding in some areas and drought in others (e.g. Irvine et al., 2010) . Polar amplification is the phenomenon in which the poles warm by more than the tropics when atmospheric CO_2 concentrations are increased. While the reasons for polar amplification are not yet completely understood, it has already been observed in the instrumental temperature record (*e.g.* Bekryaev et al., 2010) and is a robust behavior in climate models (*e.g.* Holland and Bitz, 2003). Since reflecting sunlight would affect Earth's radiation

~~budget through different physical mechanisms from changes in CO_2 concentrations~~the tropics more strongly than the poles, it has been hypothesized that ~~solar geoengineering may insufficiently cool the polar regions~~it would reduce the meridional temperature gradient (e.g. Keith and Dowlatabadi, 1992) , leading to tropical cooling and polar warming under the combined CO_2 and geoengineering forcings. We refer to this effect as "residual polar amplification". Early model simulations of solar geoengineering scenarios, involving a simultaneous CO_2 increase and solar constant decrease (Govindasamy and Caldeira, 2000; Govindasamy et al., 2003), found that ~~most of the difference in warming between the poles and the tropics was , in fact, eliminated~~the residual polar amplification was relatively small, with latitudinal temperature patterns looking much more like the preindustrial climate than the climate under increased CO_2 without geoengineering. However, ~~these types of experiments still result in some warming at the poles and cooling in the tropics if the global mean temperature is held constant; we refer to this effect as "~~some residual polar amplification ~~"~~still occurs as a robust feature of these types of model experiments (e.g. Kravitz et al., 2013a) .

Questions about shifts in regional precipitation under solar geoengineering are motivated by evidence from paleoclimate data and climate model studies that if one hemisphere is preferentially warmed, the intertropical convergence zone (ITCZ) shifts toward that hemisphere (*e.g.* Broccoli et al., 2006). Model studies have shown that such an effect could occur for changes in many different variables that affect the inter-hemispheric albedo contrast, such as high-latitude ice cover (Chiang and Bitz, 2005), mid-latitude forest extent ~~(Swann et al., 2012)~~ (Swann et al., 2012; Laguë and Swann, 2016) , and tropospheric sulfate aerosol concentration (Hwang et al., 2013). In the context of solar geoengineering, Haywood et al. (2013) demonstrated that preferentially injecting reflective aerosols into one hemisphere shifts the ITCZ towards the other hemisphere, causing drought in some ~~subtropical~~ tropical areas. Even ~~for~~ under a hemispherically symmetric solar geoengineering deployment, ~~ITCZ shifts might still occur , due to differing albedos and/or radiative feedbacks between hemispheres~~such as space-based mirrors (represented by a solar constant reduction), ITCZ shifts can still occur (Smyth et al., 2017) .

Both polar amplification and ITCZ shifts are closely related to the meridional transport of energy by the atmosphere~~. Much progress has been made understanding atmospheric energy transport in a changing climate through~~ , which makes atmospheric energy transport an important aspect of the effects of solar geoengineering to study. The sensitivity of the ITCZ, in particular, to energy transport in the atmosphere and ocean in present and future climates has recently been a topic of great research interest. Studies with slab ocean models with imposed hemispherically asymmetric energy fluxes (e.g. Kang et al., 2008; Yoshimori and Broccoli, 2008) found that an anomalous Hadley circulation transports energy from the warmed hemisphere across the equator, shifting the ITCZ towards the warmed hemisphere (because moisture is transported by the lower branch of the Hadley cell, while energy is transported by the upper branch). However, later studies (e.g. Kay et al., 2016; Hawcroft that this effect is substantially weaker in GCM simulations that include a full ocean circulation coupled to the atmosphere. This is because an anomalous wind-driven ocean circulation develops in response to changes in the atmospheric Hadley circulation, allowing the ocean to do most of the work of transporting the excess energy in one hemisphere across the equator (Green and Marshall, 2017) . Still, we can consider the ITCZ position in the framework of the atmosphere and take ocean heat transport and storage into account via surface energy fluxes.

This study builds off the methods of a particular set of studies of atmospheric energy transport in projects in which multiple global climate models (GCMs) ~~are~~ were run for the same radiative forcing scenarios. Hwang and Frierson (2010) showed that poleward transport of atmospheric moist static energy (MSE) increases under increased CO_2 concentrations in Coupled Model Intercomparison Project, Phase 3 (CMIP3) models. They used a moist energy balance model (EBM) to attribute the change in MSE transport across 40° latitude to different forcing and feedback terms, and found that cloud feedbacks are responsible for most of the inter-model spread in this quantity. Hwang et al. (2011) found that poleward dry static energy (DSE) transport in mid-to-high latitudes decreases with warming due to the reduced equator-to-pole temperature gradient (since warming is amplified at the poles), but moisture transport increases due to the overall warming combined with the nonlinearity of the Clausius-Clapeyron equation and the increase in moisture transport is enough to lead to an increase in MSE transport overall. Frierson and Hwang (2012) found that shifts in the ITCZ with warming in the CMIP3 slab ocean ensemble are anticorrelated with changes in atmospheric energy transport across the equator, with cloud feedbacks again being the largest source of uncertainty.

The Geoengineering Model Intercomparison Project (GeoMIP) provides an opportunity to use similar methods to investigate how atmospheric energy transport may change under solar geoengineering conditions, which can help us understand the reasons for residual polar amplification and tropical precipitation shifts. We analyze the results of GeoMIP experiment G1 (Kravitz et al., 2011), in which the solar constant is reduced at the same time as the CO_2 concentration is quadrupled in order to maintain top of atmosphere (TOA) energy balance and therefore keep the global mean temperature approximately at preindustrial levels. For comparison, we also examine two CMIP5 model runs: piControl, a preindustrial run, and abrupt4xCO2, in which CO_2 is quadrupled but the solar constant remains the same.

GeoMIP has yielded insights into how temperature and precipitation patterns may change under solar geoengineering. Kravitz et al. (2013a) found that residual polar amplification occurs in all models running the G1 experiment. Global mean precipitation decreases in G1 because the reduction in solar radiative flux at the surface is primarily balanced by a reduction in evaporation (Kravitz et al., 2013b). The precipitation reduction is evident over monsoonal land regions, as well as in the global mean, and extreme precipitation events are reduced in G1, in contrast to an increase in abrupt4xCO2 (Tilmes et al., 2013).

Reducing the solar constant is an approximation of more realistic proposals for solar geoengineering, such as injecting aerosols into the stratosphere. One example of how the physics differs between these scenarios involves the magnitude of the reduction in global mean precipitation. Solar constant reduction experiments underestimate the precipitation reduction compared to model runs that increase the concentration of sulfate aerosols in the stratosphere (Niemeier et al., 2013; Ferraro and Griffiths, 2016). This is because sulfate aerosols absorb longwave radiation, which reduces the net atmospheric radiative cooling rate and therefore allows for less precipitation, since the latent heat release from precipitation formation must be balanced by net radiative cooling. (See, *e.g.*, Pendergrass and Hartmann (2014) for a discussion of the atmospheric energy constraints on global mean precipitation). Even with this caveat, the G1 experiment is useful because of its simplicity and because it eliminates confounding effects from global mean temperature changes.

We use the G1 experiment to investigate changes in meridional energy transport under solar geoengineering, the factors responsible for these changes, and the associated effects on tropical precipitation and polar amplification. Section 2 describes the energy and moisture latent heat transport changes that occur in the G1 and abrupt4xCO2 experiments. Section 3 attributes these energy transport changes to different forcing and feedback terms, using the moist energy balance model (EBM) of Hwang and Frierson (2010). Conclusions are provided in Section 4.

2 Energy and moisture transport changes

Using the top of atmosphere (TOA) TOA and surface energy and moisture fluxes from the GeoMIP GCM experiments, we calculate changes in the meridional transport of MSE by the atmosphere. By subtracting the MSE transport in piControl from that in G1, we can understand how the combined CO_2 increase and solar constant decrease affect MSE transport, or, in other words, how well solar reductions can restore preindustrial patterns of atmospheric energy transport. For comparison, we also examine how the CO_2 increase alone affects MSE transport by subtracting the MSE transport in piControl from that in abrupt4xCO2. Following Kravitz et al. (2013a) and other papers analyzing GeoMIP results, we use the average of years 11-50 of the G1 and abrupt4xCO2 experiments in order to exclude the rapid changes that occur during the first few years. For piControl, we average over the first 40 years of model output provided by the modeling groups. (The period analyzed does not include any model spin-up period.) All averages are multi-annual means including all months.

We calculate the energy flux into the atmosphere from the GCM output as the sum of terms on the right-hand side of the following energy budget equation:

$$\nabla \cdot F_M = R^{\downarrow}_{\mathrm{net,TOA}} + R^{\uparrow}_{\mathrm{net,surface}} + \mathrm{SH} + \mathrm{LH} \tag{1}$$

where F_M is the vertically integrated horizontal moist static energy flux, $R^{\downarrow}_{\mathrm{net,TOA}}$ is the net downward radiative flux at the top of the atmosphere, $R^{\uparrow}_{\mathrm{net,surface}}$ is the net upward radiative flux at the surface, SH is the net upward surface sensible heat flux, and LH is the net upward surface latent heat flux. Since the net energy flux into the atmospheric column must be balanced by energy transport out of the column, we can calculate the northward atmospheric moist static energy transport as a function of latitude by integrating $\nabla \cdot F_M$, first zonally and then cumulatively northward from the south pole. It is also useful to decompose the MSE transport into latent energy (moisture) transport and dry static energy (DSE) transport, in order to identify how moisture changes affect the total energy transport changes, following the methodology of Hwang et al. (2011) . We calculate the latent energy transport from the latent heat flux and precipitation GCM output by integrating the following equation zonally and meridionally:

$$\nabla \cdot F_L = \mathrm{LH} - L_v P \tag{2}$$

where F_L is the vertically integrated horizontal latent energy flux, L_v is the latent heat of vaporization of water and P is precipitation. We calculate the DSE transport by subtracting the latent energy transport from the MSE transport.

Table 1 lists the GeoMIP models included in this analysis. The models in this study all had solar constant reductions between 3.2% and 5.0% and global mean temperatures in G1 within 0.3 K of those in piControl. Three of the original 13 GeoMIP models are excluded: BNU-ESM, because it did not adequately restore the global mean temperature in the G1 and because the

Table 1. Models included in this study, with references, institutions, ~~and~~ solar constant reduction in the G1 experiment (ΔS_0), and global mean temperature change in G1 - piControl (ΔT).

Model	Reference	Institution	~~S_0 reduction in G1~~ ΔS_0
CanESM-2	Arora et al. (2011)	Canadian Centre for Climate Modeling and Analysis	4.0%
CCSM4	Gent et al. (2011)	National Center for Atmospheric Research	4.1%
CESM-CAM5.1-FV	Hurrell et al. (2013)	National Center for Atmospheric Research	4.7%
CSIRO-Mk3L-1-2*	Phipps et al. (2011)	Commonwealth Scientific and Industrial Research Organization/ Bureau of Meteorology	3.2%
GISS-E2-R*	Schmidt et al. (2014)	NASA Goddard Institute for Space Studies	4.5%
HadGEM2-ES	Collins et al. (2011)	Met Office Hadley Centre	3.9%
IPSL-CM5A-LR	Dufresne et al. (2013)	Institut Pierre Simon Laplace	3.5%
MIROC-ESM	Watanabe et al. (2011)	Atmosphere and Ocean Research Institute (The University of Tokyo), National Institute for Environmental Studies, and Japan Agency for Marine-Earth Science and Technology	5.0%
MPI-ESM-LR	Giorgetta et al. (2013)	Max Planck Institute for Meteorology	4.7%
NorESM1	Bentsen et al. (2013)	Bjerknes Centre for Climate Research, Norwegian Meteorological Institute	4.0%

* These models are excluded from the second part of this study (the EBM analysis) because the necessary output fields were not archived.

~~surface upwelling LW radiation is less than the downwelling LW, an unphysical result~~realizations that were available when our analysis was done; EC-Earth, because the precipitation output file was corrupted; and HadCM3, because many of the output fields required for this study are no longer available. Methodological details of these calculations are described in Appendix A.

2.1 Poleward transport in mid-latitudes

Changes in the zonal mean northward MSE, latent energy and dry static energy (DSE) transport for G1 minus piControl are shown in Figure 1. Poleward MSE transport in mid-latitudes is reduced under G1 in all 10 models and, when decomposed into the latent and DSE components, both of these terms are reduced as well. Figure 2 shows the same calculations for abrupt4xCO2 minus piControl. In this case, poleward DSE transport decreases but moisture transport increases by more than enough to compensate, leading to an increase in total MSE transport. This corroborates the result seen by Held and Soden (2006) and Hwang et al. (2011) in CMIP3 global warming scenarios.

To understand why the energy transport changes are different for global warming and geoengineering conditions, we look at zonal mean changes in temperature and saturation vapor pressure. Figures 3a,b show the zonal mean temperature change in G1 and abrupt4xCO2 relative to preindustrial. (These are also plotted in Figure 1 of Kravitz et al. (2013a), but our plots include only the models analyzed here and, for G1, we use a smaller y-axis range to show more detail.) In G1, the tropics are cooled while the poles are warmed (Figure 3a). There is warming everywhere in abrupt4xCO2 but more so in the polar regions, G1 minus piControl (Figure 1)

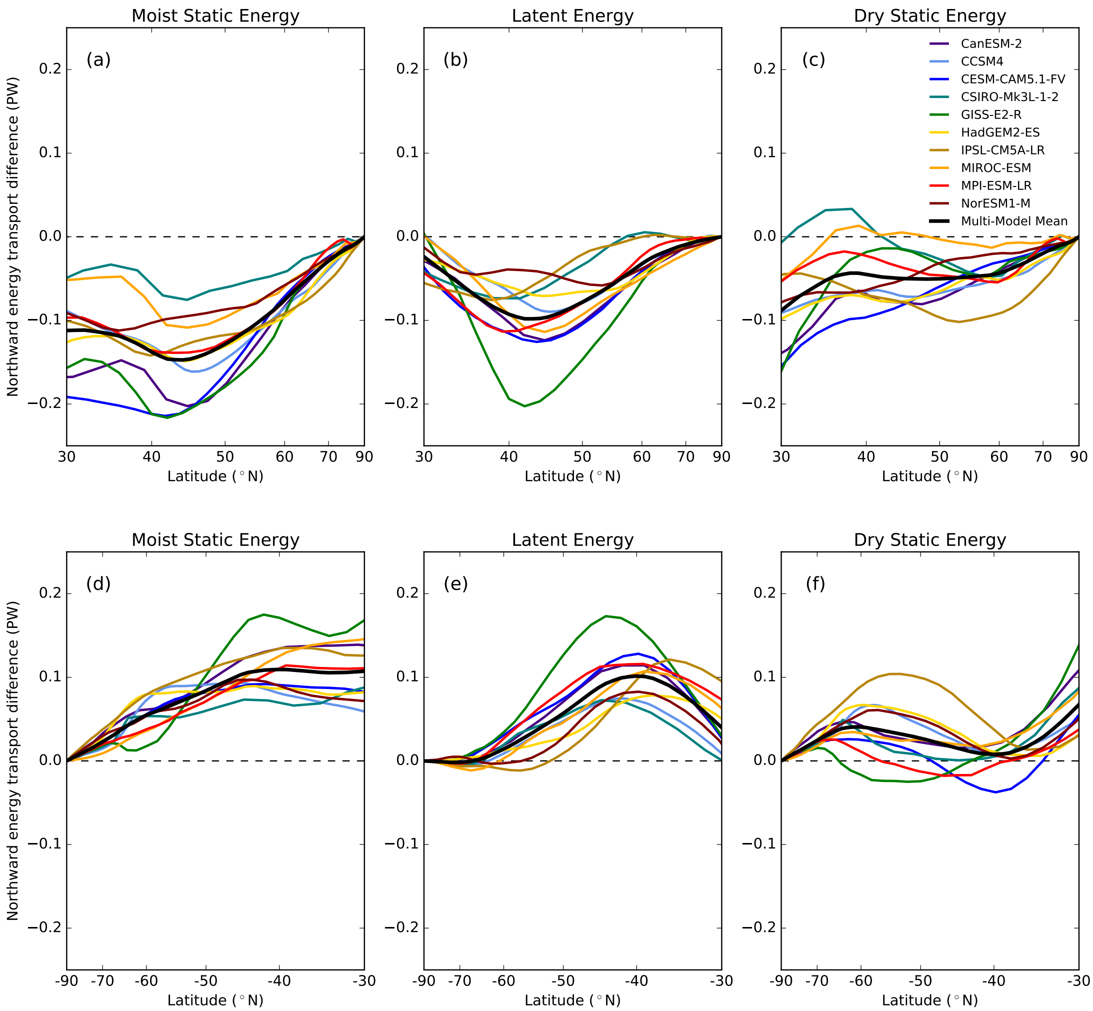

Figure 1. Northward energy transport (PW) for G1 minus piControl, poleward of 30° N (a-c) and 30° S (d-f), for total moist static energy transport (a, d), latent energy transport (b, e), and dry static energy transport (c, f), in the GeoMIP models and the multi-model mean.

especially the Arctic (Figure 3b). In both cases, this pattern of temperature change results in a weakening of the equator-to-pole temperature gradient and reduces the poleward transport of dry static energy (Figures 1c,f and 2c,f), similar to the result found by Hwang et al. (2011) .

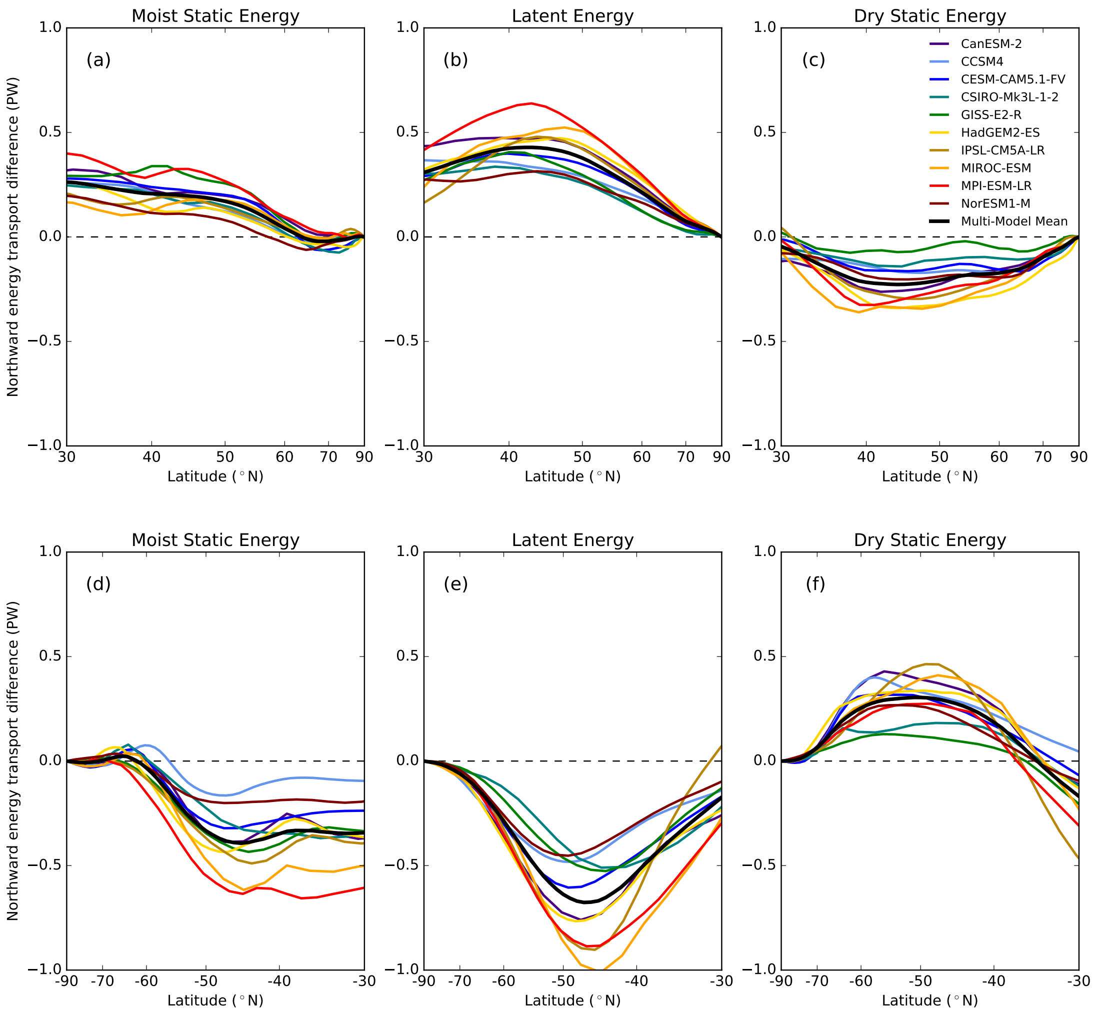

Figure 2. As in Figure 1 but for abrupt4xCO2 minus piControl.

The mechanism for the difference in moisture transport is apparent from changes in saturation vapor pressure, e_s, which we calculate using an approximate form of the Clausius-Clapeyron equation (*e.g.* Hartmann, 2016, eq. 1.11):

$$e_s = (6.11\,\mathrm{hPa})\exp\left\{\frac{L_v}{R_v}\left(\frac{1}{273}-\frac{1}{T}\right)\right\} \tag{3}$$

where L_v is the latent heat of vaporization of water, R_v is the gas constant for water vapor, and T is the temperature in K. In abrupt4xCO2 (Figure 3d), e_s increases more in the tropics than it does near the poles because e_s is approximately exponential with respect to temperature. A slight warming in the tropics leads to a larger increase in e_s because the tropics were initially warmer than the poles. In G1, however (Figure 3c), the tropics cool and the poles warm, so saturation vapor

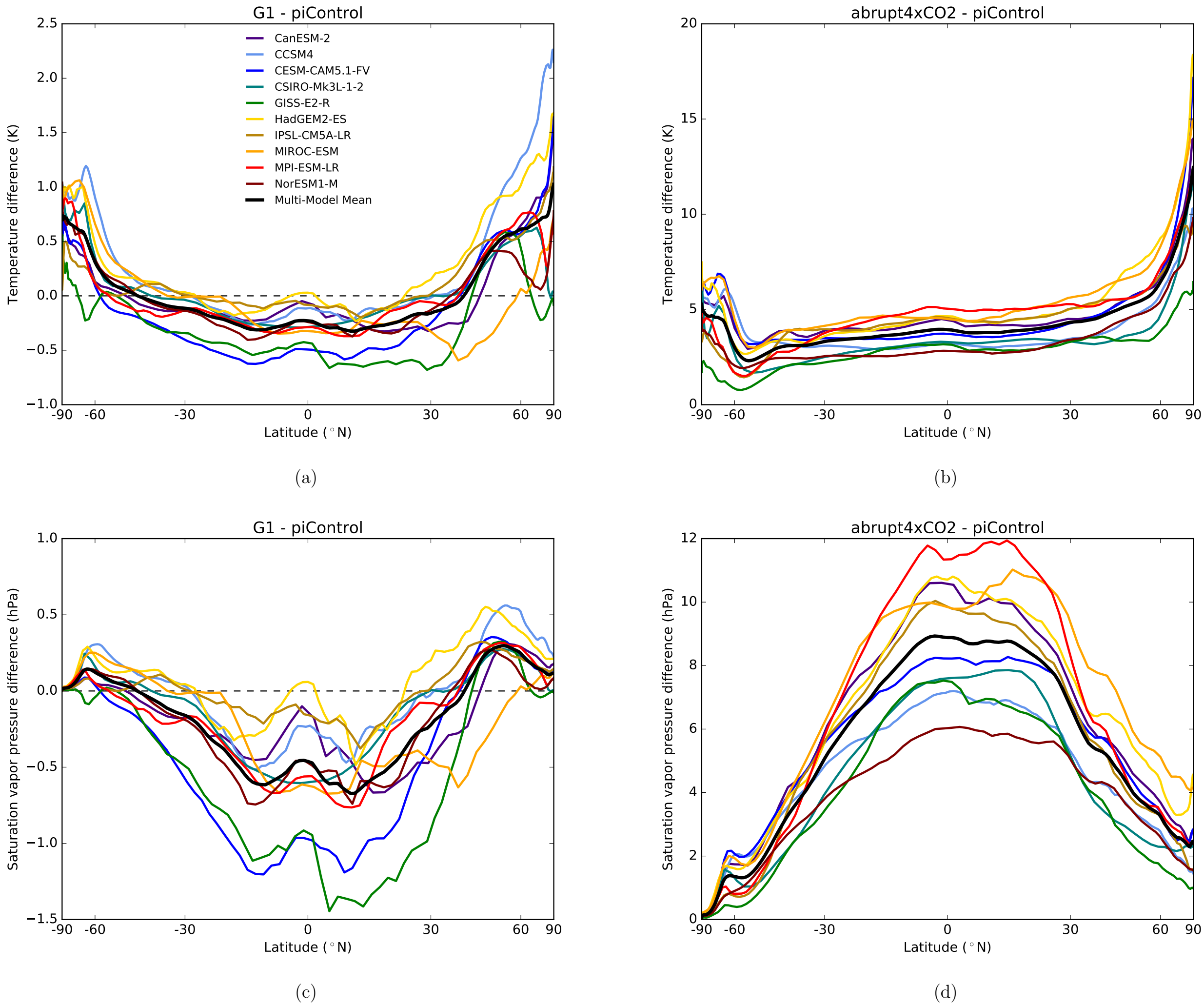

Figure 3. Zonal mean surface air temperature changes relative to piControl for G1 (a) and abrupt4xCO2 (b), and analogous zonal mean surface saturation vapor pressure changes (c,d), in GeoMIP models and multi-model mean.

pressure, like temperature, decreases in the tropics and increases (to a lesser extent) at high latitudes relative to piControl. Assuming the moisture content in the atmosphere scales with Clausius-Clapeyron, and the meridional winds are roughly the same, poleward moisture transport increases in abrupt4xCO2 and decreases in G1 because the equator-to-pole moisture gradient has strengthened in abrupt4xCO2 and weakened in G1.

A decrease in poleward energy transport has been previously reported in a single-model study running the G1 setup (Schaller et al., 2014) . In addition to a G1 experiment, that study also included runs which included only the CO_2 increase or solar constant decrease. The decrease in poleward energy transport in their G1 run is not equal to the sum of the increase in the

"CO2+" run and the decrease in the "solar-" run in either hemisphere (see their Table 3). Also, the changes in poleward energy transport are not symmetrical in their solar increase and solar decrease run. This indicates that the response of meridional MSE transport to various climate forcings is nonlinear, and we cannot simply add and subtract the responses to individual climate forcings to predict the responses to combined forcings. The nonlinearity of the Clausius-Clapeyron equation is a likely source of these nonlinear responses.

In G1, poleward MSE transport decreases, but the poles are still warmed relative to the tropics. This implies that the residual polar amplification in G1 must be due to the differing spatial patterns of the opposing solar and CO_2 forcings, with the solar forcing being greater in absolute magnitude in the tropics, where there is more sunlight to reduce. Local radiative feedbacks such as the ice-albedo feedback cannot be responsible for the residual polar amplification because these can only amplify or dampen a temperature change, but cannot reverse its sign. Another possible explanation would be an increase in ocean heat transport; we have not calculated this explicitly, but Hong et al. (2017) found that the Atlantic Meridional Overturning Circulation, which transports heat to the Arctic, slightly weakens in G1. While they only looked at heat transport in the Atlantic, there is a net decrease in energy flux into the ocean in the tropics (see their Figure 4b), so there is no reason to expect an increase in poleward ocean heat transport. In addition, the poleward energy transport by the oceans is much less than that by the atmosphere at high latitudes (e.g. Hawcroft et al., 2017, Figure 6) , so small changes to it would not be expected to significantly affect the polar warming. This leaves the differing spatial patterns of the forcings as the only possible explanation for the polar warming and tropical cooling in G1.

The decrease in poleward MSE transport likely diminishes the polar warming in G1, relative to what would happen if forcings and feedbacks were allowed to operate locally but energy transport was fixed at piControl levels. It would be a useful avenue for future research to quantify the effect of reduced energy transport, as well as local feedbacks, on the polar warming in G1, similar to the study of Arctic amplification under global warming by Pithan and Mauritsen (2014). The reduction in poleward moisture transport may help explain the reduction in mid-latitude precipitation seen in Tilmes et al. (2013); quantifying this effect would also be a useful research direction.

2.2 Cross-equatorial energy transport and ITCZ shifts

Figure 4a shows the relationship between shifts in the ITCZ in G1 relative to piControl and changes in the transport of moist static energy across the equator. We define the position of the ITCZ as the latitude where half of the zonally integrated rainfall between 15°S and 15°N lies to the south and half lies to the north, following Hwang and Frierson (2010). In the multi-model mean, the ITCZ shifts northward by 0.14 degrees, but there is significant inter-model spread, ranging from -0.33 to 0.89 degrees. ~~These shifts~~ A multi-model mean northward ITCZ shift is consistent with the result of Viale and Merlis (2017) that the ITCZ shifts northward by a greater amount for a CO_2 increase than for solar constant increase in slab ocean aquaplanet GCM runs with a prescribed northward ocean heat transport that keeps the ITCZ in the northern hemisphere. However, caution must be taken in assuming that the results from CO_2 and solar forcing runs can be added linearly, for reasons discussed above. The ITCZ shifts in G1 are moderately anticorrelated with the change in cross-equatorial energy transport (correlation coefficient r = ~~-0.768~~ -0.77). Anticorrelation between these quantities is consistent with previous work (e.g. Frierson and Hwang, 2012;

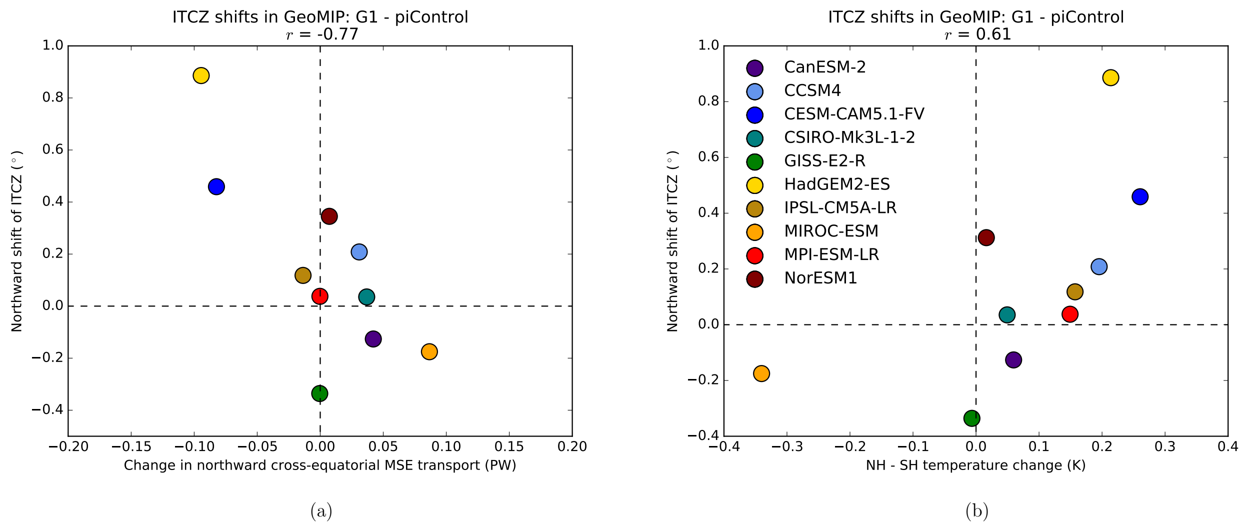

Figure 4. Shift in the ITCZ in GeoMIP models for G1 minus piControl, plotted against change in northward MSE transport across the equator (a) and northern hemisphere mean surface temperature change minus southern hemisphere mean temperature change (b). The quantity r is the correlation coefficient.

Hwang et al., 2013), and is expected because the Hadley cell transports energy primarily in its upper branch but moisture primarily in its lower branch.

For ITCZ shifts in abrupt4xCO2, however, there is no correlation between shifts in the precipitation-median ITCZ and cross-equatorial energy transport (r = ~~0.071~~0.07; not shown). ~~This may be due to changes in ocean heat storage and transport that occur following an abrupt quadrupling of CO_2, which creates a large TOA energy imbalance. The G1 experiment was designed to keep the top of atmosphere in approximate~~ There are several possible reasons for this, and for the fact that some models have close to zero change in cross-equatorial energy flux but nonzero ITCZ shifts in Figure 4a. First, the ITCZ is more closely connected to the "energy flux equator", or the latitude at which the meridional transport of energy by the atmosphere is zero, than it is to the cross-equatorial energy flux. Bischoff and Schneider (2014) developed a theory for the relationship between cross-equatorial energy transport and the energy flux equator, assuming the latter was correlated with the ITCZ position, and argued that while the energy flux equator is proportional to the cross-equatorial energy flux, the constant of proportionality is governed by the net energy input into the tropical atmosphere, which can allow the energy flux equator to move while cross-equatorial energy transport does not change. We might expect this effect to occur when the atmosphere is suddenly thrown far out of energy balance, ~~which limits changes in energy storage by the ocean~~as happens when CO_2 is abruptly quadrupled. Furthermore, the ITCZ, when defined as the precipitation median or maximum, does not necessarily always follow the energy flux equator, because the the gross moist stability, or the efficiency with which the Hadley circulation exports energy, can change (Seo et al., 2017) .

Figure 4b shows the ITCZ shifts in G1 plotted against the warming of the northern hemisphere relative to the southern hemisphere in the same experiment. This is similar to Figure 7 of Smyth et al. (2017), but for the specific set of models included in this study. Here, there is a positive correlation (r = ~~0.606~~0.61), slightly weaker than that for cross-equatorial MSE transport. ~~This corresponds to the idea that the ITCZ "shifts toward the warmed hemisphere". It implies~~ While Haywood et al. (2013) found ITCZ shifts away from the cooled hemisphere in the extreme case of aerosol injections in only one hemisphere, the ITCZ shifts in Figure 4b imply that solar reductions applied equally in both hemispheres could still cause regional shifts in precipitation based on factors like the base state albedo and local radiative feedbacks that might warm one hemisphere relative to the other. This, along with reductions in the seasonal ITCZ migration due to preferential cooling of the summer hemisphere, is discussed elsewhere (Smyth et al., 2017). Our focus here is on the reasons for the inter-model spread in the ITCZ shifts. These are more easily diagnosed using energy balance model attribution experiments aimed at understanding the causes for the changes in cross-equatorial energy flux.

3 Attribution of changes using a moist EBM

In order to investigate the causes of robust changes in meridional energy transport in the G1 experiment and the largest sources of inter-model spread, we ran attribution experiments in which we perturbed different forcing and feedback terms one at a time. These experiments involved the moist energy balance model (EBM) first used by Hwang and Frierson (2010). We used the GCM output to calculate the magnitude of various forcings and feedbacks, including the greenhouse and solar forcings and cloud, surface albedo and non-cloud atmosphere feedbacks, and we used the EBM to understand how atmospheric energy transport would respond to each forcing or feedback in isolation. The advantage of using a moist EBM over directly integrating the energy fluxes associated with each forcing or feedback is that it allows for a coupled response between the energy transport, local temperature, and longwave radiative cooling.

The EBM takes as input the zonal mean surface and TOA energy fluxes and the LW cloud radiative effect from each GCM, and calculates the outgoing longwave radiation (OLR) as a function of surface temperature based on a linear fit of the clear-sky OLR and surface temperature output from each GCM. The net atmospheric energy flux input term is perturbed to account for the influence of various individual forcings and feedbacks, while the intercept of the clear-sky OLR-surface temperature relationship is re-fit in the perturbation climates (G1 and abrupt4xCO2) to account for the enhanced greenhouse effect. Net vertical energy flux convergences at each latitude are balanced by meridional diffusion of MSE. We obtained a meridional energy transport estimate from the EBM by meridionally integrating this diffusion term. Several limitations of the EBM experiments must be noted. The approach of prescribing energy perturbations associated with feedbacks that are static in time does not take into account the interactions of different feedbacks with each other (analyzed by Feldl et al. (2017)) or changes in the feedbacks that arise from the changing energy transport (Merlis, 2014; Rose et al., 2014; Rose and Rayborn, 2016) . Also, changing the intercept of the OLR-temperature fit does not account for the nonuniformity of the CO_2 radiative forcing with latitude (Huang and Zhang, 2014) . Appendix B describes the methods for these experiments in more detail.

3.1 Comparison of EBM and GCM-derived energy transport

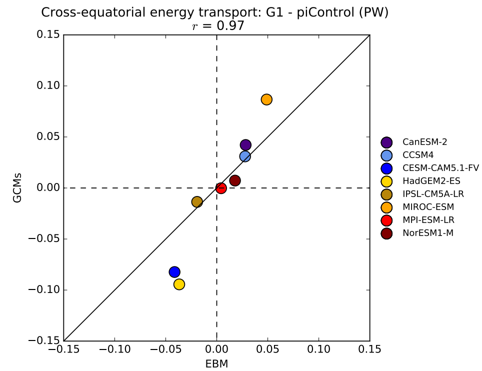

(a)

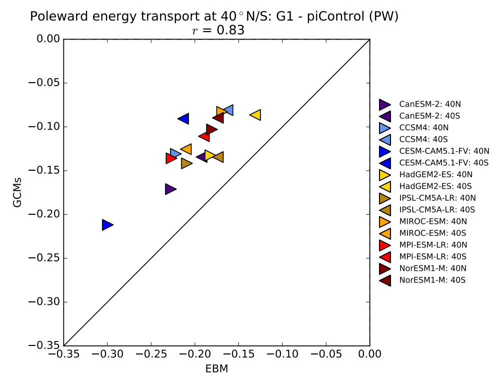

(b)

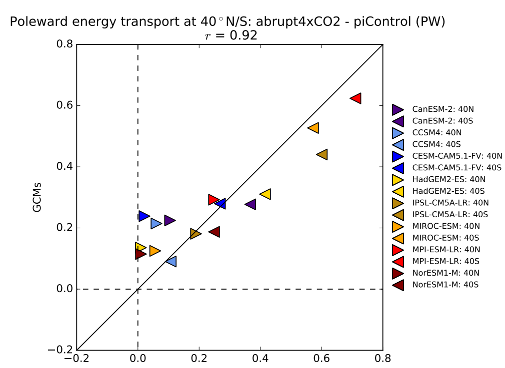

(c)

Figure 5. Meridional energy transport changes calculated by moist EBM (x-axis) versus those diagnosed from the GCM output (y-axis). (a): northward energy transport across the equator, for G1 minus piControl; (b): poleward energy transport changes across 40° N and S, for G1 minus piControl; (c): as in (b) but for abrupt4xCO2 minus piControl. Diagonal solid lines are 1:1 lines.

Table 2. Summary of attribution experiments run with moist energy balance model.

Name	Effects considered	OLR fit from
APRPcloud	SW radiative response at TOA due to cloud changes	piControl
APRPnoncloud	SW radiative response at TOA due to non-cloud atmosphere changes	piControl
APRPsurface	SW radiative response at TOA due to surface albedo changes	piControl
solarForcing	solar constant change (for G1), or nonlinear SW feedbacks (for abrupt4xCO2)	piControl
surfaceFlux	net SW, LW, sensible and latent heat flux changes at surface; *i.e.* surface energy storage	piControl
LWCRE	difference in net TOA LW radiation between clear-sky and all-sky conditions	piControl
greenhouse	enhanced greenhouse effect	G1 or abrupt4xCO2
all_G1	sum of effects listed in first 7 rows	G1
all_4xCO2	sum of effects listed in first 7 rows	abrupt4xCO2

The "OLR fit" refers to the fitting of coefficients for a linearized greenhouse effect based on surface air temperature and clear-sky OLR output from the GCMs; shown in the table is the GCM experiment from which these fits were drawn. Table 4 shows the actual fit coefficients.

In order to be helpful in understanding the causes of the GCM behaviors, the EBM needs to predict changes in GCM-derived energy fluxes reasonably well when all forcing and feedback terms are considered. Figure 5 shows the meridional MSE transport across specific latitudes calculated by the EBM versus the same quantities diagnosed directly from the output of each GCM, for cross-equatorial transport in G1 minus piControl (Figure 5a), for poleward transport across 40°N/S in G1 minus piControl (Figure 5b), and for the same comparison in abrupt4xCO2 minus piControl (Figure 5c). There are generally strong correlations in each of these cases. Cross-equatorial energy transport changes in abrupt4xCO2 minus piControl are not examined because these did not correlate well with ITCZ shifts. Note that, for G1 minus piControl, the cross-equatorial energy transport appears to change more easily in the GCMs than in the EBM, ~~and the intercept is nonzero in Figure 5c~~while the poleward energy transport across 40° N/S changes more in the EBM than in the GCMs. Also, for abrupt4xCO2 - piControl, the EBM tends to underestimate poleward energy transport changes in the Northern Hemisphere and overestimate them in the Southern Hemisphere. With these cautions in mind regarding the exact magnitude of the changes, the EBM predicts changes in GCM-derived energy fluxes well enough to proceed to the attribution experiments.

3.2 Attribution of cross-equatorial energy transport changes

The attribution experiments are summarized in Table 2. Two experiments, "all_G1" and "all_4xCO2", consider all of the forcing and feedback terms for the two perturbation climates. There are three experiments that perturb shortwave feedbacks, based on the Approximate Partial Radiation Perturbation (APRP) method (Taylor et al., 2007). APRP uses a single-layer radiative transfer model to estimate the TOA radiative response to changes in clouds, non-cloud atmospheric scattering and absorption, and surface albedo, based on monthly mean GCM cloud fraction output and SW radiative flux output at the surface and TOA. We refer to our SW feedback attribution experiments as the "APRPcloud", "APRPnoncloud", and "APRPsurface" experiments, which consider cloud, non-cloud atmosphere, and surface albedo feedbacks, respectively. The "solarForcing"

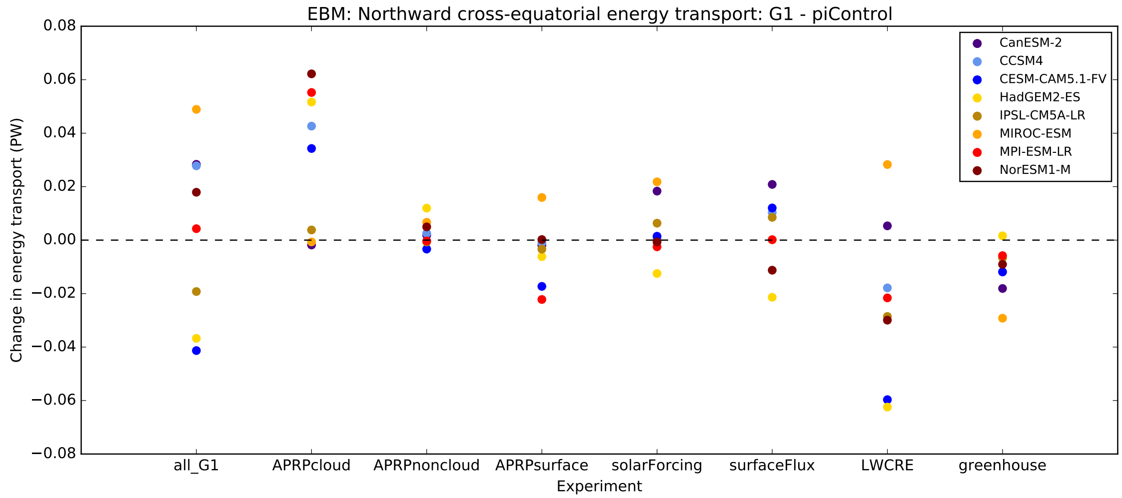

Figure 6. Changes in northward cross-equatorial energy transport calculated by moist EBM for G1 minus piControl in various attribution experiments.

experiment considers the change in insolation at the TOA due to the solar constant change. The "surfaceFlux" experiment considers the change in the net downward energy flux at the surface, which represents energy storage and transport by the ocean. The "LWCRE" experiment considers changes in the LW cloud radiative effect, or the difference between clear-sky and all-sky net TOA LW fluxes. Finally, the "greenhouse" experiment considers the enhanced clear-sky greenhouse effect, which includes the CO_2 forcing and the water vapor, Planck and lapse rate feedbacks. The calculations of the input terms for the EBM for each experiment are described in more detail in Appendix B.

Figure 6 shows the changes in northward energy transport across the equator for G1 minus piControl in each of the experiments listed in Table 2. The "all_G1" results are the same as those plotted on the x-axis on Figure 5a and show that there is considerable inter-model spread in the value of the cross-equatorial energy transport changes. None of the experiments shown in Figure 6 moves cross-equatorial energy transport in the same direction in all 8 models (although the APRPcloud ~~experiment comes~~ and greenhouse experiments come close), so we cannot say with much confidence that any one forcing or feedback is likely to push the ITCZ one way or the other under a solar geoengineering scenario. However, it is useful to examine the inter-model spread in each experiment in order to determine which terms cause the most uncertainty in response of the ITCZ to solar geoengineering.

The two attribution experiments with the largest inter-model spread are the APRPcloud and LWCRE experiments, which correspond to SW and LW cloud feedbacks. This indicates that changes in clouds are the largest source of uncertainty regarding how cross-equatorial energy transport and, therefore, the ITCZ would respond to a hemispherically symmetric solar geoengineering scenario. This is similar to the finding of Frierson and Hwang (2012) that cloud feedbacks are the largest source of uncertainty for cross-equatorial energy transport changes in slab ocean simulations of CO_2-induced warming.

~~The experiment with the next-largest~~ The APRPsurface, solarForcing, surfaceFlux, and greenhouse experiments have smaller inter-model ~~spread is surfaceFlux, indicating that the hemispheric asymmetry of the ocean heat uptake response to the combined solar and CO_2 forcings differs between the models. Solar forcing and surface albedo changes have smaller effects on~~ spread than the two cloud experiments but are similar to each other. The spread in the surfaceFlux experiment indicates different responses of the atmosphere in different models to changes in either heat storage or cross-equatorial energy transport ~~. The enhanced greenhouse effect, non-cloud atmospheric SW feedbacks, and solar forcing have the smallest effects on cross-equatorial energy transport. The impact of the solar forcing term depends on~~ by the ocean. The appreciable inter-model spread in the solarForcing experiment suggests that the base state ~~surface and atmospheric albedo , because a spatially uniform solar constant reduction will have different effects on net TOA insolation depending on what fraction of the solar radiation would have otherwise been reflected back to space had it not been reduced. Haywood et al. (2016) showed~~ inter-hemispheric albedo difference is an important factor in the ITCZ response to solar geoengineering and solar forcings in general. This is interesting in the light of the result of Haywood et al. (2016) that tropical precipitation in the HadGEM2-ES is highly sensitive to the difference in the mean albedo between the hemispheres, ~~but the small inter-model spread in the solarForcing experiment in Figure 6 suggests that the base state inter-hemispheric albedo difference is not the main source of inter-model spread in the ITCZ response to solar geoengineering~~and that equalizing them can improve GCM tropical precipitation biases.

3.3 Attribution of poleward energy transport changes

3.3.1 G1 minus piControl

Figure 7 shows the results of the same attribution experiments shown in Figure 6, but for poleward energy transport at 40° N (Figure 7a) and 40° S (Figure 7b). In the all_G1 experiment, poleward energy transport decreases at this latitude in both hemispheres. Poleward energy transport decreases in the solarForcing experiment for each model, and increases in the greenhouse experiment, but not by enough to compensate. The increase in poleward transport in the greenhouse experiment can be understood in terms of the increasing moisture transport argument discussed in Section 2 for the abrupt4xCO2 experiment. The ~~radiative forcing is roughly spatially uniform~~ CO_2 radiative forcing in the EBM is spatially uniform since OLR, in the initial perturbation, is reduced by the same amount everywhere (see Appendix B), but atmospheric moisture increases more in the tropics than at the poles because the atmosphere was warmer in the tropics to begin with. The reduction in tropical moisture in the solarForcing case is greater than the increase in the greenhouse case because there is more sunlight to reduce in the tropics, causing a greater ~~radiative~~ temperature perturbation there for solar reductions than for greenhouse gas increases. One caveat to this point is that in the actual atmosphere the CO_2 radiative forcing is stronger in the tropics than at the poles (although by as much as the solar forcing), which contributes to stronger poleward energy transport (Huang and Zhang, 2014) ; this mechanism for increased energy transport under greenhouse gas forcings is not captured by the EBM.

The APRPcloud experiment exhibits an increase in poleward energy transport in both hemispheres in all models, which is consistent with a decrease in low cloud cover causing heating in the tropics. Schmidt et al. (2012) noted that low cloud cover decreased in four GCMs running G1. A more detailed investigation of the cloud changes in the full G1 ensemble and their

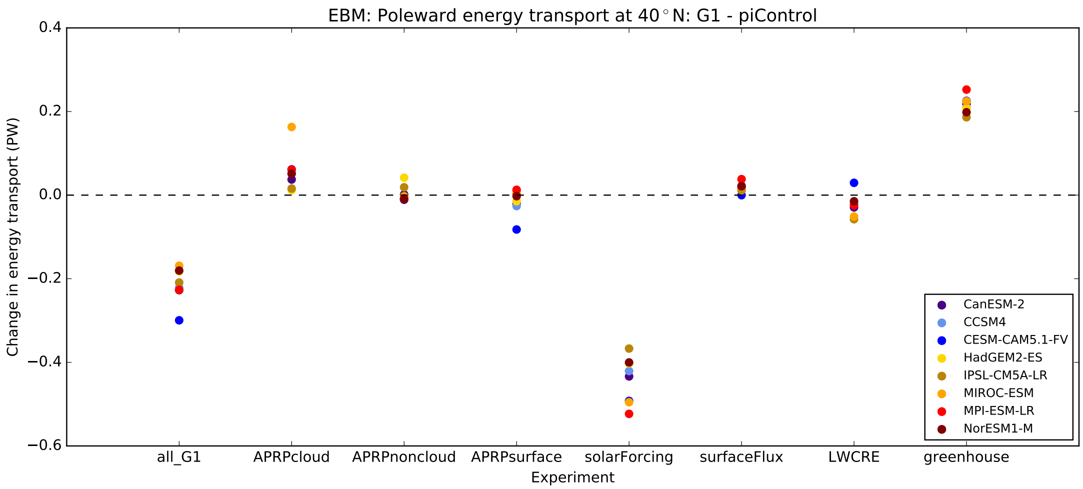

(a)

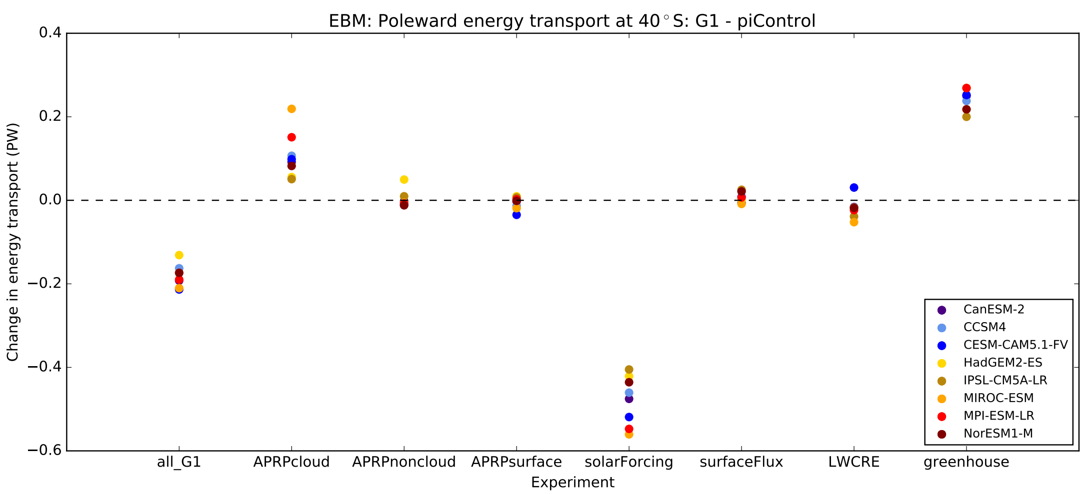

(b)

Figure 7. As in Figure 6 but for changes in poleward atmospheric energy transport across 40° N (a) and 40° S (b), for G1 minus piControl.

physical mechanisms and radiative effects will be the subject of a future study. None of the ~~various feedback experiments has~~ other feedback experiments have a consistent effect on ~~the sign of the change of~~ poleward energy transport ~~in both hemispheres~~across 40° N/S, but the different feedback terms appear to rearrange the models in the all_G1 experiment, and contribute to the inter-model spread, with SW cloud feedbacks being the largest contributor. Models with a greater negative change in the solarForcing experiment (e.g. MPI-ESM-LR) also tend to have a greater positive change in the greenhouse experiment, and the compensation between these effects tends to reduce the inter-model spread. This implies that the remaining inter-model spread comes from the feedback terms. The ~~lack of a reduction in poleward energy transport associated with the surfaceFlux experiment rules out changes in ocean heat transport as a reason for the reduction in poleward energy transport. The~~ fact that the solar forcing is the only term contributing to the reduction of poleward energy transport in G1 in all models implies that the imperfect compensation between SW and LW forcings, not local feedbacks, causes this reduction.

3.3.2 abrupt4xCO2 minus piControl

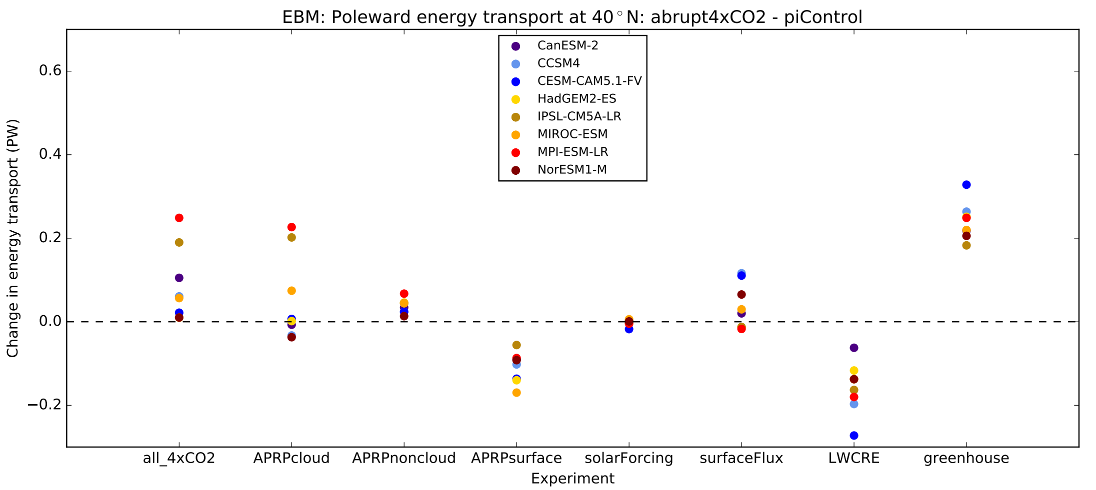

(a)

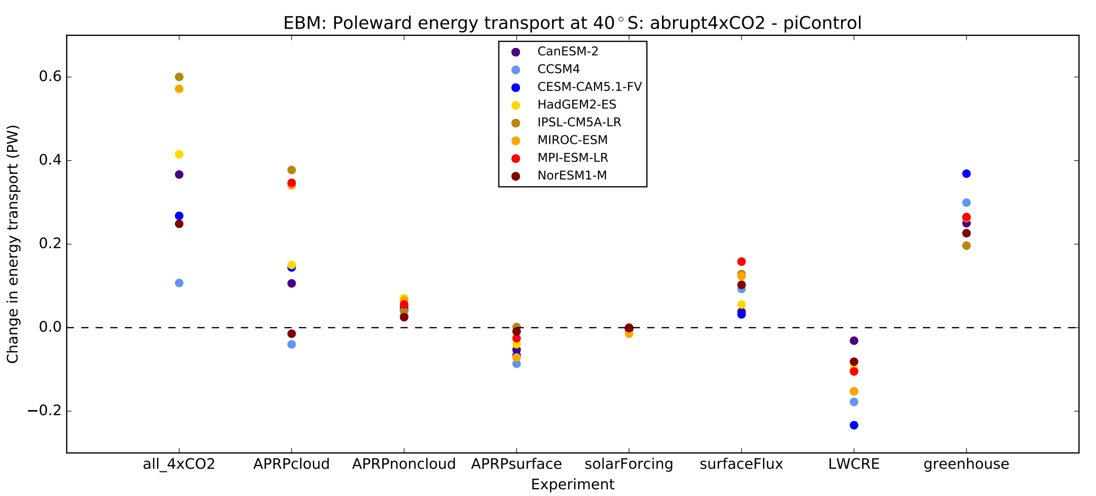

(b)

Figure 8. As in Figure 7 but for abrupt4xCO2 minus piControl.

Figure 8 is the equivalent of Figure 7, but for abrupt4xCO2 minus piControl. For abrupt4xCO2, the greenhouse attribution experiment results in an increase in poleward energy transport, similar to the same experiment for G1. SW cloud feedbacks (APRPcloud experiment) are the largest contributor to the inter-model spread, followed by LW cloud feedbacks. Surface albedo feedbacks (APRPsurface) also contribute to the inter-model spread, but generally reduce poleward energy transport. (The increase in moisture due to tropical warming that results in greater poleward energy transport in the ~~full abrupt4xCO2~~ all_4xCO2 experiment does not show up when only surface albedo is perturbed.) This feedback term is mainly due to ice melt at high latitudes, which would be expected to reduce the equator-to-pole temperature gradient and therefore also reduce poleward energy transport. The LWCRE experiment also reduces poleward energy transport for abrupt4xCO2, because the LW cloud feedback is positive at high latitudes due to an increase in the optical depth of high clouds (Zelinka et al., 2012). As with G1, non-cloud atmosphere SW feedbacks have small effects on the poleward energy transport for abrupt4xCO2, but there is a consistent increase in this case, presumably due to increases in SW absorption by water vapor. The solarForcing experiment in this case represents the residual between the total TOA net shortwave radiation changes and the individual feedback terms calculated using APRP; these effects are minor.

The surfaceFlux experiment has a much greater impact on poleward energy transport for abrupt4xCO2 than for G1, or for the 20th and 21st century CMIP3 runs analyzed by Hwang and Frierson (2010). This is because, while the TOA was kept approximately in energy balance in G1, and the imbalance is relatively small in 20th and 21st century runs, the abrupt4xCO2 case represents a response to an impulse that throws the climate system far out of equilibrium, with much energy being stored in the oceans over time. The ~~abrupt4xCO2 surfaceFlux experiment results in an increase in poleward atmospheric energy transport, which compensates for the energy lost~~ energy loss from the atmosphere to the ocean ~~at high latitudes.~~

~~The allEBM experiment shows a reduction in poleward energy transport for some models, especially at 40° N, whereas there is an increase in every model in the GCM output (See Figures 2a,d and 5c). Therefore, there must be a mechanism for increased poleward MSE transport at high latitudesthat is missed or underestimated by the EBM experiments, or a mechanism for decreased transport that is exaggerated by the EBM. Still, it is useful to see here that cloud feedbacks are significant contributors to the uncertainty in the poleward energy transport changes in abrupt4xCO2 as well as G1. The energy storage term contributes much more to this uncertainty in~~ is strongest in high latitudes, leading to a compensating increase in poleward atmospheric energy transport in the abrupt4xCO2 ~~, which is far out of equilibrium, than in G1, where the global mean energy balance at the TOA is approximately maintained~~surfaceFlux experiment.

4 Conclusions

Our analysis of the GeoMIP G1 ensemble shows that, when CO_2 concentrations are increased and the solar constant is reduced to compensate, poleward atmospheric energy transport decreases (Figures 1a,d). This is because of an increase in polar temperatures and decrease in tropical temperatures, or "residual polar amplification", that results from the different spatial patterns of the opposing solar and CO_2 forcings. The polar warming and tropical cooling cause a decrease in both dry static energy transport, which depends on the equator-to-pole temperature gradient, and latent heat transport, which depends on the meridional gradient of saturation vapor pressure. Residual polar amplification cannot be due to increases in poleward atmospheric energy transport, as might have been thought, because poleward energy transport actually decreases. It cannot be due to local feedbacks such as the ice-albedo feedback because these feedbacks cannot reverse the sign of an initial temperature change. Poleward energy transport by the ocean in the North Atlantic decreases (Hong et al., 2017) , and there is no reason to expect an increase in poleward energy transport by the ocean overall given the decrease in net energy flux into the ocean in the tropics. Instead, the spatial distribution of the combined CO_2 and solar forcing causes this pattern of temperature change, while the decrease in poleward energy transport then acts as a negative feedback that limits the polar warming in G1.

The reduction of poleward energy transport helps explain why the difference in temperature change in the poles and the tropics is not nearly as much in G1 as it is in abrupt4xCO2, or in other words, why solar geoengineering in the form of a uniform solar constant reduction manages to eliminate most (but not all) of the polar amplification of CO_2-induced warming. The role of moisture transport is critical here. When CO_2 is increased by itself, poleward latent heat transport increases because of the large increase in moisture in the tropics, and this amplifies polar warming. In the G1 scenario, by contrast, the cooling of the tropics reduces the amount of moisture in the air, lessening the energy transport to the poles. This indicates that tropical moisture content is a very important control on the meridional temperature gradient. Geoengineering schemes have been designed that, in GCMs, avoid the problem of over-cooling the tropics by preferentially reducing sunlight in high latitudes (Ban-Weiss and Caldeira, 2010; Kravitz et al., 2016). It would be useful to analyze the changes in atmospheric energy transport in these scenarios in order to better understand the role moisture transport would play in attempting to regulate temperatures in various latitudes.

Our EBM attribution experiments illustrate the specific forcings and feedbacks responsible for the changes in meridional energy transport in G1. The solar forcing causes a reduction in poleward energy transport in mid-latitudes; the enhanced greenhouse effect only partially counteracts this. Cloud feedbacks are generally the largest contributors to the inter-model spread in both mid-latitude poleward energy transport changes and cross-equatorial energy transport changes, which are a predictor of ITCZ shifts. The large uncertainty in these quantities associated with clouds implies that an improved physical understanding of the changes in clouds in G1 would help our understanding of how regional precipitation and temperature changes would play out under a solar geoengineering scenario. A more in-depth analysis of the cloud changes in the GeoMIP G1 ensemble will be the subject of a future study.

The finding that poleward atmospheric energy transport decreases in the G1 experiment relative to piControl is relevant for understanding why polar amplification of warming happens under increased CO_2. In warmer climates, the increased poleward energy transport contributes to the amount of polar amplification that occurs, as evidenced by model studies in which surface albedo is held constant (Alexeev et al., 2005; Graversen and Wang, 2009). However, our analysis of G1 shows that increases in poleward atmospheric energy transport are not necessary in order to have a decrease in the equator-to-pole temperature gradient. These results are particularly interesting in the light of the finding by Hwang et al. (2011) that polar amplification is actually negatively correlated with changes in atmospheric energy transport into the polar regions in CMIP3 global warming simulations. Our results reinforce the conclusion of Hwang et al. (2011) that changes in energy transport alone cannot predict changes in the meridional temperature gradient, which is actually governed by the coupling between energy transport and local feedbacks. It is useful to remember as well that radiative forcings are not spatially uniform, and the structure of the CO_2 forcing can affect atmospheric circulations in warming simulations ~~(Merlis, 2015)~~ (e.g. Huang and Zhang, 2014; Merlis, 2015) . The spatial structure of radiative forcing is part of the set of processes, including local feedbacks and energy transport by the atmosphere and ocean, that interactively determine the Earth's meridional temperature pattern. Due to the complexity of these interactions, changes in the temperature gradient cannot be quantitatively predicted without a general circulation model. To better understand these interactions, it would be useful to do further analysis to quantify the contributions of different local feedbacks to the amount of polar warming in the G1 experiment.

Appendix A: Details of GCM-derived energy transport calculations

Often, when calculating meridional energy transport based on a cumulative integration of energy flux convergence into the column from GCM output, there is a residual energy transport at the north pole, because the models' internal energy conservation involves terms that are not included in the reported fields energy flux fields, or else because the models used slightly different values of physical constants than we used in our diagnostics. For some models (CCSM4, CESM-CAM5.1-FV, GISS-E2-R, HadGEM2-ES, MIROC-ESM and NorESM1-M), this error can be reduced or nearly eliminated by adding $L_f P_{\mathrm{snow}}$ to the right side of Equation 1, where L_f is the latent heat of fusion of ice and P_{snow} is the mass flux of snowfall at the surface. This term accounts for the net energy flux into the atmosphere when snow crystals form in the atmosphere and then melt on land or in the ocean. (We also do this for the calculation of moisture transport in Eq. 2.) For the rest of the models, including this term increases the north pole residual, so we omitted it, assuming that this term had been already accounted for inside the latent heat flux output field. Omitting this term in the first set of models as well did not significantly affect our results.

To correct for any remaining energy flux residual, we subtract the following error function E from the northward energy transport profile:

$$E(\phi) = \frac{N}{2}\left(1 + \sin(\phi)\right) \tag{A1}$$

where ϕ is the latitude and N is the residual northward energy transport at the north pole. This correction function assumes that each unit area of Earth's surface contributes equally to the error. To demonstrate that the error is small, Table 3 shows the values of N in piControl and the change in N in the other 2 runs relative to piControl. The errors are generally small ($<$ .15 PW), except for MIROC-ESM, but even in this case the difference in the error between the runs is still small (all models have error $<$ .06 PW for G1 minus piControl, or .09 PW for abrupt4xCO2 minus piControl). Once the correction in Eq. (A1) is applied, the energy transport residual should only affect the results (in terms of differences between runs) if the errors are spatially nonuniform and the spatial pattern of the error differs between the runs. Since even the total error differences are small between runs, these residuals should not be a significant source of error in our analysis.

Table 3. Northward energy transport residual error at north pole in different models and runs, to 4 decimal places.

Model	N (piControl) (PW)	N (G1 - piControl) (PW)	N (abrupt4xCO2 - piControl) (PW)
CanESM-2	-0.0531	0.0411	0.0809
CCSM4	0.0162	-0.0025	0.0015
CESM-CAM5.1-FV	0.0172	-0.0138	0.0027
CSIRO-Mk3L-1-2	0.1429	-0.0093	0.0857
GISS-E2-R	0.0135	-0.0002	0.0033
HadGEM2-ES	-0.0270	0.0137	0.0164
IPSL-CM5A-LR	0.0373	-0.0549	0.0027
MIROC-ESM	-1.9135	0.0593	0.0734
MPI-ESM-LR	-0.1174	0.0526	-0.0515
NorESM1	0.0137	-0.00004	0.0027

Appendix B: Details of moist EBM calculations

We use the moist energy balance model first used in Hwang and Frierson (2010). Here we describe how the model works, with an emphasis on new changes made for the solar geoengineering experiments.

The core equation of the model, as in other energy balance models (e.g. North, 1975), is a heat diffusion equation:

$$\frac{\partial T_s}{\partial t} = C\left(\mathrm{EI} - \mathrm{OLR} + D\frac{p_s}{g}\frac{\partial^2 \mathrm{MSE}}{\partial x^2} D\nabla^2\mathrm{MSE}\right) \tag{B1}$$

or

$$\frac{\partial T_s}{\partial t} = C\left(\mathrm{EI} - \mathrm{OLR} + \frac{p_s}{g}\frac{D}{r^2}\frac{\partial}{\partial x}\left[(1-x^2)\frac{\partial \mathrm{MSE}}{\partial x}\right]\right), \tag{B2}$$

where MSE is the moist static energy, T_s is surface temperature, C is an arbitrary surface heat capacity, OLR is the outgoing longwave radiation at the top of the atmosphere, EI ("energy in") is the net surface and TOA energy flux into the atmospheric column excluding OLR, D is a diffusivity coefficient for MSE, p_s is the surface pressure, g is the acceleration due to gravity, and x is sine of latitude (the sine accounts for area weighting). r is the radius of the earth, and $x = \sin\theta$ where θ is the latitude. We have explicitly written out the r^2 that comes from the Laplacian operator in equation B2 rather than absorbing it into D as is often done (e.g. North, 1975) . Noting that $\mathrm{d}x = \cos\theta \mathrm{d}\theta$, equation B2 can also be written in terms of latitude, which is more convenient in terms of specifying inputs for EI as functions of latitude without converting to sine latitude first:

$$\frac{\partial T_s}{\partial t} = C\left(\mathrm{EI} - \mathrm{OLR} + \frac{p_s}{g}\frac{D}{r^2}\frac{\partial}{\cos\theta\partial\theta}\left[\cos\theta\frac{\partial \mathrm{MSE}}{\partial\theta}\right]\right). \tag{B3}$$

Table 4. Values of fit coefficients for clear-sky OLR as a function of temperature for use in moist EBM analysis.

Model	a (W m^{-2} K^{-1})	~~a' (G1) a' (abrupt4xCO2)~~ b (W m^{-2})	b' (G1)	b' (abrupt4xCO2)
CanESM-2	2.0667	~~1.9934 2.0139~~ 326.83	~~314.74~~ 334.99	~~320.04~~ 335.00
CCSM4	2.1604	~~2.0898 2.0946~~ 350.06	~~338.74~~ 358.31	~~341.84~~ 360.35
CESM-CAM5.1-FV	2.0724	~~1.9907 1.9837~~ 328.98	~~315.19~~ 337.74	~~316.62~~ 341.62
HadGEM2-ES	2.1531	~~2.0942 2.1200~~ 349.37	~~341.00~~ 357.38	~~349.61~~ 358.99
IPSL-CM5A-LR	2.2149	~~2.1429 2.1504~~ 363.39	~~350.70~~ 370.58	~~352.36~~ 370.46
MIROC-ESM	2.0512	~~1.9585 1.9732~~ 327.40	~~310.59~~ 336.37	~~313.99~~ 336.18
MPI-ESM-LR	2.0157	~~1.9284 1.9314~~ 315.55	~~300.22~~ 324.47	~~300.50~~ 324.34
NorESM1	2.1403	~~2.0665 2.1043~~ 346.36	~~333.94~~ 354.38	~~344.57~~ 354.68

We assume a value of 1.06×10^6 m^2 s^{-1} for D, following Hwang and Frierson (2010), and a flat topography with g = 9.8 m s^{-2} and p_s = 980 hPa. ~~Numerically, we use a 2nd-order finite difference for the 2nd derivative of MSE with respect to x, and~~ We step forward in time with a relative time step of $\frac{dt}{C} = 1 \times 10^{-4}$. The model is considered to have converged when T_s differs by less than .001 K everywhere in the domain between successive time steps.

The moist static energy is calculated according to:

$$\text{MSE} = C_p T_s + L_v q \tag{B4}$$

where C_p is the heat capacity of air at constant pressure, L_v is the latent heat of vaporization of water, and q is the specific humidity. We calculate q as a function of T_s using Equation 3, assuming a relative humidity of 80%.

The OLR is treated as a linear function of temperature:

$$\text{OLR} = aT_s - b \tag{B5}$$

where the coefficients a and b are calculated as linear least-squares fits from the monthly surface air temperature and clear-sky OLR output in each of the GCMs over the first 40 years of piControl. To consider the enhanced greenhouse effect in "perturbation" climates (G1 and abrupt4xCO2), we fit new coefficients ~~a' and~~ b', maintaining the original value of a (following Hwang and Frierson (2010)), based on the surface temperature and clear-sky OLR output in those experiments. ~~(Hwang and Frierson (2010) state that they only re-fit b' while keeping a the same, but this appears to be stated in error because when we did the "greenhouse" experiments this way, we found virtually no effect on the EBM results, in contrast to their Figure 4.)~~ Table 4 shows the values of a, b, ~~a'~~ and b' we calculated for each of the GCMs.

To run the EBM, we input the a and b coefficients shown in Table 4, and an EI term calculated differently for the different attribution experiments. For the EBM runs representing piControl conditions, we combine the following terms from the zonal mean output of each GCM:

$$\text{EI}_{\text{piControl}} = S - L_C + F_s \tag{B6}$$

where S is the net downward SW radiation at the TOA, L_C is the LW cloud radiative effect (clear-sky OLR minus all-sky OLR), and F_s is the net upward surface flux, including SW and LW radiation, sensible heat flux and latent heat flux.

For the "full" perturbation runs emulating the G1 and abrupt4xCO2 experiments, we use ~~a' and~~ b' instead of ~~a and~~ b for the OLR calculation, and the EI term is:

$$\mathrm{EI}_{\mathrm{perturb}} = \mathrm{EI}_{\mathrm{piControl}} + C_S + A_s + I + \Delta L_C + O + \Delta S \tag{B7}$$

where C_S, A_s and I are the change in the net downward TOA SW radiation associated with cloud, non-cloud atmosphere, and surface albedo feedbacks, respectively, calculated using the Approximate Partial Radiation Perturbation (APRP) method (Taylor et al., 2007); ΔL_C is the change in the LW cloud radiative effect in the GCM output; O is the change in the net surface flux in the GCM output; and ΔS is the change in the solar forcing. We calculate ΔS by taking the change in net TOA SW radiation between the control and perturbation climates, and subtracting C_S, A_s, and I to get the change in solar radiation that is not due to any of the three feedback terms. In G1 this represents the effect of changing the solar constant; in abrupt4xCO2 this represents a residual feedback not accounted for by a linear sum of the other 3 feedbacks.

For the individual attribution experiments (except "greenhouse"), we use ~~a and~~ b in the OLR calculation, and the EI terms are calculated as follows (experiment labels following Table 2):

$$\mathrm{EI}_{\mathrm{APRPcloud}} = \mathrm{EI}_{\mathrm{piControl}} + C_S \tag{B8}$$

$$\mathrm{EI}_{\mathrm{APRPnoncloud}} = \mathrm{EI}_{\mathrm{piControl}} + A_s \tag{B9}$$

$$\mathrm{EI}_{\mathrm{APRPsurface}} = \mathrm{EI}_{\mathrm{piControl}} + I \tag{B10}$$

$$\mathrm{EI}_{\mathrm{solarForcing}} = \mathrm{EI}_{\mathrm{piControl}} + \Delta S \tag{B11}$$

$$\mathrm{EI}_{\mathrm{surfaceFlux}} = \mathrm{EI}_{\mathrm{piControl}} + O \tag{B12}$$

$$\mathrm{EI}_{\mathrm{LWCRE}} = \mathrm{EI}_{\mathrm{piControl}} + \Delta L_C \tag{B13}$$

For the "greenhouse" experiment, we use the control value of EI, but use ~~a' and~~ b' instead of ~~a and~~ b for the OLR calculation.

The northward energy transport output by the EBM and shown in figures 6 through 8 is the cumulative meridional integration of the MSE diffusion term in Eq. (B2). The discretization of the diffusion equation for numerical solving inevitably results in some loss of energy, so after integrating, we apply a correction for residual northward transport at the North Pole for the EBM results, using Eq. (A1).

Author contributions. R.D. Russotto analyzed the GCM output, ran the EBM attribution experiments, produced the figures, and wrote the bulk of the paper. T.P. Ackerman provided general guidance and assisted with the preparation of the manuscript text.

Code availability All scripts used to analyze data and create plots are available here: atmos.washington.edu/articles/GeoMIP_EnergyTransport_PolarAmplification_ITCZ. A standalone Python code for the APRP method is available at: https://github.com/rdrussotto/pyAPRP.

Acknowledgements. This work was supported by the U.S. Department of Defense (DoD) through the National Defense Science and Engineering Graduate Fellowship (NDSEG) Program and by a grant to JISAO from the Fund for Innovative Climate and Energy Research. We thank Dargan Frierson for providing helpful guidance regarding the direction of this research, and Kyle Armour for pointing out a possible connection between decreased poleward moisture transport and reductions in mid-latitude precipitation. For their roles in producing, coordinating, and making available the CMIP5 and GeoMIP model output, we acknowledge the climate modeling groups (listed in Table 1 of this paper), the World Climate Research Programme's (WCRP) Working Group on Coupled Modelling (WGCM), and the Global Organization for Earth System Science Portals (GO-ESSP). We are grateful to Ben Kravitz, Helene Muri, Ulrike Niemeier, Stephen Phipps, and Jin-Ho Yoon for helping to provide access to GeoMIP output that was not yet available online; Phil Rasch, Balwinder Singh, and Ashly Spevacek for helpful discussions on technical issues with energy budgets in CMIP5 models; and Yen-Ting Hwang for providing us with codes for the APRP method and the moist EBM that formed the basis of this analysis. Two anonymous reviewers provided comments that greatly helped to improve the manuscript. We are particularly grateful to Reviewer 2 for their detailed commentary on the methodology of our EBM experiments. This led to us finding and fixing a major error in our implementation of the EBM.

References

Alexeev, V. A., Langen, P. L., and Bates, J. R.: Polar amplification of surface warming on an aquaplanet in "ghost forcing" experiments without sea ice feedbacks, Climate Dynamics, 24, 655–666, doi:10.1007/s00382-005-0018-3, http://dx.doi.org/10.1007/s00382-005-0018-3, 2005.

Arora, V. K., Scinocca, J. F., Boer, G. J., Christian, J. R., Denman, K. L., Flato, G. M., Kharin, V. V., Lee, W. G., and Merryfield, W. J.: Carbon emission limits required to satisfy future representative concentration pathways of greenhouse gases, Geophysical Research Letters, 38, L05805, doi:10.1029/2010GL046270, 2011.

Ban-Weiss, G. and Caldeira, K.: Geoengineering as an optimization problem, Environmental Research Letters, 5, 034009, doi:10.1088/1748-9326/5/3/034009, 2010.

Bekryaev, R. V., Polyakov, I. V., and Alexeev, V. A.: Role of Polar Amplification in Long-Term Surface Air Temperature Variations and Modern Arctic Warming, Journal of Climate, 23, 3888–3906, doi:10.1175/2010JCLI3297.1, 2010.

Bentsen, M., Bethke, I., Debernard, J. B., Iversen, T., Kirkevåg, A., Seland, Ø., Drange, H., Roelandt, C., Seierstad, I. A., Hoose, C., and Kristjánsson, J. E.: The Norwegian Earth System Model, NorESM1-M – Part 1: Description and basic evaluation of the physical climate, Geoscientific Model Development, 6, 687–720, doi:10.5194/gmd-6-687-2013, 2013.

Bischoff, T. and Schneider, T.: Energetic Constraints on the Position of the Intertropical Convergence Zone, Journal of Climate, 27, 4937–4951, doi:10.1175/JCLI-D-13-00650.1, 2014.

Broccoli, A. J., Dahl, K. A., and Stouffer, R. J.: Response of the ITCZ to Northern Hemisphere cooling, Geophysical Research Letters, 33, L01702, doi:10.1029/2005GL024546, 2006.

Chiang, J. C. H. and Bitz, C. M.: Influence of high latitude ice cover on the marine Intertropical Convergence Zone, Climate Dynamics, 25, 477–496, doi:10.1007/s00382-005-0040-5, 2005.

Collins, W. J., Bellouin, N., Doutriaux-Boucher, M., Gedney, N., Halloran, P., Hinton, T., Hughes, J., Jones, C. D., Joshi, M., Liddicoat, S., Martin, G., O'Connor, F., Rae, J., Senior, C., Sitch, S., Totterdell, I., Wiltshire, A., and Woodward, S.: Development and evaluation of an Earth-System model – HadGEM2, Geoscientific Model Development, 4, 1051–1075, doi:10.5194/gmd-4-1051-2011, 2011.

Dufresne, J.-L., Foujols, M.-A., Denvil, S., Caubel, A., Marti, O., Aumont, O., Balkanski, Y., Bekki, S., Bellenger, H., Benshila, R., Bony, S., Bopp, L., Braconnot, P., Brockmann, P., Cadule, P., Cheruy, F., Codron, F., Cozic, A., Cugnet, D., de Noblet, N., Duvel, J.-P., Ethé, C., Fairhead, L., Fichefet, T., Flavoni, S., Friedlingstein, P., Grandpeix, J.-Y., Guez, L., Guilyardi, E., Hauglustaine, D., Hourdin, F., Idelkadi, A., Ghattas, J., Joussaume, S., Kageyama, M., Krinner, G., Labetoulle, S., Lahellec, A., Lefebvre, M.-P., Lefevre, F., Levy, C., Li, Z. X., Lloyd, J., Lott, F., Madec, G., Mancip, M., Marchand, M., Masson, S., Meurdesoif, Y., Mignot, J., Musat, I., Parouty, S., Polcher, J., Rio, C., Schulz, M., Swingedouw, D., Szopa, S., Talandier, C., Terray, P., Viovy, N., and Vuichard, N.: Climate change projections using the IPSL-CM5 Earth System Model: from CMIP3 to CMIP5, Climate Dynamics, 40, 2123–2165, doi:10.1007/s00382-012-1636-1, 2013.

Feldl, N., Bordoni, S., and Merlis, T. M.: Coupled High-Latitude Climate Feedbacks and Their Impact on Atmospheric Heat Transport, Journal of Climate, 30, 189–201, doi:10.1175/JCLI-D-16-0324.1, 2017.

Ferraro, A. J. and Griffiths, H. G.: Quantifying the temperature-independent effect of stratospheric aerosol geoengineering on global-mean precipitation in a multi-model ensemble, Environmental Research Letters, 11, 034012, doi:10.1088/1748-9326/11/3/034012, 2016.

Frierson, D. M. W. and Hwang, Y.-T.: Extratropical Influence on ITCZ Shifts in Slab Ocean Simulations of Global Warming, Journal of Climate, 25, 720–733, doi:10.1175/JCLI-D-11-00116.1, 2012.

Gent, P. R., Danabasoglu, G., Donner, L. J., Holland, M. M., Hunke, E. C., Jayne, S. R., Lawrence, D. M., Neale, R. B., Rasch, P. J., Vertenstein, M., Worley, P. H., Yang, Z.-L., and Zhang, M.: The Community Climate System Model Version 4, Journal of Climate, 24, 4973–4991, doi:10.1175/2011JCLI4083.1, 2011.

Giorgetta, M. A., Jungclaus, J., Reick, C. H., Legutke, S., Bader, J., Böttinger, M., Brovkin, V., Crueger, T., Esch, M., Fieg, K., Glushak, K., Gayler, V., Haak, H., Hollweg, H.-D., Ilyina, T., Kinne, S., Kornblueh, L., Matei, D., Mauritsen, T., Mikolajewicz, U., Mueller, W., Notz, D., Pithan, F., Raddatz, T., Rast, S., Redler, R., Roeckner, E., Schmidt, H., Schnur, R., Segschneider, J., Six, K. D., Stockhause, M., Timmreck, C., Wegner, J., Widmann, H., Wieners, K.-H., Claussen, M., Marotzke, J., and Stevens, B.: Climate and carbon cycle changes from 1850 to 2100 in MPI-ESM simulations for the Coupled Model Intercomparison Project phase 5, Journal of Advances in Modeling Earth Systems, 5, 572–597, doi:10.1002/jame.20038, 2013.

Govindasamy, B. and Caldeira, K.: Geoengineering Earth's radiation balance to mitigate CO2-induced climate change, Geophysical Research Letters, 27, 2141–2144, doi:10.1029/1999GL006086, http://dx.doi.org/10.1029/1999GL006086, 2000.

Govindasamy, B., Caldeira, K., and Duffy, P.: Geoengineering Earth's radiation balance to mitigate climate change from a quadrupling of CO2, Global and Planetary Change, 37, 157 – 168, doi:http://dx.doi.org/10.1016/S0921-8181(02)00195-9, http://www.sciencedirect.com/science/article/pii/S0921818102001959, evaluation, Intercomparison and Application of Global Climate Models, 2003.

Graversen, R. G. and Wang, M.: Polar amplification in a coupled climate model with locked albedo, Climate Dynamics, 33, 629–643, doi:10.1007/s00382-009-0535-6, http://dx.doi.org/10.1007/s00382-009-0535-6, 2009.

Green, B. and Marshall, J.: Coupling of Trade Winds with Ocean Circulation Damps ITCZ Shifts, Journal of Climate, 30, 4395–4411, doi:10.1175/JCLI-D-16-0818.1, 2017.

Hartmann, D. L.: Global Physical Climatology, Elsevier, Amsterdam, Netherlands, 2nd edn., 2016.

Hawcroft, M., Haywood, J. M., Collins, M., Jones, A., Jones, A. C., and Stephens, G.: Southern Ocean albedo, inter-hemispheric energy transports and the double ITCZ: global impacts of biases in a coupled model, Climate Dynamics, 48, 2279–2295, doi:10.1007/s00382-016-3205-5, 2017.

Haywood, J. M., Jones, A., Bellouin, N., and Stephenson, D.: Asymmetric forcing from stratospheric aerosols impacts Sahelian rainfall, Nature Climate Change, 3, 660–665, doi:10.1038/NCLIMATE1857, 2013.

Haywood, J. M., Jones, A., Dunstone, N., Milton, S., Vellinga, M., Bodas-Salcedo, A., Hawcroft, M., Kravitz, B., Cole, J., Watanabe, S., and Stephens, G.: The impact of equilibrating hemispheric albedos on tropical performance in the HadGEM2-ES coupled climate model, Geophysical Research Letters, 43, 395–403, doi:10.1002/2015GL066903, http://dx.doi.org/10.1002/2015GL066903, 2015GL066903, 2016.

Held, I. M. and Soden, B. J.: Robust Responses of the Hydrological Cycle to Global Warming, Journal of Climate, 19, 5686–5699, doi:http://dx.doi.org/10.1175/JCLI3990.1, 2006.

Holland, M. M. and Bitz, C. M.: Polar amplification of climate change in coupled models, Climate Dynamics, 21, 221–232, doi:10.1007/s00382-003-0332-6, 2003.

Hong, Y., Moore, J. C., Jevrejeva, S., Ji, D., Phipps, S. J., Lenton, A., Tilmes, S., Watanabe, S., and Zhao, L.: Impact of the GeoMIP G1 sunshade geoengineering experiment on the Atlantic meridional overturning circulation, Enviornmental Research Letters, 12, 034009, doi:10.1088/1748-9326/aa5fb8, 2017.

Huang, Y. and Zhang, M.: The implication of radiative forcing and feedback for meridional energy transport, Geophysical Research Letters, 41, 1665–1672, doi:10.1002/2013GL059079, http://dx.doi.org/10.1002/2013GL059079, 2013GL059079, 2014.

Hurrell, J. W., Holland, M. M., Gent, P. R., Ghan, S., Kay, J. E., Kushner, P. J., Lamarque, J.-F., Large, W. G., Lawrence, D., Lindsay, K., Lipscomb, W. H., Long, M. C., Mahowald, N., Marsh, D. R., Neale, R. B., Rasch, P., Vavrus, S., Vertenstein, M., Bader, D., Collins, W. D., Hack, J. J., Kiehl, J., and Marshall, S.: The Community Earth System Model: A Framework for Collaborative Research, Bulletin of the American Meteorological Society, 94, 1339–1360, doi:10.1175/BAMS-D-12-00121.1, 2013.

Hwang, Y.-T. and Frierson, D. M. W.: Increasing atmospheric poleward energy transport with global warming, Geophysical Research Letters, 37, L24807, doi:10.1029/2010GL045440, 2010.

Hwang, Y.-T., Frierson, D. M. W., and Kay, J. E.: Coupling between Arctic feedbacks and changes in poleward energy transport, Geophysical Research Letters, 38, L17704, doi:10.1029/2011GL048546, 2011.

Hwang, Y.-T., Frierson, D. M. W., and Kang, S. M.: Anthropogenic sulfate aerosol and the southward shift of tropical precipitation in the late 20th century, Geophysical Research Letters, 40, 2845–2850, doi:10.1002/grl.50502, 2013.

Irvine, P. J., Ridgwell, A., and Lunt, D. J.: Assessing the regional disparities in geoengineering impacts, Geophysical Research Letters, 37, L18702, doi:10.1029/2010GL044447, 2010.

Kang, S. M., Held, I. M., Frierson, D. M. W., and Zhao, M.: The Response of the ITCZ to Extratropical Thermal Forcing: Idealized Slab-Ocean Experiments with a GCM, Journal of Climate, 21, 3521–3532, doi:10.1175/2007JCLI2146.1, 2008.

Kay, J. E., Wall, C., Yettella, V., Medeiros, B., Hannay, C., Caldwell, P., and Bitz, C.: Global Climate Impacts of Fixing the Southern Ocean Shortwave Radiation Bias in the Community Earth System Model (CESM), Journal of Climate, 29, 4617–4636, doi:10.1175/JCLI-D-15-0358.1, 2016.

Keith, D. W. and Dowlatabadi, H.: A serious look at geoengineering, Eos, Transactions American Geophysical Union, 73, 289–293, doi:10.1029/91EO00231, 1992.

Kravitz, B., Robock, A., Boucher, O., Schmidt, H., Taylor, K. E., Stenchikov, G., and Schulz, M.: The Geoengineering Model Intercomparison Project (GeoMIP), Atmospheric Science Letters, 12, 162–167, doi:10.1002/asl.316, 2011.

Kravitz, B., Caldeira, K., Boucher, O., Robock, A., Rasch, P. J., Alterskjær, K., Karam, D. B., Cole, J. N. S., Curry, C. L., Haywood, J. M., Irvine, P. J., Ji, D., Jones, A., Kristjánsson, J. E., Lunt, D. J., Moore, J. C., Niemeier, U., Schmidt, H., Schulz, M., Singh, B., Tilmes, S., Watanabe, S., Yang, S., and Yoon, J.-H.: Climate model response from the Geoengineering Model Intercomparison Project (GeoMIP), Journal of Geophysical Research: Atmospheres, 118, 8320–8332, doi:10.1002/jgrd.50646, 2013a.

Kravitz, B., Rasch, P. J., Forster, P. M., Andrews, T., Cole, J. N. S., Irvine, P. J., Ji, D., Kristjánsson, J. E., Moore, J. C., Muri, H., Niemeier, U., Robock, A., Singh, B., Tilmes, S., Watanabe, S., and Yoon, J.-H.: An energetic perspective on hydrological cycle changes in the Geoengineering Model Intercomparison Project, Journal of Geophysical Research: Atmospheres, 118, 13,087–13,102, doi:10.1002/2013JD020502, 2013b.

Kravitz, B., MacMartin, D., Wang, H., and Rasch, P.: Geoengineering as a design problem, Earth System Dynamics, 7, 469–497, doi:10.5194/esd-7-469-2016, 2016.

Laguë, M. M. and Swann, A. L. S.: Progressive Midlatitude Afforestation: Impacts on Clouds, Global Energy Transport, and Precipitation, Journal of Climate, 29, 5561–5573, doi:10.1175/JCLI-D-15-0748.1, 2016.

Merlis, T. M.: Interacting components of the top-of-atmosphere energy balance affect changes in regional surface temperature, Geophysical Research Letters, 41, 7291–7297, doi:10.1002/2014GL061700, http://dx.doi.org/10.1002/2014GL061700, 2014.

Merlis, T. M.: Direct weakening of tropical circulations from masked CO2 radiative forcing, Proceedings of the National Academy of Sciences, 112, 13 167–13 171, doi:10.1073/pnas.1508268112, http://www.pnas.org/content/112/43/13167.abstract, 2015.

Niemeier, U., Schmidt, H., Alterskjær, K., and Kristjánsson, J. E.: Solar irradiance reduction via climate engineering: Impact of different techniques on the energy balance and the hydrological cycle, Journal of Geophysical Research: Atmospheres, 118, 11,905–11,917, doi:10.1002/2013JD020445, 2013.

North, G. R.: Theory of Energy-Balance Climate Models, Journal of the Atmospheric Sciences, 32, 2033–2043, 1975.

Pendergrass, A. G. and Hartmann, D. L.: The Atmospheric Energy Constraint on Global-Mean Precipitaton Change, Journal of Climate, 27, 757–768, 2014.

Phipps, S. J., Rotstayn, L. D., Gordon, H. B., Roberts, J. L., Hirst, A. C., and Budd, W. F.: The CSIRO Mk3L climate system model version 1.0 – Part 1: Description and evaluation, Geoscientific Model Development, 4, 483–509, doi:10.5194/gmd-4-483-2011, 2011.

Pithan, F. and Mauritsen, T.: Arctic amplification dominated by temperature feedbacks in contemporary climate models, Nature Geoscience, 7, 181–184, doi:10.1038/ngeo2071, 2014.

Rose, B. E. J. and Rayborn, L.: The Effects of Ocean Heat Uptake on Transient Climate Sensitivity, Current Climate Change Reports, 2, 190–201, doi:10.1007/s40641-016-0048-4, 2016.

Rose, B. E. J., Armour, K. C., Battisti, D. S., Feldl, N., and Koll, D. D. B.: The dependence of transient climate sensitivity and radiative feedbacks on the spatial pattern of ocean heat uptake, Geophysical Research Letters, 41, 1071–1078, doi:10.1002/2013GL058955, http://dx.doi.org/10.1002/2013GL058955, 2014.

Schaller, N., Sedláček, J., and Knutti, R.: The asymmetry of the climate system's response to solar forcing changes and its implications for geoengineering scenarios, Journal of Geophysical Research: Atmospheres, 119, 5171–5184, doi:10.1002/2013JD021258, 2014.

Schmidt, G. A., Kelley, M., Nazarenko, L., Ruedy, R., Russell, G. L., Aleinov, I., Bauer, M., Bauer, S. E., Bhat, M. K., Bleck, R., Canuto, V., Chen, Y.-H., Cheng, Y., Clune, T. L., Del Genio, A., de Fainchtein, R., Faluvegi, G., Hansen, J. E., Healy, R. J., Kiang, N. Y., Koch, D., Lacis, A. A., LeGrande, A. N., Lerner, J., Lo, K. K., Matthews, E. E., Menon, S., Miller, R. L., Oinas, V., Oloso, A. O., Perlwitz, J. P., Puma, M. J., Putman, W. M., Rind, D., Romanou, A., Sato, M., Shindell, D. T., Sun, S., Syed, R. A., Tausnev, N., Tsigaridis, K., Unger, N., Voulgarakis, A., Yao, M.-S., and Zhang, J.: Configuration and assessment of the GISS ModelE2 contributions to the CMIP5 archive, Journal of Advances in Modeling Earth Systems, 6, 141–184, doi:10.1002/2013MS000265, 2014.

Schmidt, H., Alterskjær, K., Bou Karam, D., Boucher, O., Jones, A., Kristjánsson, J. E., Niemeier, U., Schulz, M., Aaheim, A., Benduhn, F., Lawrence, M., and Timmreck, C.: Solar irradiance reduction to counteract radiative forcing from a quadrupling of CO_2: climate responses simulated by four earth system models, Earth System Dynamics, 3, 63–78, doi:10.5194/esd-3-63-2012, 2012.

Seo, J., Kang, S. M., and Merlis, T. M.: A model intercomparison of the tropical precipitation response to a CO2 doubling in aquaplanet simulations, Geophysical Research Letters, 44, 993–1000, doi:10.1002/2016GL072347, 2016GL072347, 2017.

Smyth, J. E., Russotto, R. D., and Storelvmo, T.: Thermodynamic and dynamic responses of the hydrological cycle to solar dimming, Atmospheric Chemistry and Physics, pp. 1–17, doi:10.5194/acp-2016-886, http://www.atmos-chem-phys-discuss.net/acp-2016-886/, accepted article, 2017.

Swann, A. L. S., Fung, I. Y., and Chiang, J. C. H.: Mid-latitude afforestation shifts general circulation and tropical precipitation, Proceedings of the National Academy of Sciences, 109, 712–716, doi:10.1073/pnas.1116706108, 2012.

Taylor, K. E., Crucifix, M., Braconnot, P., Hewitt, C. D., Doutriaux, C., Broccoli, A. J., Mitchell, J. F. B., and Webb, M. J.: Estimating Shortwave Radiative Forcing and Response in Climate Models, Journal of Climate, 20, 2530–2543, doi:10.1175/JCLI4143.1, 2007.

Tilmes, S., Fasullo, J., Lamarque, J.-F., Marsh, D. R., Mills, M., Alterskjær, K., Muri, H., Kristjánsson, J. E., Boucher, O., Schulz, M., Cole, J. N. S., Curry, C. L., Jones, A., Haywood, J., Irvine, P. J., Ji, D., Moore, J. C., Karam, D. B., Kravitz, B., Rasch, P. J., Singh, B., Yoon, J.-H., Niemeier, U., Schmidt, H., Robock, A., Yang, S., and Watanabe, S.: The hydrological impact of geoengineering in the Geoengineering Model Intercomparison Project (GeoMIP), Journal of Geophysical Research: Atmospheres, 118, 11,036–11,058, doi:10.1002/jgrd.50868, 2013.

Viale, F. and Merlis, T. M.: Variations in tropical cyclone frequency response to solar and CO2 forcing in aquaplanet simulations, Journal of Advances in Modeling Earth Systems, 9, 4–18, doi:10.1002/2016MS000785, http://dx.doi.org/10.1002/2016MS000785, 2017.

Watanabe, S., Hajima, T., Sudo, K., Nagashima, T., Takemura, T., Okajima, H., Nozawa, T., Kawase, H., Abe, M., Yokohata, T., Ise, T., Sato, H., Kato, E., Takata, K., Emori, S., and Kawamiya, M.: MIROC-ESM 2010: model description and basic results of CMIP5-20C3M experiments, Geoscientific Model Development, 4, 845–872, doi:10.5194/gmd-4-845-2011, 2011.

Yoshimori, M. and Broccoli, A. J.: Equilibrium Response of an Atmosphere–Mixed Layer Ocean Model to Different Radiative Forcing Agents: Global and Zonal Mean Response, Journal of Climate, 21, 4399–4423, doi:10.1175/2008JCLI2172.1, 2008.

Zelinka, M. D., Klein, S. A., and Hartmann, D. L.: Computing and Partitioning Cloud Feedbacks Using Cloud Property Histograms. Part II: Attribution to Changes in Cloud Amount, Altitude, and Optical Depth, J. Climate, 25, 3736–3754, doi:10.1175/JCLI-D-11-00249.1, 2012.

Energy transport, polar amplification, and ITCZ shifts in the GeoMIP G1 ensemble

Rick D. Russotto[1] and Thomas P. Ackerman[1,2]

[1]Department of Atmospheric Sciences, University of Washington, Seattle, Washington, USA
[2]Joint Institute for the Study of the Atmosphere and Ocean, University of Washington, Seattle, Washington, USA

Correspondence to: Rick D. Russotto (russotto@uw.edu)

Abstract.

The polar amplification of warming and the ability of the inter-tropical convergence zone (ITCZ) to shift to the north or south are two very important problems in climate science. Examining these behaviors in global climate models (GCMs) running solar geoengineering experiments is helpful not only for predicting the effects of solar geoengineering, but also for understanding how these processes work under increased carbon dioxide (CO_2). Both polar amplification and ITCZ shifts are closely related to the meridional transport of moist static energy (MSE) by the atmosphere. This study examines changes in MSE transport in 10 fully coupled GCMs in Experiment G1 of the Geoengineering Model Intercomparison Project, in which the solar constant is reduced to compensate for the radiative forcing from abruptly quadrupled CO_2 concentrations. In G1, poleward MSE transport decreases relative to preindustrial conditions in all models, in contrast to the CMIP5 abrupt4xCO2 experiment, in which poleward MSE transport increases. We show that since poleward energy transport decreases rather than increasing, and local feedbacks cannot change the sign of an initial temperature change, the residual polar amplification in the G1 experiment must be due to the net positive forcing in the polar regions and net negative forcing in the tropics, which arises from the different spatial patterns of the simultaneously imposed solar and CO_2 forcings. However, the reduction in poleward energy transport likely plays a role in limiting the polar warming in G1. An attribution study with a moist energy balance model shows that cloud feedbacks are the largest source of uncertainty regarding changes in poleward energy transport in mid-latitudes in G1, as well as for changes in cross-equatorial energy transport, which are anticorrelated with ITCZ shifts.

1 Introduction

As solar geoengineering, or the artificial cooling of earth by reflecting sunlight, increasingly gains attention as part of a possible strategy to deal with the effects of climate change, two important issues are whether the polar amplification of CO_2-induced warming can be fully counteracted, and whether regional precipitation patterns will shift, exacerbating flooding in some areas and drought in others (e.g. Irvine et al., 2010). Polar amplification is the phenomenon in which the poles warm by more than the tropics when atmospheric CO_2 concentrations are increased. While the reasons for polar amplification are not yet completely understood, it has already been observed in the instrumental temperature record (*e.g.* Bekryaev et al., 2010) and is a robust behavior in climate models (*e.g.* Holland and Bitz, 2003). Since reflecting sunlight would affect the tropics more strongly than the poles, it has been hypothesized that it would reduce the meridional temperature gradient (e.g. Keith and Dowlatabadi, 1992), leading to tropical cooling and polar warming under the combined CO_2 and geoengineering forcings. We refer to this effect as "residual polar amplification". Early model simulations of solar geoengineering scenarios, involving a simultaneous CO_2 increase and solar constant decrease (Govindasamy and Caldeira, 2000; Govindasamy et al., 2003), found that the residual polar amplification was relatively small, with latitudinal temperature patterns looking much more like the preindustrial climate than the climate under increased CO_2 without geoengineering. However, some residual polar amplification still occurs as a robust feature of these types of model experiments (e.g. Kravitz et al., 2013a).

Questions about shifts in regional precipitation under solar geoengineering are motivated by evidence from paleoclimate data and climate model studies that if one hemisphere is preferentially warmed, the intertropical convergence zone (ITCZ) shifts toward that hemisphere (*e.g.* Broccoli et al., 2006). Model studies have shown that such an effect could occur for changes in many different variables that affect the inter-hemispheric albedo contrast, such as high-latitude ice cover (Chiang and Bitz, 2005), mid-latitude forest extent (Swann et al., 2012; Laguë and Swann, 2016), and tropospheric sulfate aerosol concentration (Hwang et al., 2013). In the context of solar geoengineering, Haywood et al. (2013) demonstrated that preferentially injecting reflective aerosols into one hemisphere shifts the ITCZ towards the other hemisphere, causing drought in some tropical areas. Even under a hemispherically symmetric solar geoengineering deployment, such as space-based mirrors (represented by a solar constant reduction), ITCZ shifts can still occur (Smyth et al., 2017).

Both polar amplification and ITCZ shifts are closely related to the meridional transport of energy by the atmosphere, which makes atmospheric energy transport an important aspect of the effects of solar geoengineering to study. The sensitivity of the ITCZ, in particular, to energy transport in the atmosphere and ocean in present and future climates has recently been a topic of great research interest. Studies with slab ocean models with imposed hemispherically asymmetric energy fluxes (e.g. Kang et al., 2008; Yoshimori and Broccoli, 2008) found that an anomalous Hadley circulation transports energy from the warmed hemisphere across the equator, shifting the ITCZ towards the warmed hemisphere (because moisture is transported by the lower branch of the Hadley cell, while energy is transported by the upper branch). However, later studies (e.g. Kay et al., 2016; Hawcroft et al., 2017) found that this effect is substantially weaker in GCM simulations that include a full ocean circulation coupled to the atmosphere. This is because an anomalous wind-driven ocean circulation develops in response to changes in the atmospheric Hadley circulation, allowing the ocean to do most of the work of transporting the excess energy in one hemisphere across the equator (Green and Marshall, 2017). Still, we can consider the ITCZ position in the framework of the atmosphere and take ocean heat transport and storage into account via surface energy fluxes.

This study builds off the methods of a particular set of studies of atmospheric energy transport in projects in which multiple global climate models (GCMs) were run for the same radiative forcing scenarios. Hwang and Frierson (2010) showed that poleward transport of atmospheric moist static energy (MSE) increases under increased CO_2 concentrations in Coupled Model Intercomparison Project, Phase 3 (CMIP3) models. They used a moist energy balance model (EBM) to attribute the change in MSE transport across 40° latitude to different forcing and feedback terms, and found that cloud feedbacks are responsible for most of the inter-model spread in this quantity. Hwang et al. (2011) found that poleward dry static energy (DSE) transport in mid-to-high latitudes decreases with warming due to the reduced equator-to-pole temperature gradient (since warming is amplified at the poles), but moisture transport increases due to the overall warming combined with the nonlinearity of the Clausius-Clapeyron equation and the increase in moisture transport is enough to lead to an increase in MSE transport overall. Frierson and Hwang (2012) found that shifts in the ITCZ with warming in the CMIP3 slab ocean ensemble are anticorrelated with changes in atmospheric energy transport across the equator, with cloud feedbacks again being the largest source of uncertainty.

The Geoengineering Model Intercomparison Project (GeoMIP) provides an opportunity to use similar methods to investigate how atmospheric energy transport may change under solar geoengineering conditions, which can help us understand the reasons for residual polar amplification and tropical precipitation shifts. We analyze the results of GeoMIP experiment G1 (Kravitz et al., 2011), in which the solar constant is reduced at the same time as the CO_2 concentration is quadrupled in order to maintain top of atmosphere (TOA) energy balance and therefore keep the global mean temperature approximately at preindustrial levels. For comparison, we also examine two CMIP5 model runs: piControl, a preindustrial run, and abrupt4xCO2, in which CO_2 is quadrupled but the solar constant remains the same.

GeoMIP has yielded insights into how temperature and precipitation patterns may change under solar geoengineering. Kravitz et al. (2013a) found that residual polar amplification occurs in all models running the G1 experiment. Global mean precipitation decreases in G1 because the reduction in solar radiative flux at the surface is primarily balanced by a reduction in evaporation (Kravitz et al., 2013b). The precipitation reduction is evident over monsoonal land regions, as well as in the global mean, and extreme precipitation events are reduced in G1, in contrast to an increase in abrupt4xCO2 (Tilmes et al., 2013).

Reducing the solar constant is an approximation of more realistic proposals for solar geoengineering, such as injecting aerosols into the stratosphere. One example of how the physics differs between these scenarios involves the magnitude of the reduction in global mean precipitation. Solar constant reduction experiments underestimate the precipitation reduction compared to model runs that increase the concentration of sulfate aerosols in the stratosphere (Niemeier et al., 2013; Ferraro and Griffiths, 2016). This is because sulfate aerosols absorb longwave radiation, which reduces the net atmospheric radiative cooling rate and therefore allows for less precipitation, since the latent heat release from precipitation formation must be balanced by net radiative cooling. (See, *e.g.*, Pendergrass and Hartmann (2014) for a discussion of the atmospheric energy constraints on global mean precipitation). Even with this caveat, the G1 experiment is useful because of its simplicity and because it eliminates confounding effects from global mean temperature changes.

We use the G1 experiment to investigate changes in meridional energy transport under solar geoengineering, the factors responsible for these changes, and the associated effects on tropical precipitation and polar amplification. Section 2 describes the energy and latent heat transport changes that occur in the G1 and abrupt4xCO2 experiments. Section 3 attributes these energy transport changes to different forcing and feedback terms, using the moist energy balance model (EBM) of Hwang and Frierson (2010). Conclusions are provided in Section 4.

2 Energy and moisture transport changes

Using the TOA and surface energy and moisture fluxes from the GeoMIP GCM experiments, we calculate changes in the meridional transport of MSE by the atmosphere. By subtracting the MSE transport in piControl from that in G1, we can understand how the combined CO_2 increase and solar constant decrease affect MSE transport, or, in other words, how well solar reductions can restore preindustrial patterns of atmospheric energy transport. For comparison, we also examine how the CO_2 increase alone affects MSE transport by subtracting the MSE transport in piControl from that in abrupt4xCO2. Following Kravitz et al. (2013a) and other papers analyzing GeoMIP results, we use the average of years 11-50 of the G1 and abrupt4xCO2 experiments in order to exclude the rapid changes that occur during the first few years. For piControl, we average over the first 40 years of model output provided by the modeling groups. (The period analyzed does not include any model spin-up period.) All averages are multi-annual means including all months.

We calculate the energy flux into the atmosphere from the GCM output as the sum of terms on the right-hand side of the following energy budget equation:

$$\nabla \cdot F_M = R^{\downarrow}_{\mathrm{net,TOA}} + R^{\uparrow}_{\mathrm{net,surface}} + \mathrm{SH} + \mathrm{LH} \tag{1}$$

where F_M is the vertically integrated horizontal moist static energy flux, $R^{\downarrow}_{\mathrm{net,TOA}}$ is the net downward radiative flux at the top of the atmosphere, $R^{\uparrow}_{\mathrm{net,surface}}$ is the net upward radiative flux at the surface, SH is the net upward surface sensible heat flux, and LH is the net upward surface latent heat flux. Since the net energy flux into the atmospheric column must be balanced by energy transport out of the column, we can calculate the northward atmospheric moist static energy transport as a function of latitude by integrating $\nabla \cdot F_M$, first zonally and then cumulatively northward from the south pole. It is also useful to decompose the MSE transport into latent energy (moisture) transport and dry static energy (DSE) transport, in order to identify how moisture changes affect the total energy transport changes, following the methodology of Hwang et al. (2011). We calculate the latent energy transport from the latent heat flux and precipitation GCM output by integrating the following equation zonally and meridionally:

$$\nabla \cdot F_L = \mathrm{LH} - L_v P \tag{2}$$

where F_L is the vertically integrated horizontal latent energy flux, L_v is the latent heat of vaporization of water and P is precipitation. We calculate the DSE transport by subtracting the latent energy transport from the MSE transport.

Table 1 lists the GeoMIP models included in this analysis. The models in this study all had solar constant reductions between 3.2% and 5.0% and global mean temperatures in G1 within 0.3 K of those in piControl. Three of the original 13 GeoMIP models are excluded: BNU-ESM, because it did not adequately restore the global mean temperature in the G1 realizations that were available when our analysis was done; EC-Earth, because the precipitation output file was corrupted; and HadCM3, because many of the output fields required for this study are no longer available. Methodological details of these calculations are described in Appendix A.

Table 1. Models included in this study, with references, institutions, solar constant reduction in the G1 experiment (ΔS_0), and global mean temperature change in G1 - piControl (ΔT).

Model	Reference	Institution	ΔS_0	ΔT (K)
CanESM-2	Arora et al. (2011)	Canadian Centre for Climate Modeling and Analysis	4.0%	-0.013
CCSM4	Gent et al. (2011)	National Center for Atmospheric Research	4.1%	0.233
CESM-CAM5.1-FV	Hurrell et al. (2013)	National Center for Atmospheric Research	4.7%	-0.157
CSIRO-Mk3L-1-2*	Phipps et al. (2011)	Commonwealth Scientific and Industrial Research Organization/ Bureau of Meteorology	3.2%	0.034
GISS-E2-R*	Schmidt et al. (2014)	NASA Goddard Institute for Space Studies	4.5%	-0.292
HadGEM2-ES	Collins et al. (2011)	Met Office Hadley Centre	3.9%	0.241
IPSL-CM5A-LR	Dufresne et al. (2013)	Institut Pierre Simon Laplace	3.5%	0.109
MIROC-ESM	Watanabe et al. (2011)	Atmosphere and Ocean Research Institute (The University of Tokyo), National Institute for Environmental Studies, and Japan Agency for Marine-Earth Science and Technology	5.0%	-0.065
MPI-ESM-LR	Giorgetta et al. (2013)	Max Planck Institute for Meteorology	4.7%	-0.011
NorESM1	Bentsen et al. (2013)	Bjerknes Centre for Climate Research, Norwegian Meteorological Institute	4.0%	-0.044

* These models are excluded from the second part of this study (the EBM analysis) because the necessary output fields were not archived.

2.1 Poleward transport in mid-latitudes

Changes in the zonal mean northward MSE, latent energy and dry static energy (DSE) transport for G1 minus piControl are shown in Figure 1. Poleward MSE transport in mid-latitudes is reduced under G1 in all 10 models and, when decomposed into the latent and DSE components, both of these terms are reduced as well. Figure 2 shows the same calculations for abrupt4xCO2 minus piControl. In this case, poleward DSE transport decreases but moisture transport increases by more than enough to compensate, leading to an increase in total MSE transport. This corroborates the result seen by Held and Soden (2006) and Hwang et al. (2011) in CMIP3 global warming scenarios.

To understand why the energy transport changes are different for global warming and geoengineering conditions, we look at zonal mean changes in temperature and saturation vapor pressure. Figures 3a,b show the zonal mean temperature change in G1 and abrupt4xCO2 relative to preindustrial. (These are also plotted in Figure 1 of Kravitz et al. (2013a), but our plots include only the models analyzed here and, for G1, we use a smaller y-axis range to show more detail.) In G1, the tropics are cooled while the poles are warmed (Figure 3a). There is warming everywhere in abrupt4xCO2 but more so in the polar regions, especially the Arctic (Figure 3b). In both cases, this pattern of temperature change results in a weakening of the equator-to-pole temperature gradient and reduces the poleward transport of dry static energy (Figures 1c,f and 2c,f), similar to the result found by Hwang et al. (2011).

G1 minus piControl (Figure 1)

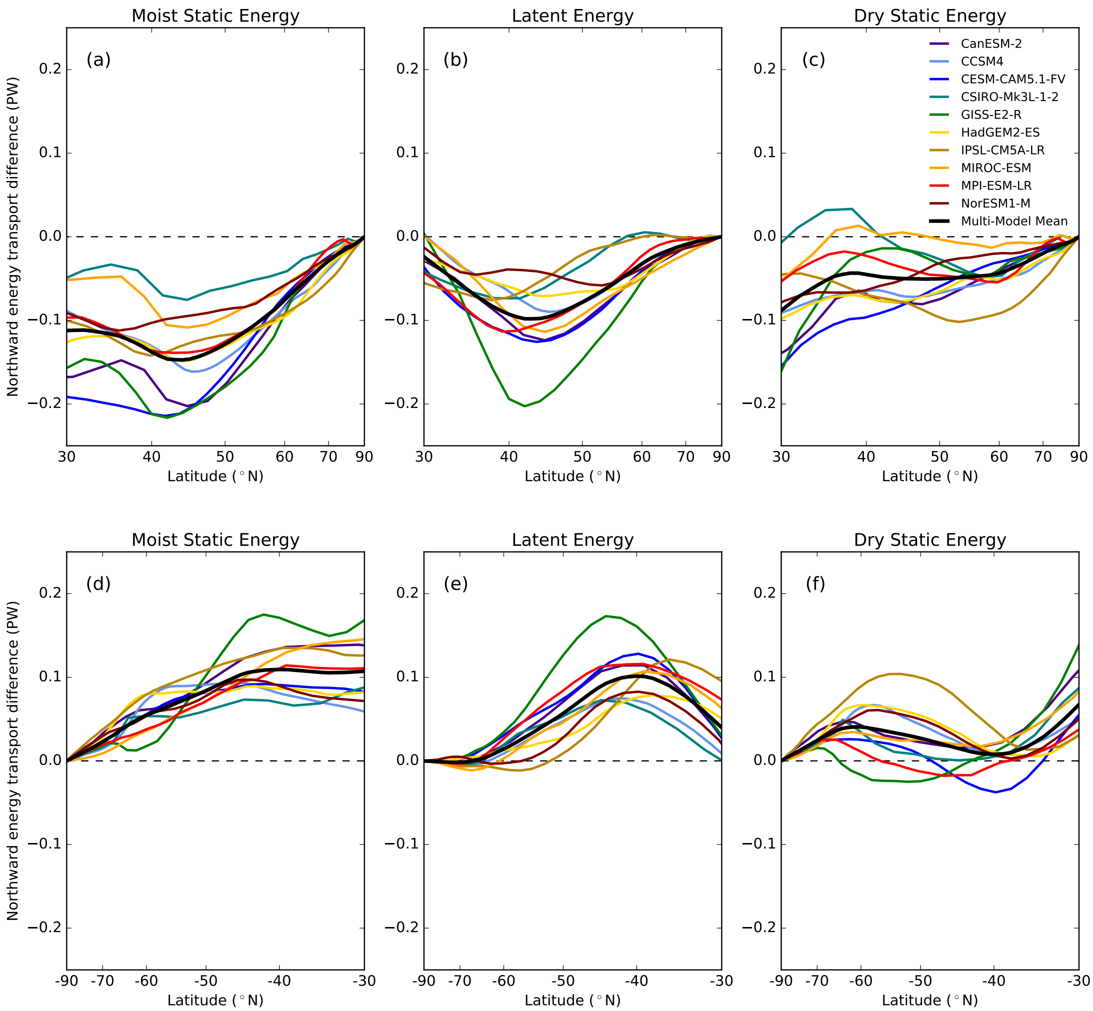

Figure 1. Northward energy transport (PW) for G1 minus piControl, poleward of 30° N (a-c) and 30° S (d-f), for total moist static energy transport (a, d), latent energy transport (b, e), and dry static energy transport (c, f), in the GeoMIP models and the multi-model mean.

The mechanism for the difference in moisture transport is apparent from changes in saturation vapor pressure, e_s, which we calculate using an approximate form of the Clausius-Clapeyron equation (*e.g.* Hartmann, 2016, eq. 1.11):

$$e_s = (6.11\text{hPa})\exp\left\{\frac{L_v}{R_v}\left(\frac{1}{273} - \frac{1}{T}\right)\right\} \quad (3)$$

where L_v is the latent heat of vaporization of water, R_v is the gas constant for water vapor, and T is the temperature in K. In abrupt4xCO2 (Figure 3d), e_s increases more in the tropics than it does near the poles because e_s is approximately

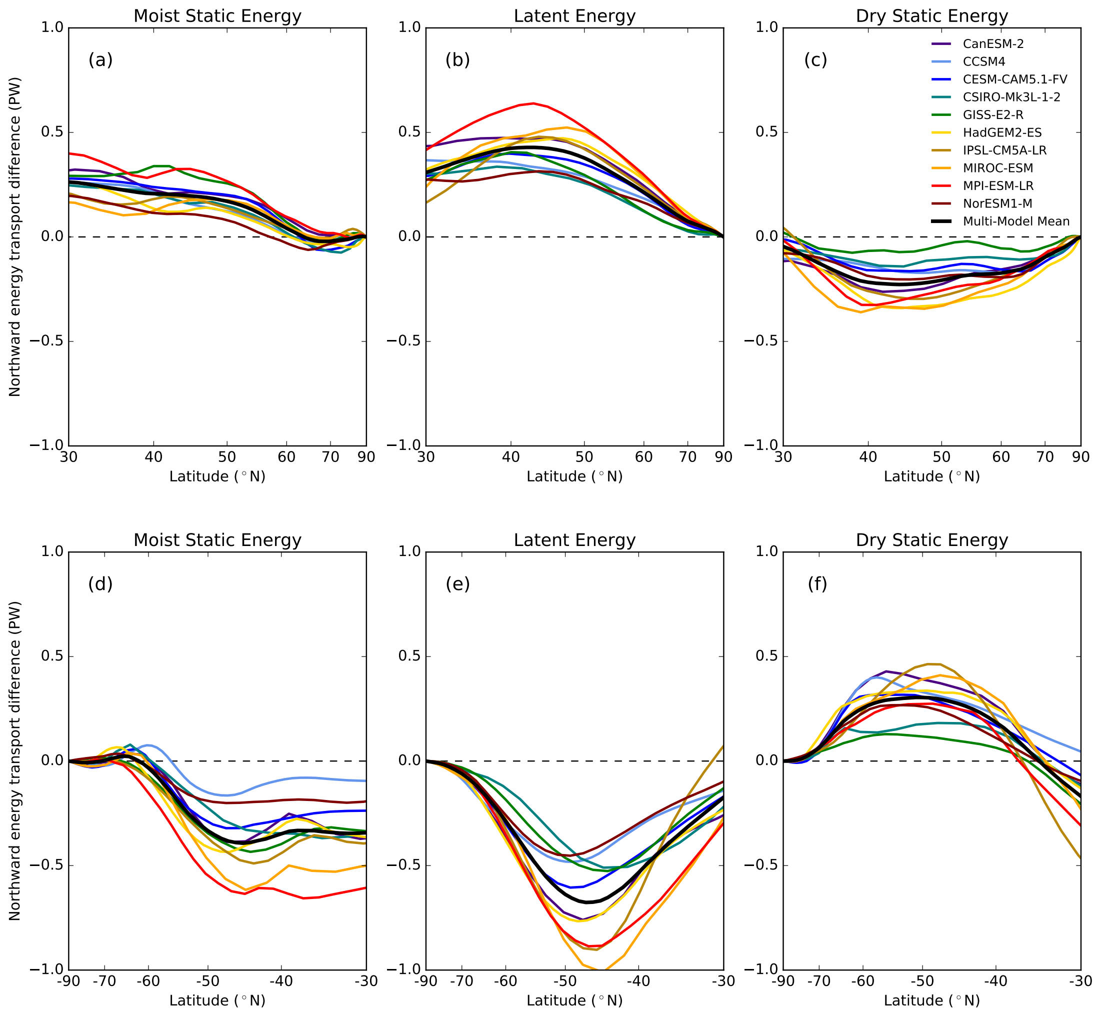

Figure 2. As in Figure 1 but for abrupt4xCO2 minus piControl.

exponential with respect to temperature. A slight warming in the tropics leads to a larger increase in e_s because the tropics were initially warmer than the poles. In G1, however (Figure 3c), the tropics cool and the poles warm, so saturation vapor pressure, like temperature, decreases in the tropics and increases (to a lesser extent) at high latitudes relative to piControl. Assuming the moisture content in the atmosphere scales with Clausius-Clapeyron, and the meridional winds are roughly the same, poleward moisture transport increases in abrupt4xCO2 and decreases in G1 because the equator-to-pole moisture gradient has strengthened in abrupt4xCO2 and weakened in G1.

A decrease in poleward energy transport has been previously reported in a single-model study running the G1 setup (Schaller et al., 2014). In addition to a G1 experiment, that study also included runs which included only the CO_2 increase or solar

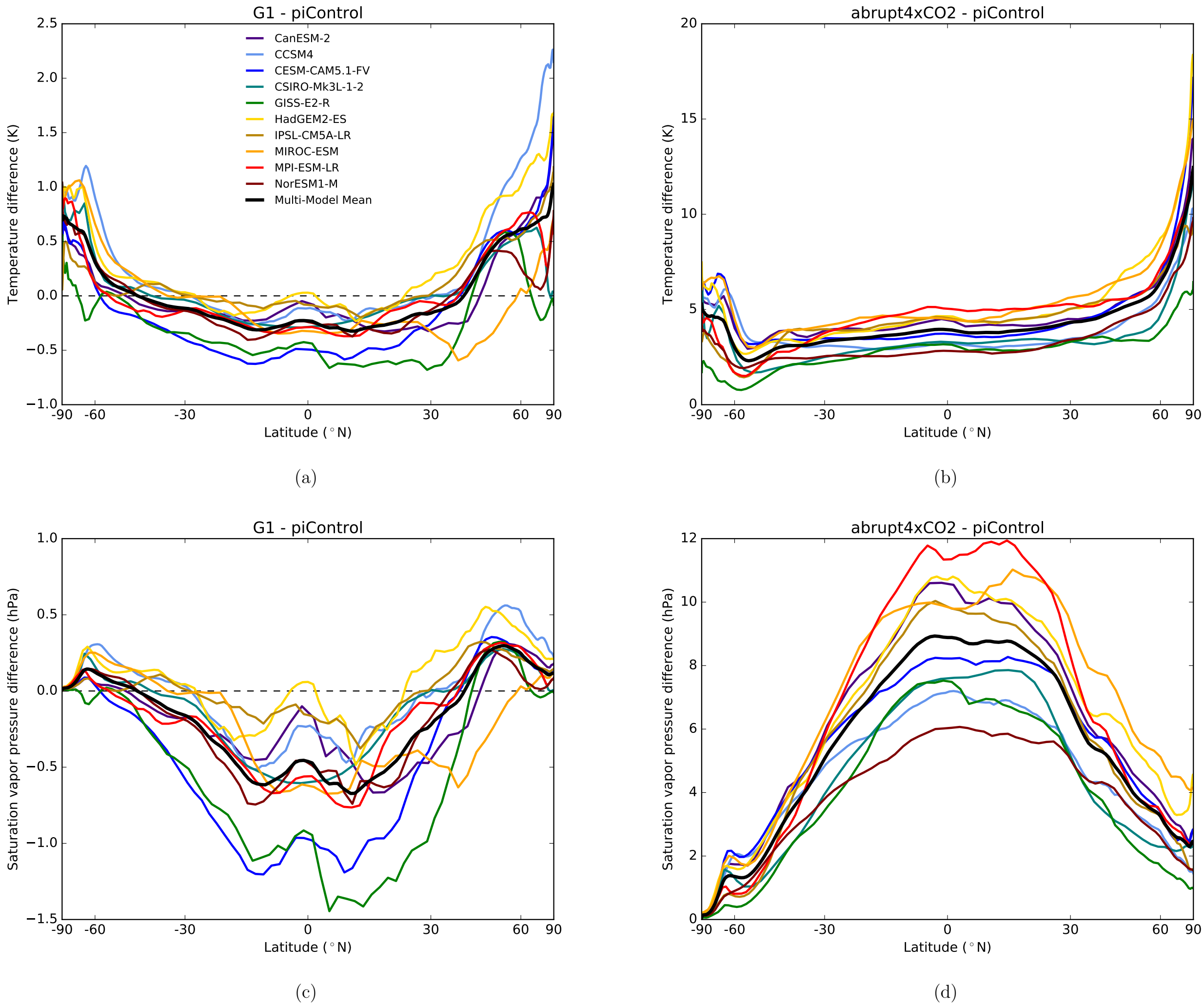

Figure 3. Zonal mean surface air temperature changes relative to piControl for G1 (a) and abrupt4xCO2 (b), and analogous zonal mean surface saturation vapor pressure changes (c,d), in GeoMIP models and multi-model mean.

constant decrease. The decrease in poleward energy transport in their G1 run is not equal to the sum of the increase in the "CO2+" run and the decrease in the "solar-" run in either hemisphere (see their Table 3). Also, the changes in poleward energy transport are not symmetrical in their solar increase and solar decrease run. This indicates that the response of meridional MSE transport to various climate forcings is nonlinear, and we cannot simply add and subtract the responses to individual climate forcings to predict the responses to combined forcings. The nonlinearity of the Clausius-Clapeyron equation is a likely source of these nonlinear responses.

In G1, poleward MSE transport decreases, but the poles are still warmed relative to the tropics. This implies that the residual polar amplification in G1 must be due to the differing spatial patterns of the opposing solar and CO_2 forcings, with the solar forcing being greater in absolute magnitude in the tropics, where there is more sunlight to reduce. Local radiative feedbacks such as the ice-albedo feedback cannot be responsible for the residual polar amplification because these can only amplify or dampen a temperature change, but cannot reverse its sign. Another possible explanation would be an increase in ocean heat transport; we have not calculated this explicitly, but Hong et al. (2017) found that the Atlantic Meridional Overturning Circulation, which transports heat to the Arctic, slightly weakens in G1. While they only looked at heat transport in the Atlantic, there is a net decrease in energy flux into the ocean in the tropics (see their Figure 4b), so there is no reason to expect an increase in poleward ocean heat transport. In addition, the poleward energy transport by the oceans is much less than that by the atmosphere at high latitudes (e.g. Hawcroft et al., 2017, Figure 6), so small changes to it would not be expected to significantly affect the polar warming. This leaves the differing spatial patterns of the forcings as the only possible explanation for the polar warming and tropical cooling in G1.

The decrease in poleward MSE transport likely diminishes the polar warming in G1, relative to what would happen if forcings and feedbacks were allowed to operate locally but energy transport was fixed at piControl levels. It would be a useful avenue for future research to quantify the effect of reduced energy transport, as well as local feedbacks, on the polar warming in G1, similar to the study of Arctic amplification under global warming by Pithan and Mauritsen (2014). The reduction in poleward moisture transport may help explain the reduction in mid-latitude precipitation seen in Tilmes et al. (2013); quantifying this effect would also be a useful research direction.

2.2 Cross-equatorial energy transport and ITCZ shifts

Figure 4a shows the relationship between shifts in the ITCZ in G1 relative to piControl and changes in the transport of moist static energy across the equator. We define the position of the ITCZ as the latitude where half of the zonally integrated rainfall between 15°S and 15°N lies to the south and half lies to the north, following Hwang and Frierson (2010). In the multi-model mean, the ITCZ shifts northward by 0.14 degrees, but there is significant inter-model spread, ranging from -0.33 to 0.89 degrees. A multi-model mean northward ITCZ shift is consistent with the result of Viale and Merlis (2017) that the ITCZ shifts northward by a greater amount for a CO_2 increase than for solar constant increase in slab ocean aquaplanet GCM runs with a prescribed northward ocean heat transport that keeps the ITCZ in the northern hemisphere. However, caution must be taken in assuming that the results from CO_2 and solar forcing runs can be added linearly, for reasons discussed above. The ITCZ shifts in G1 are moderately anticorrelated with the change in cross-equatorial energy transport (correlation coefficient r = -0.77). Anticorrelation between these quantities is consistent with previous work (e.g. Frierson and Hwang, 2012; Hwang et al., 2013), and is expected because the Hadley cell transports energy primarily in its upper branch but moisture primarily in its lower branch.

For ITCZ shifts in abrupt4xCO2, however, there is no correlation between shifts in the precipitation-median ITCZ and cross-equatorial energy transport (r = 0.07; not shown). There are several possible reasons for this, and for the fact that some models have close to zero change in cross-equatorial energy flux but nonzero ITCZ shifts in Figure 4a. First, the ITCZ is more closely

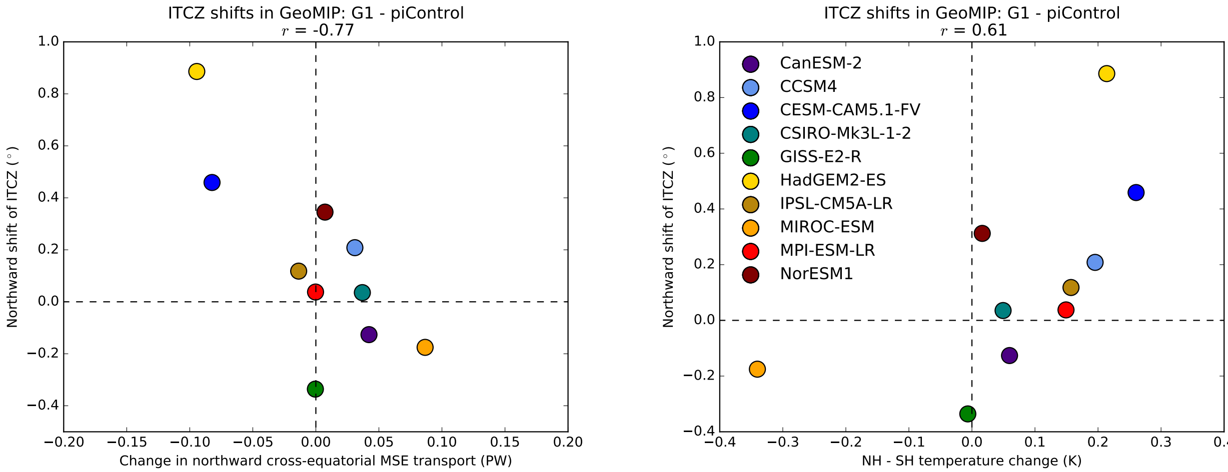

(a) (b)

Figure 4. Shift in the ITCZ in GeoMIP models for G1 minus piControl, plotted against change in northward MSE transport across the equator (a) and northern hemisphere mean surface temperature change minus southern hemisphere mean temperature change (b). The quantity r is the correlation coefficient.

connected to the “energy flux equator”, or the latitude at which the meridional transport of energy by the atmosphere is zero, than it is to the cross-equatorial energy flux. Bischoff and Schneider (2014) developed a theory for the relationship between cross-equatorial energy transport and the energy flux equator, assuming the latter was correlated with the ITCZ position, and argued that while the energy flux equator is proportional to the cross-equatorial energy flux, the constant of proportionality is governed by the net energy input into the tropical atmosphere, which can allow the energy flux equator to move while cross-equatorial energy transport does not change. We might expect this effect to occur when the atmosphere is suddenly thrown far out of energy balance, as happens when CO_2 is abruptly quadrupled. Furthermore, the ITCZ, when defined as the precipitation median or maximum, does not necessarily always follow the energy flux equator, because the the gross moist stability, or the efficiency with which the Hadley circulation exports energy, can change (Seo et al., 2017).

Figure 4b shows the ITCZ shifts in G1 plotted against the warming of the northern hemisphere relative to the southern hemisphere in the same experiment. This is similar to Figure 7 of Smyth et al. (2017), but for the specific set of models included in this study. Here, there is a positive correlation ($r = 0.61$), slightly weaker than that for cross-equatorial MSE transport. While Haywood et al. (2013) found ITCZ shifts away from the cooled hemisphere in the extreme case of aerosol injections in only one hemisphere, the ITCZ shifts in Figure 4b imply that solar reductions applied equally in both hemispheres could still cause regional shifts in precipitation based on factors like the base state albedo and local radiative feedbacks that might warm one hemisphere relative to the other. This, along with reductions in the seasonal ITCZ migration due to preferential cooling of the summer hemisphere, is discussed elsewhere (Smyth et al., 2017). Our focus here is on the reasons for the inter-model spread in the ITCZ shifts. These are more easily diagnosed using energy balance model attribution experiments aimed at understanding the causes for the changes in cross-equatorial energy flux.

3 Attribution of changes using a moist EBM

In order to investigate the causes of robust changes in meridional energy transport in the G1 experiment and the largest sources of inter-model spread, we ran attribution experiments in which we perturbed different forcing and feedback terms one at a time. These experiments involved the moist energy balance model (EBM) first used by Hwang and Frierson (2010). We used the GCM output to calculate the magnitude of various forcings and feedbacks, including the greenhouse and solar forcings and cloud, surface albedo and non-cloud atmosphere feedbacks, and we used the EBM to understand how atmospheric energy transport would respond to each forcing or feedback in isolation. The advantage of using a moist EBM over directly integrating the energy fluxes associated with each forcing or feedback is that it allows for a coupled response between the energy transport, local temperature, and longwave radiative cooling.

The EBM takes as input the zonal mean surface and TOA energy fluxes and the LW cloud radiative effect from each GCM, and calculates the outgoing longwave radiation (OLR) as a function of surface temperature based on a linear fit of the clear-sky OLR and surface temperature output from each GCM. The net atmospheric energy flux input term is perturbed to account for the influence of various individual forcings and feedbacks, while the intercept of the clear-sky OLR-surface temperature relationship is re-fit in the perturbation climates (G1 and abrupt4xCO2) to account for the enhanced greenhouse effect. Net vertical energy flux convergences at each latitude are balanced by meridional diffusion of MSE. We obtained a meridional energy transport estimate from the EBM by meridionally integrating this diffusion term. Several limitations of the EBM experiments must be noted. The approach of prescribing energy perturbations associated with feedbacks that are static in time does not take into account the interactions of different feedbacks with each other (analyzed by Feldl et al. (2017)) or changes in the feedbacks that arise from the changing energy transport (Merlis, 2014; Rose et al., 2014; Rose and Rayborn, 2016). Also, changing the intercept of the OLR-temperature fit does not account for the nonuniformity of the CO_2 radiative forcing with latitude (Huang and Zhang, 2014). Appendix B describes the methods for these experiments in more detail.

3.1 Comparison of EBM and GCM-derived energy transport

In order to be helpful in understanding the causes of the GCM behaviors, the EBM needs to predict changes in GCM-derived energy fluxes reasonably well when all forcing and feedback terms are considered. Figure 5 shows the meridional MSE transport across specific latitudes calculated by the EBM versus the same quantities diagnosed directly from the output of each GCM, for cross-equatorial transport in G1 minus piControl (Figure 5a), for poleward transport across 40°N/S in G1 minus piControl (Figure 5b), and for the same comparison in abrupt4xCO2 minus piControl (Figure 5c). There are generally strong correlations in each of these cases. Cross-equatorial energy transport changes in abrupt4xCO2 minus piControl are not examined because these did not correlate well with ITCZ shifts. Note that, for G1 minus piControl, the cross-equatorial energy transport appears to change more easily in the GCMs than in the EBM, while the poleward energy transport across 40° N/S

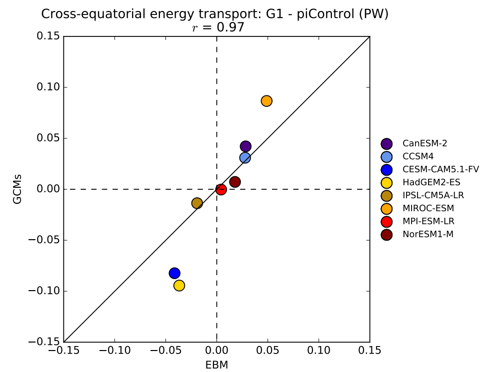

(a)

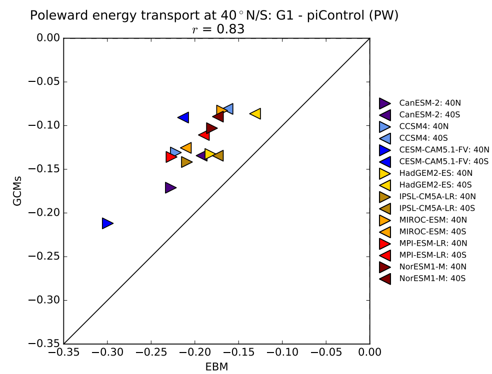

(b)

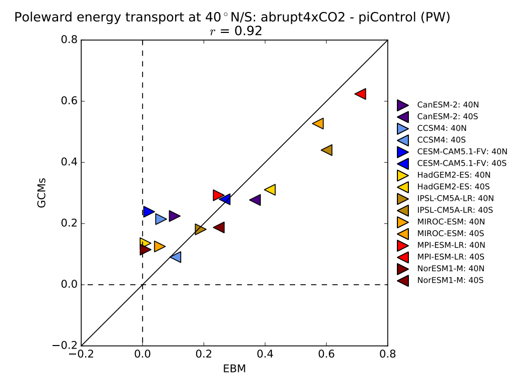

(c)

Figure 5. Meridional energy transport changes calculated by moist EBM (x-axis) versus those diagnosed from the GCM output (y-axis). (a): northward energy transport across the equator, for G1 minus piControl; (b): poleward energy transport changes across 40° N and S, for G1 minus piControl; (c): as in (b) but for abrupt4xCO2 minus piControl. Diagonal solid lines are 1:1 lines.

Table 2. Summary of attribution experiments run with moist energy balance model.

Name	Effects considered	OLR fit from
APRPcloud	SW radiative response at TOA due to cloud changes	piControl
APRPnoncloud	SW radiative response at TOA due to non-cloud atmosphere changes	piControl
APRPsurface	SW radiative response at TOA due to surface albedo changes	piControl
solarForcing	solar constant change (for G1), or nonlinear SW feedbacks (for abrupt4xCO2)	piControl
surfaceFlux	net SW, LW, sensible and latent heat flux changes at surface; *i.e.* surface energy storage	piControl
LWCRE	difference in net TOA LW radiation between clear-sky and all-sky conditions	piControl
greenhouse	enhanced greenhouse effect	G1 or abrupt4xCO2
all_G1	sum of effects listed in first 7 rows	G1
all_4xCO2	sum of effects listed in first 7 rows	abrupt4xCO2

The "OLR fit" refers to the fitting of coefficients for a linearized greenhouse effect based on surface air temperature and clear-sky OLR output from the GCMs; shown in the table is the GCM experiment from which these fits were drawn. Table 4 shows the actual fit coefficients.

changes more in the EBM than in the GCMs. Also, for abrupt4xCO2 - piControl, the EBM tends to underestimate poleward energy transport changes in the Northern Hemisphere and overestimate them in the Southern Hemisphere. With these cautions in mind regarding the exact magnitude of the changes, the EBM predicts changes in GCM-derived energy fluxes well enough to proceed to the attribution experiments.

3.2 Attribution of cross-equatorial energy transport changes

The attribution experiments are summarized in Table 2. Two experiments, "all_G1" and "all_4xCO2", consider all of the forcing and feedback terms for the two perturbation climates. There are three experiments that perturb shortwave feedbacks, based on the Approximate Partial Radiation Perturbation (APRP) method (Taylor et al., 2007). APRP uses a single-layer radiative transfer model to estimate the TOA radiative response to changes in clouds, non-cloud atmospheric scattering and absorption, and surface albedo, based on monthly mean GCM cloud fraction output and SW radiative flux output at the surface and TOA. We refer to our SW feedback attribution experiments as the "APRPcloud", "APRPnoncloud", and "APRPsurface" experiments, which consider cloud, non-cloud atmosphere, and surface albedo feedbacks, respectively. The "solarForcing" experiment considers the change in insolation at the TOA due to the solar constant change. The "surfaceFlux" experiment considers the change in the net downward energy flux at the surface, which represents energy storage and transport by the ocean. The "LWCRE" experiment considers changes in the LW cloud radiative effect, or the difference between clear-sky and all-sky net TOA LW fluxes. Finally, the "greenhouse" experiment considers the enhanced clear-sky greenhouse effect, which includes the CO_2 forcing and the water vapor, Planck and lapse rate feedbacks. The calculations of the input terms for the EBM for each experiment are described in more detail in Appendix B.

Figure 6 shows the changes in northward energy transport across the equator for G1 minus piControl in each of the experiments listed in Table 2. The "all_G1" results are the same as those plotted on the x-axis on Figure 5a and show that there is

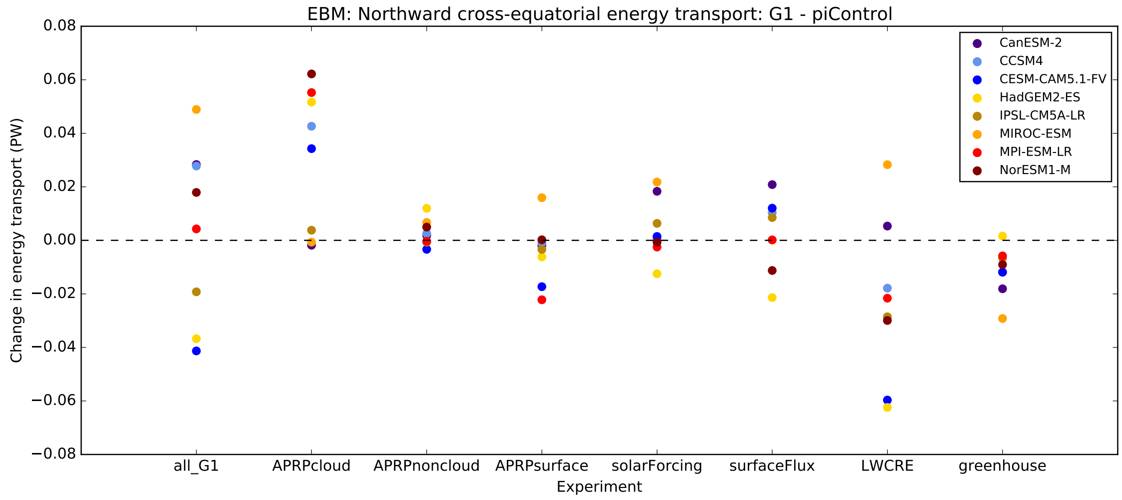

Figure 6. Changes in northward cross-equatorial energy transport calculated by moist EBM for G1 minus piControl in various attribution experiments.

considerable inter-model spread in the value of the cross-equatorial energy transport changes. None of the experiments shown in Figure 6 moves cross-equatorial energy transport in the same direction in all 8 models (although the APRPcloud and greenhouse experiments come close), so we cannot say with much confidence that any one forcing or feedback is likely to push the ITCZ one way or the other under a solar geoengineering scenario. However, it is useful to examine the inter-model spread in each experiment in order to determine which terms cause the most uncertainty in response of the ITCZ to solar geoengineering.

The two attribution experiments with the largest inter-model spread are the APRPcloud and LWCRE experiments, which correspond to SW and LW cloud feedbacks. This indicates that changes in clouds are the largest source of uncertainty regarding how cross-equatorial energy transport and, therefore, the ITCZ would respond to a hemispherically symmetric solar geoengineering scenario. This is similar to the finding of Frierson and Hwang (2012) that cloud feedbacks are the largest source of uncertainty for cross-equatorial energy transport changes in slab ocean simulations of CO_2-induced warming.

The APRPsurface, solarForcing, surfaceFlux, and greenhouse experiments have smaller inter-model spread than the two cloud experiments but are similar to each other. The spread in the surfaceFlux experiment indicates different responses of the atmosphere in different models to changes in either heat storage or cross-equatorial energy transport by the ocean. The appreciable inter-model spread in the solarForcing experiment suggests that the base state inter-hemispheric albedo difference is an important factor in the ITCZ response to solar geoengineering and solar forcings in general. This is interesting in the light of the result of Haywood et al. (2016) that tropical precipitation in the HadGEM2-ES is highly sensitive to the difference in the mean albedo between the hemispheres, and that equalizing them can improve GCM tropical precipitation biases.

3.3 Attribution of poleward energy transport changes

3.3.1 G1 minus piControl

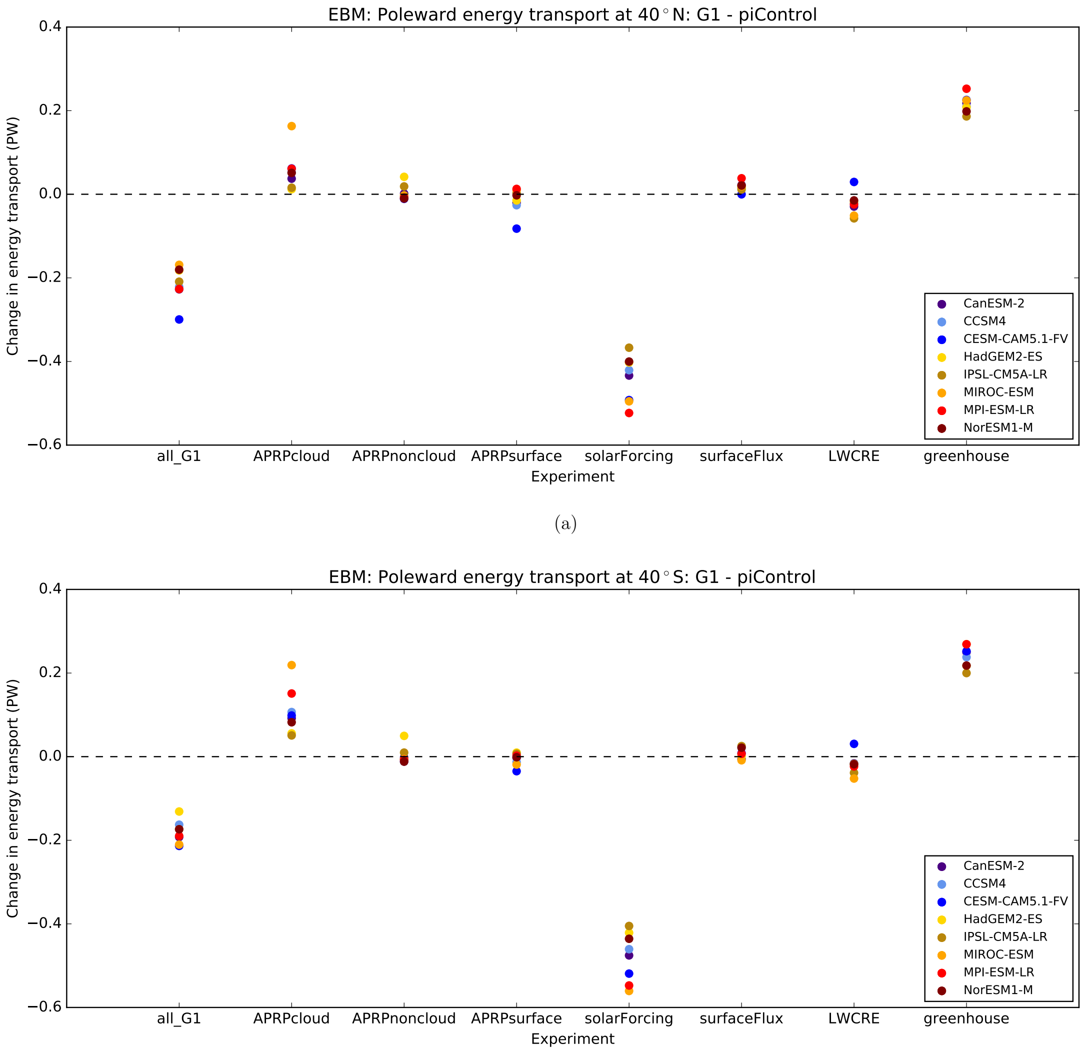

Figure 7. As in Figure 6 but for changes in poleward atmospheric energy transport across 40° N (a) and 40° S (b), for G1 minus piControl.

Figure 7 shows the results of the same attribution experiments shown in Figure 6, but for poleward energy transport at 40° N (Figure 7a) and 40° S (Figure 7b). In the all_G1 experiment, poleward energy transport decreases at this latitude in both hemispheres. Poleward energy transport decreases in the solarForcing experiment for each model, and increases in the greenhouse experiment, but not by enough to compensate. The increase in poleward transport in the greenhouse experiment can be understood in terms of the increasing moisture transport argument discussed in Section 2 for the abrupt4xCO2 experiment. The CO_2 radiative forcing in the EBM is spatially uniform since OLR, in the initial perturbation, is reduced by the same amount everywhere (see Appendix B), but atmospheric moisture increases more in the tropics than at the poles because the atmosphere was warmer in the tropics to begin with. The reduction in tropical moisture in the solarForcing case is greater than the increase in the greenhouse case because there is more sunlight to reduce in the tropics, causing a greater temperature perturbation there for solar reductions than for greenhouse gas increases. One caveat to this point is that in the actual atmosphere the CO_2 radiative forcing is stronger in the tropics than at the poles (although by as much as the solar forcing), which contributes to stronger poleward energy transport (Huang and Zhang, 2014); this mechanism for increased energy transport under greenhouse gas forcings is not captured by the EBM.

The APRPcloud experiment exhibits an increase in poleward energy transport in both hemispheres in all models, which is consistent with a decrease in low cloud cover causing heating in the tropics. Schmidt et al. (2012) noted that low cloud cover decreased in four GCMs running G1. A more detailed investigation of the cloud changes in the full G1 ensemble and their physical mechanisms and radiative effects will be the subject of a future study. None of the other feedback experiments have a consistent effect on poleward energy transport across 40° N/S, but the different feedback terms appear to rearrange the models in the all_G1 experiment, and contribute to the inter-model spread, with SW cloud feedbacks being the largest contributor. Models with a greater negative change in the solarForcing experiment (e.g. MPI-ESM-LR) also tend to have a greater positive change in the greenhouse experiment, and the compensation between these effects tends to reduce the inter-model spread. This implies that the remaining inter-model spread comes from the feedback terms. The fact that the solar forcing is the only term contributing to the reduction of poleward energy transport in G1 in all models implies that the imperfect compensation between SW and LW forcings, not local feedbacks, causes this reduction.

3.3.2 abrupt4xCO2 minus piControl

Figure 8 is the equivalent of Figure 7, but for abrupt4xCO2 minus piControl. For abrupt4xCO2, the greenhouse attribution experiment results in an increase in poleward energy transport, similar to the same experiment for G1. SW cloud feedbacks (APRPcloud experiment) are the largest contributor to the inter-model spread, followed by LW cloud feedbacks. Surface albedo feedbacks (APRPsurface) also contribute to the inter-model spread, but generally reduce poleward energy transport. (The increase in moisture due to tropical warming that results in greater poleward energy transport in the all_4xCO2 experiment does not show up when only surface albedo is perturbed.) This feedback term is mainly due to ice melt at high latitudes, which would be expected to reduce the equator-to-pole temperature gradient and therefore also reduce poleward energy transport. The LWCRE experiment also reduces poleward energy transport for abrupt4xCO2, because the LW cloud feedback is positive at high latitudes due to an increase in the optical depth of high clouds (Zelinka et al., 2012). As with G1, non-cloud atmosphere SW feedbacks have small effects on the poleward energy transport for abrupt4xCO2, but there is a consistent increase in this case, presumably due to increases in SW absorption by water vapor. The solarForcing experiment in this case represents the

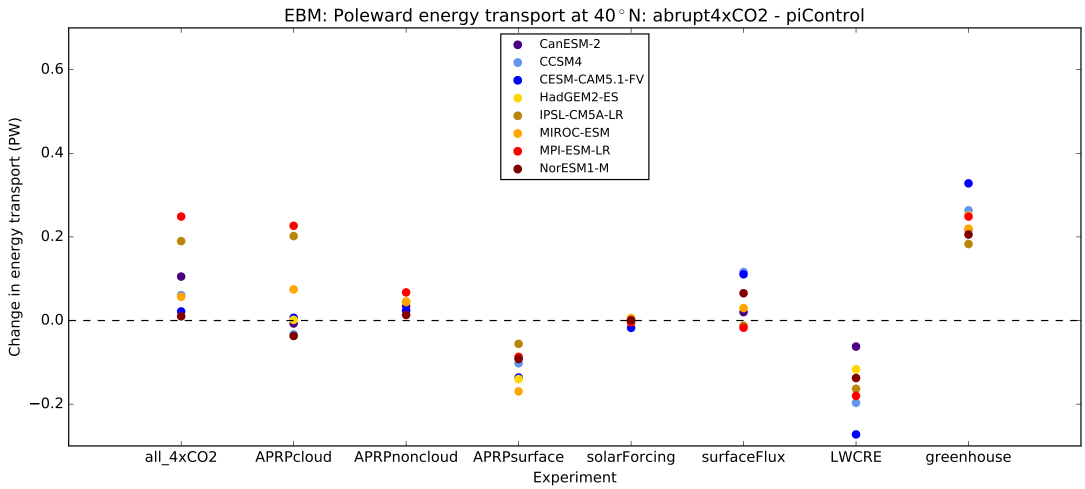

(a)

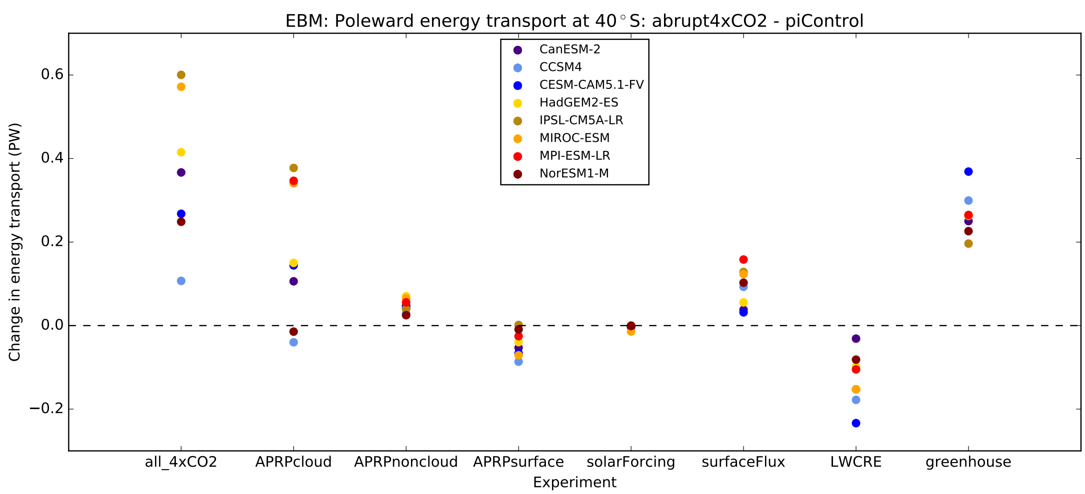

(b)

Figure 8. As in Figure 7 but for abrupt4xCO2 minus piControl.

residual between the total TOA net shortwave radiation changes and the individual feedback terms calculated using APRP; these effects are minor.

The surfaceFlux experiment has a much greater impact on poleward energy transport for abrupt4xCO2 than for G1, or for the 20th and 21st century CMIP3 runs analyzed by Hwang and Frierson (2010). This is because, while the TOA was kept approximately in energy balance in G1, and the imbalance is relatively small in 20th and 21st century runs, the abrupt4xCO2 case represents a response to an impulse that throws the climate system far out of equilibrium, with much energy being stored in the oceans over time. The energy loss from the atmosphere to the ocean is strongest in high latitudes, leading to a compensating increase in poleward atmospheric energy transport in the abrupt4xCO2 surfaceFlux experiment.

4 Conclusions

Our analysis of the GeoMIP G1 ensemble shows that, when CO_2 concentrations are increased and the solar constant is reduced to compensate, poleward atmospheric energy transport decreases (Figures 1a,d). This is because of an increase in polar temperatures and decrease in tropical temperatures, or "residual polar amplification", that results from the different spatial patterns of the opposing solar and CO_2 forcings. The polar warming and tropical cooling cause a decrease in both dry static energy transport, which depends on the equator-to-pole temperature gradient, and latent heat transport, which depends on the meridional gradient of saturation vapor pressure. Residual polar amplification cannot be due to increases in poleward atmospheric energy transport, as might have been thought, because poleward energy transport actually decreases. It cannot be due to local feedbacks such as the ice-albedo feedback because these feedbacks cannot reverse the sign of an initial temperature change. Poleward energy transport by the ocean in the North Atlantic decreases (Hong et al., 2017), and there is no reason to expect an increase in poleward energy transport by the ocean overall given the decrease in net energy flux into the ocean in the tropics. Instead, the spatial distribution of the combined CO_2 and solar forcing causes this pattern of temperature change, while the decrease in poleward energy transport then acts as a negative feedback that limits the polar warming in G1.

The reduction of poleward energy transport helps explain why the difference in temperature change in the poles and the tropics is not nearly as much in G1 as it is in abrupt4xCO2, or in other words, why solar geoengineering in the form of a uniform solar constant reduction manages to eliminate most (but not all) of the polar amplification of CO_2-induced warming. The role of moisture transport is critical here. When CO_2 is increased by itself, poleward latent heat transport increases because of the large increase in moisture in the tropics, and this amplifies polar warming. In the G1 scenario, by contrast, the cooling of the tropics reduces the amount of moisture in the air, lessening the energy transport to the poles. This indicates that tropical moisture content is a very important control on the meridional temperature gradient. Geoengineering schemes have been designed that, in GCMs, avoid the problem of over-cooling the tropics by preferentially reducing sunlight in high latitudes (Ban-Weiss and Caldeira, 2010; Kravitz et al., 2016). It would be useful to analyze the changes in atmospheric energy transport in these scenarios in order to better understand the role moisture transport would play in attempting to regulate temperatures in various latitudes.

Our EBM attribution experiments illustrate the specific forcings and feedbacks responsible for the changes in meridional energy transport in G1. The solar forcing causes a reduction in poleward energy transport in mid-latitudes; the enhanced greenhouse effect only partially counteracts this. Cloud feedbacks are generally the largest contributors to the inter-model spread in both mid-latitude poleward energy transport changes and cross-equatorial energy transport changes, which are a predictor of ITCZ shifts. The large uncertainty in these quantities associated with clouds implies that an improved physical understanding of the changes in clouds in G1 would help our understanding of how regional precipitation and temperature changes would play out under a solar geoengineering scenario. A more in-depth analysis of the cloud changes in the GeoMIP G1 ensemble will be the subject of a future study.

The finding that poleward atmospheric energy transport decreases in the G1 experiment relative to piControl is relevant for understanding why polar amplification of warming happens under increased CO_2. In warmer climates, the increased poleward energy transport contributes to the amount of polar amplification that occurs, as evidenced by model studies in which surface albedo is held constant (Alexeev et al., 2005; Graversen and Wang, 2009). However, our analysis of G1 shows that increases in poleward atmospheric energy transport are not necessary in order to have a decrease in the equator-to-pole temperature gradient. These results are particularly interesting in the light of the finding by Hwang et al. (2011) that polar amplification is actually negatively correlated with changes in atmospheric energy transport into the polar regions in CMIP3 global warming simulations. Our results reinforce the conclusion of Hwang et al. (2011) that changes in energy transport alone cannot predict changes in the meridional temperature gradient, which is actually governed by the coupling between energy transport and local feedbacks. It is useful to remember as well that radiative forcings are not spatially uniform, and the structure of the CO_2 forcing can affect atmospheric circulations in warming simulations (e.g. Huang and Zhang, 2014; Merlis, 2015). The spatial structure of radiative forcing is part of the set of processes, including local feedbacks and energy transport by the atmosphere and ocean, that interactively determine the Earth's meridional temperature pattern. Due to the complexity of these interactions, changes in the temperature gradient cannot be quantitatively predicted without a general circulation model. To better understand these interactions, it would be useful to do further analysis to quantify the contributions of different local feedbacks to the amount of polar warming in the G1 experiment.

Appendix A: Details of GCM-derived energy transport calculations

Often, when calculating meridional energy transport based on a cumulative integration of energy flux convergence into the column from GCM output, there is a residual energy transport at the north pole, because the models' internal energy conservation involves terms that are not included in the reported fields energy flux fields, or else because the models used slightly different values of physical constants than we used in our diagnostics. For some models (CCSM4, CESM-CAM5.1-FV, GISS-E2-R, HadGEM2-ES, MIROC-ESM and NorESM1-M), this error can be reduced or nearly eliminated by adding $L_f P_{\mathrm{snow}}$ to the right side of Equation 1, where L_f is the latent heat of fusion of ice and P_{snow} is the mass flux of snowfall at the surface. This term accounts for the net energy flux into the atmosphere when snow crystals form in the atmosphere and then melt on land or in the ocean. (We also do this for the calculation of moisture transport in Eq. 2.) For the rest of the models, including this term increases the north pole residual, so we omitted it, assuming that this term had been already accounted for inside the latent heat flux output field. Omitting this term in the first set of models as well did not significantly affect our results.

To correct for any remaining energy flux residual, we subtract the following error function E from the northward energy transport profile:

$$E(\phi) = \frac{N}{2}\left(1 + \sin(\phi)\right) \tag{A1}$$

Table 3. Northward energy transport residual error at north pole in different models and runs, to 4 decimal places.

Model	N (piControl) (PW)	N (G1 - piControl) (PW)	N (abrupt4xCO2 - piControl) (PW)
CanESM-2	-0.0531	0.0411	0.0809
CCSM4	0.0162	-0.0025	0.0015
CESM-CAM5.1-FV	0.0172	-0.0138	0.0027
CSIRO-Mk3L-1-2	0.1429	-0.0093	0.0857
GISS-E2-R	0.0135	-0.0002	0.0033
HadGEM2-ES	-0.0270	0.0137	0.0164
IPSL-CM5A-LR	0.0373	-0.0549	0.0027
MIROC-ESM	-1.9135	0.0593	0.0734
MPI-ESM-LR	-0.1174	0.0526	-0.0515
NorESM1	0.0137	-0.00004	0.0027

where ϕ is the latitude and N is the residual northward energy transport at the north pole. This correction function assumes that each unit area of Earth's surface contributes equally to the error. To demonstrate that the error is small, Table 3 shows the values of N in piControl and the change in N in the other 2 runs relative to piControl. The errors are generally small ($<$ .15 PW), except for MIROC-ESM, but even in this case the difference in the error between the runs is still small (all models have error $<$ .06 PW for G1 minus piControl, or .09 PW for abrupt4xCO2 minus piControl). Once the correction in Eq. (A1) is applied, the energy transport residual should only affect the results (in terms of differences between runs) if the errors are spatially nonuniform and the spatial pattern of the error differs between the runs. Since even the total error differences are small between runs, these residuals should not be a significant source of error in our analysis.

Appendix B: Details of moist EBM calculations

We use the moist energy balance model first used in Hwang and Frierson (2010). Here we describe how the model works, with an emphasis on new changes made for the solar geoengineering experiments.

The core equation of the model, as in other energy balance models (e.g. North, 1975), is a heat diffusion equation:

$$\frac{\partial T_s}{\partial t} = C\left(\mathrm{EI} - \mathrm{OLR} + \frac{p_s}{g} D \nabla^2 \mathrm{MSE}\right) \tag{B1}$$

or

$$\frac{\partial T_s}{\partial t} = C\left(\mathrm{EI} - \mathrm{OLR} + \frac{p_s}{g}\frac{D}{r^2}\frac{\partial}{\partial x}\left[(1-x^2)\frac{\partial \mathrm{MSE}}{\partial x}\right]\right), \tag{B2}$$

where MSE is the moist static energy, T_s is surface temperature, C is an arbitrary surface heat capacity, OLR is the outgoing longwave radiation at the top of the atmosphere, EI ("energy in") is the net surface and TOA energy flux into the atmospheric column excluding OLR, D is a diffusivity coefficient for MSE, p_s is the surface pressure, g is the acceleration due to gravity, r is the radius of the earth, and $x = \sin\theta$ where θ is the latitude. We have explicitly written out the r^2 that comes from the Laplacian operator in equation B2 rather than absorbing it into D as is often done (e.g. North, 1975). Noting that $\mathrm{d}x = \cos\theta\mathrm{d}\theta$, equation B2 can also be written in terms of latitude, which is more convenient in terms of specifying inputs for EI as functions of latitude without converting to sine latitude first:

$$\frac{\partial T_s}{\partial t} = C\left(\mathrm{EI} - \mathrm{OLR} + \frac{p_s}{g}\frac{D}{r^2}\frac{\partial}{\cos\theta\partial\theta}\left[\cos\theta\frac{\partial\mathrm{MSE}}{\partial\theta}\right]\right). \tag{B3}$$

We assume a value of 1.06×10^6 m^2 s^{-1} for D, following Hwang and Frierson (2010), and a flat topography with g = 9.8 m s^{-2} and p_s = 980 hPa. We step forward in time with a relative time step of $\frac{dt}{C} = 1\times10^{-4}$. The model is considered to have converged when T_s differs by less than .001 K everywhere in the domain between successive time steps.

The moist static energy is calculated according to:

$$\mathrm{MSE} = C_pT_s + L_vq \tag{B4}$$

where C_p is the heat capacity of air at constant pressure, L_v is the latent heat of vaporization of water, and q is the specific humidity. We calculate q as a function of T_s using Equation 3, assuming a relative humidity of 80%.

The OLR is treated as a linear function of temperature:

$$\mathrm{OLR} = aT_s - b \tag{B5}$$

where the coefficients a and b are calculated as linear least-squares fits from the monthly surface air temperature and clear-sky OLR output in each of the GCMs over the first 40 years of piControl. To consider the enhanced greenhouse effect in "perturbation" climates (G1 and abrupt4xCO2), we fit new coefficients b', maintaining the original value of a (following Hwang and Frierson (2010)), based on the surface temperature and clear-sky OLR output in those experiments. Table 4 shows the values of a, b, and b' we calculated for each of the GCMs.

To run the EBM, we input the a and b coefficients shown in Table 4, and an EI term calculated differently for the different attribution experiments. For the EBM runs representing piControl conditions, we combine the following terms from the zonal mean output of each GCM:

$$\mathrm{EI}_{\mathrm{piControl}} = S - L_C + F_s \tag{B6}$$

where S is the net downward SW radiation at the TOA, L_C is the LW cloud radiative effect (clear-sky OLR minus all-sky OLR), and F_s is the net upward surface flux, including SW and LW radiation, sensible heat flux and latent heat flux.

For the "full" perturbation runs emulating the G1 and abrupt4xCO2 experiments, we use b' instead of b for the OLR calculation, and the EI term is:

$$\mathrm{EI}_{\mathrm{perturb}} = \mathrm{EI}_{\mathrm{piControl}} + C_S + A_s + I + \Delta L_C + O + \Delta S \tag{B7}$$

Table 4. Values of fit coefficients for clear-sky OLR as a function of temperature for use in moist EBM analysis.

Model	a (W m^{-2} K^{-1})	b (W m^{-2})	b' (G1)	b' (abrupt4xCO2)
CanESM-2	2.0667	326.83	334.99	335.00
CCSM4	2.1604	350.06	358.31	360.35
CESM-CAM5.1-FV	2.0724	328.98	337.74	341.62
HadGEM2-ES	2.1531	349.37	357.38	358.99
IPSL-CM5A-LR	2.2149	363.39	370.58	370.46
MIROC-ESM	2.0512	327.40	336.37	336.18
MPI-ESM-LR	2.0157	315.55	324.47	324.34
NorESM1	2.1403	346.36	354.38	354.68

where C_S, A_s and I are the change in the net downward TOA SW radiation associated with cloud, non-cloud atmosphere, and surface albedo feedbacks, respectively, calculated using the Approximate Partial Radiation Perturbation (APRP) method (Taylor et al., 2007); ΔL_C is the change in the LW cloud radiative effect in the GCM output; O is the change in the net surface flux in the GCM output; and ΔS is the change in the solar forcing. We calculate ΔS by taking the change in net TOA SW radiation between the control and perturbation climates, and subtracting C_S, A_s, and I to get the change in solar radiation that is not due to any of the three feedback terms. In G1 this represents the effect of changing the solar constant; in abrupt4xCO2 this represents a residual feedback not accounted for by a linear sum of the other 3 feedbacks.

For the individual attribution experiments (except "greenhouse"), we use b in the OLR calculation, and the EI terms are calculated as follows (experiment labels following Table 2):

$$\mathrm{EI}_{\mathrm{APRPcloud}} = \mathrm{EI}_{\mathrm{piControl}} + C_S \tag{B8}$$

$$\mathrm{EI}_{\mathrm{APRPnoncloud}} = \mathrm{EI}_{\mathrm{piControl}} + A_s \tag{B9}$$

$$\mathrm{EI}_{\mathrm{APRPsurface}} = \mathrm{EI}_{\mathrm{piControl}} + I \tag{B10}$$

$$\mathrm{EI}_{\mathrm{solarForcing}} = \mathrm{EI}_{\mathrm{piControl}} + \Delta S \tag{B11}$$

$$\mathrm{EI}_{\mathrm{surfaceFlux}} = \mathrm{EI}_{\mathrm{piControl}} + O \tag{B12}$$

$$\mathrm{EI}_{\mathrm{LWCRE}} = \mathrm{EI}_{\mathrm{piControl}} + \Delta L_C \tag{B13}$$

For the "greenhouse" experiment, we use the control value of EI, but use b' instead of b for the OLR calculation.

The northward energy transport output by the EBM and shown in figures 6 through 8 is the cumulative meridional integration of the MSE diffusion term in Eq. (B2). The discretization of the diffusion equation for numerical solving inevitably results in some loss of energy, so after integrating, we apply a correction for residual northward transport at the North Pole for the EBM results, using Eq. (A1).

Author contributions. R.D. Russotto analyzed the GCM output, ran the EBM attribution experiments, produced the figures, and wrote the bulk of the paper. T.P. Ackerman provided general guidance and assisted with the preparation of the manuscript text.

Code availability All scripts used to analyze data and create plots are available here: atmos.washington.edu/articles/GeoMIP_EnergyTransport_PolarAmplification_ITCZ. A standalone Python code for the APRP method is available at: https://github.com/rdrussotto/pyAPRP.

Acknowledgements. This work was supported by the U.S. Department of Defense (DoD) through the National Defense Science and Engineering Graduate Fellowship (NDSEG) Program and by a grant to JISAO from the Fund for Innovative Climate and Energy Research. We thank Dargan Frierson for providing helpful guidance regarding the direction of this research, and Kyle Armour for pointing out a possible connection between decreased poleward moisture transport and reductions in mid-latitude precipitation. For their roles in producing, coordinating, and making available the CMIP5 and GeoMIP model output, we acknowledge the climate modeling groups (listed in Table 1 of this paper), the World Climate Research Programme's (WCRP) Working Group on Coupled Modelling (WGCM), and the Global Organization for Earth System Science Portals (GO-ESSP). We are grateful to Ben Kravitz, Helene Muri, Ulrike Niemeier, Stephen Phipps, and Jin-Ho Yoon for helping to provide access to GeoMIP output that was not yet available online; Phil Rasch, Balwinder Singh, and Ashly Spevacek for helpful discussions on technical issues with energy budgets in CMIP5 models; and Yen-Ting Hwang for providing us with codes for the APRP method and the moist EBM that formed the basis of this analysis. Two anonymous reviewers provided comments that greatly helped to improve the manuscript. We are particularly grateful to Reviewer 2 for their detailed commentary on the methodology of our EBM experiments. This led to us finding and fixing a major error in our implementation of the EBM.

References

Alexeev, V. A., Langen, P. L., and Bates, J. R.: Polar amplification of surface warming on an aquaplanet in “ghost forcing” experiments without sea ice feedbacks, Climate Dynamics, 24, 655–666, doi:10.1007/s00382-005-0018-3, http://dx.doi.org/10.1007/s00382-005-0018-3, 2005.

Arora, V. K., Scinocca, J. F., Boer, G. J., Christian, J. R., Denman, K. L., Flato, G. M., Kharin, V. V., Lee, W. G., and Merryfield, W. J.: Carbon emission limits required to satisfy future representative concentration pathways of greenhouse gases, Geophysical Research Letters, 38, L05805, doi:10.1029/2010GL046270, 2011.

Ban-Weiss, G. and Caldeira, K.: Geoengineering as an optimization problem, Environmental Research Letters, 5, 034009, doi:10.1088/1748-9326/5/3/034009, 2010.

Bekryaev, R. V., Polyakov, I. V., and Alexeev, V. A.: Role of Polar Amplification in Long-Term Surface Air Temperature Variations and Modern Arctic Warming, Journal of Climate, 23, 3888–3906, doi:10.1175/2010JCLI3297.1, 2010.

Bentsen, M., Bethke, I., Debernard, J. B., Iversen, T., Kirkevåg, A., Seland, Ø., Drange, H., Roelandt, C., Seierstad, I. A., Hoose, C., and Kristjánsson, J. E.: The Norwegian Earth System Model, NorESM1-M – Part 1: Description and basic evaluation of the physical climate, Geoscientific Model Development, 6, 687–720, doi:10.5194/gmd-6-687-2013, 2013.

Bischoff, T. and Schneider, T.: Energetic Constraints on the Position of the Intertropical Convergence Zone, Journal of Climate, 27, 4937–4951, doi:10.1175/JCLI-D-13-00650.1, 2014.

Broccoli, A. J., Dahl, K. A., and Stouffer, R. J.: Response of the ITCZ to Northern Hemisphere cooling, Geophysical Research Letters, 33, L01702, doi:10.1029/2005GL024546, 2006.

Chiang, J. C. H. and Bitz, C. M.: Influence of high latitude ice cover on the marine Intertropical Convergence Zone, Climate Dynamics, 25, 477–496, doi:10.1007/s00382-005-0040-5, 2005.

Collins, W. J., Bellouin, N., Doutriaux-Boucher, M., Gedney, N., Halloran, P., Hinton, T., Hughes, J., Jones, C. D., Joshi, M., Liddicoat, S., Martin, G., O’Connor, F., Rae, J., Senior, C., Sitch, S., Totterdell, I., Wiltshire, A., and Woodward, S.: Development and evaluation of an Earth-System model – HadGEM2, Geoscientific Model Development, 4, 1051–1075, doi:10.5194/gmd-4-1051-2011, 2011.

Dufresne, J.-L., Foujols, M.-A., Denvil, S., Caubel, A., Marti, O., Aumont, O., Balkanski, Y., Bekki, S., Bellenger, H., Benshila, R., Bony, S., Bopp, L., Braconnot, P., Brockmann, P., Cadule, P., Cheruy, F., Codron, F., Cozic, A., Cugnet, D., de Noblet, N., Duvel, J.-P., Ethé, C., Fairhead, L., Fichefet, T., Flavoni, S., Friedlingstein, P., Grandpeix, J.-Y., Guez, L., Guilyardi, E., Hauglustaine, D., Hourdin, F., Idelkadi, A., Ghattas, J., Joussaume, S., Kageyama, M., Krinner, G., Labetoulle, S., Lahellec, A., Lefebvre, M.-P., Lefevre, F., Levy, C., Li, Z. X., Lloyd, J., Lott, F., Madec, G., Mancip, M., Marchand, M., Masson, S., Meurdesoif, Y., Mignot, J., Musat, I., Parouty, S., Polcher, J., Rio, C., Schulz, M., Swingedouw, D., Szopa, S., Talandier, C., Terray, P., Viovy, N., and Vuichard, N.: Climate change projections using the IPSL-CM5 Earth System Model: from CMIP3 to CMIP5, Climate Dynamics, 40, 2123–2165, doi:10.1007/s00382-012-1636-1, 2013.

Feldl, N., Bordoni, S., and Merlis, T. M.: Coupled High-Latitude Climate Feedbacks and Their Impact on Atmospheric Heat Transport, Journal of Climate, 30, 189–201, doi:10.1175/JCLI-D-16-0324.1, 2017.

Ferraro, A. J. and Griffiths, H. G.: Quantifying the temperature-independent effect of stratospheric aerosol geoengineering on global-mean precipitation in a multi-model ensemble, Environmental Research Letters, 11, 034012, doi:10.1088/1748-9326/11/3/034012, 2016.

Frierson, D. M. W. and Hwang, Y.-T.: Extratropical Influence on ITCZ Shifts in Slab Ocean Simulations of Global Warming, Journal of Climate, 25, 720–733, doi:10.1175/JCLI-D-11-00116.1, 2012.

Gent, P. R., Danabasoglu, G., Donner, L. J., Holland, M. M., Hunke, E. C., Jayne, S. R., Lawrence, D. M., Neale, R. B., Rasch, P. J., Vertenstein, M., Worley, P. H., Yang, Z.-L., and Zhang, M.: The Community Climate System Model Version 4, Journal of Climate, 24, 4973–4991, doi:10.1175/2011JCLI4083.1, 2011.

Giorgetta, M. A., Jungclaus, J., Reick, C. H., Legutke, S., Bader, J., Böttinger, M., Brovkin, V., Crueger, T., Esch, M., Fieg, K., Glushak, K., Gayler, V., Haak, H., Hollweg, H.-D., Ilyina, T., Kinne, S., Kornblueh, L., Matei, D., Mauritsen, T., Mikolajewicz, U., Mueller, W., Notz, D., Pithan, F., Raddatz, T., Rast, S., Redler, R., Roeckner, E., Schmidt, H., Schnur, R., Segschneider, J., Six, K. D., Stockhause, M., Timmreck, C., Wegner, J., Widmann, H., Wieners, K.-H., Claussen, M., Marotzke, J., and Stevens, B.: Climate and carbon cycle changes from 1850 to 2100 in MPI-ESM simulations for the Coupled Model Intercomparison Project phase 5, Journal of Advances in Modeling Earth Systems, 5, 572–597, doi:10.1002/jame.20038, 2013.

Govindasamy, B. and Caldeira, K.: Geoengineering Earth's radiation balance to mitigate CO2-induced climate change, Geophysical Research Letters, 27, 2141–2144, doi:10.1029/1999GL006086, http://dx.doi.org/10.1029/1999GL006086, 2000.

Govindasamy, B., Caldeira, K., and Duffy, P.: Geoengineering Earth's radiation balance to mitigate climate change from a quadrupling of CO2, Global and Planetary Change, 37, 157 – 168, doi:http://dx.doi.org/10.1016/S0921-8181(02)00195-9, http://www.sciencedirect.com/science/article/pii/S0921818102001959, evaluation, Intercomparison and Application of Global Climate Models, 2003.

Graversen, R. G. and Wang, M.: Polar amplification in a coupled climate model with locked albedo, Climate Dynamics, 33, 629–643, doi:10.1007/s00382-009-0535-6, http://dx.doi.org/10.1007/s00382-009-0535-6, 2009.

Green, B. and Marshall, J.: Coupling of Trade Winds with Ocean Circulation Damps ITCZ Shifts, Journal of Climate, 30, 4395–4411, doi:10.1175/JCLI-D-16-0818.1, 2017.

Hartmann, D. L.: Global Physical Climatology, Elsevier, Amsterdam, Netherlands, 2nd edn., 2016.

Hawcroft, M., Haywood, J. M., Collins, M., Jones, A., Jones, A. C., and Stephens, G.: Southern Ocean albedo, inter-hemispheric energy transports and the double ITCZ: global impacts of biases in a coupled model, Climate Dynamics, 48, 2279–2295, doi:10.1007/s00382-016-3205-5, 2017.

Haywood, J. M., Jones, A., Bellouin, N., and Stephenson, D.: Asymmetric forcing from stratospheric aerosols impacts Sahelian rainfall, Nature Climate Change, 3, 660–665, doi:10.1038/NCLIMATE1857, 2013.

Haywood, J. M., Jones, A., Dunstone, N., Milton, S., Vellinga, M., Bodas-Salcedo, A., Hawcroft, M., Kravitz, B., Cole, J., Watanabe, S., and Stephens, G.: The impact of equilibrating hemispheric albedos on tropical performance in the HadGEM2-ES coupled climate model, Geophysical Research Letters, 43, 395–403, doi:10.1002/2015GL066903, http://dx.doi.org/10.1002/2015GL066903, 2015GL066903, 2016.

Held, I. M. and Soden, B. J.: Robust Responses of the Hydrological Cycle to Global Warming, Journal of Climate, 19, 5686–5699, doi:http://dx.doi.org/10.1175/JCLI3990.1, 2006.

Holland, M. M. and Bitz, C. M.: Polar amplification of climate change in coupled models, Climate Dynamics, 21, 221–232, doi:10.1007/s00382-003-0332-6, 2003.

Hong, Y., Moore, J. C., Jevrejeva, S., Ji, D., Phipps, S. J., Lenton, A., Tilmes, S., Watanabe, S., and Zhao, L.: Impact of the GeoMIP G1 sunshade geoengineering experiment on the Atlantic meridional overturning circulation, Enviornmental Research Letters, 12, 034009, doi:10.1088/1748-9326/aa5fb8, 2017.

Huang, Y. and Zhang, M.: The implication of radiative forcing and feedback for meridional energy transport, Geophysical Research Letters, 41, 1665–1672, doi:10.1002/2013GL059079, http://dx.doi.org/10.1002/2013GL059079, 2013GL059079, 2014.

Hurrell, J. W., Holland, M. M., Gent, P. R., Ghan, S., Kay, J. E., Kushner, P. J., Lamarque, J.-F., Large, W. G., Lawrence, D., Lindsay, K., Lipscomb, W. H., Long, M. C., Mahowald, N., Marsh, D. R., Neale, R. B., Rasch, P., Vavrus, S., Vertenstein, M., Bader, D., Collins, W. D., Hack, J. J., Kiehl, J., and Marshall, S.: The Community Earth System Model: A Framework for Collaborative Research, Bulletin of the American Meteorological Society, 94, 1339–1360, doi:10.1175/BAMS-D-12-00121.1, 2013.

Hwang, Y.-T. and Frierson, D. M. W.: Increasing atmospheric poleward energy transport with global warming, Geophysical Research Letters, 37, L24807, doi:10.1029/2010GL045440, 2010.

Hwang, Y.-T., Frierson, D. M. W., and Kay, J. E.: Coupling between Arctic feedbacks and changes in poleward energy transport, Geophysical Research Letters, 38, L17704, doi:10.1029/2011GL048546, 2011.

Hwang, Y.-T., Frierson, D. M. W., and Kang, S. M.: Anthropogenic sulfate aerosol and the southward shift of tropical precipitation in the late 20th century, Geophysical Research Letters, 40, 2845–2850, doi:10.1002/grl.50502, 2013.

Irvine, P. J., Ridgwell, A., and Lunt, D. J.: Assessing the regional disparities in geoengineering impacts, Geophysical Research Letters, 37, L18702, doi:10.1029/2010GL044447, 2010.

Kang, S. M., Held, I. M., Frierson, D. M. W., and Zhao, M.: The Response of the ITCZ to Extratropical Thermal Forcing: Idealized Slab-Ocean Experiments with a GCM, Journal of Climate, 21, 3521–3532, doi:10.1175/2007JCLI2146.1, 2008.

Kay, J. E., Wall, C., Yettella, V., Medeiros, B., Hannay, C., Caldwell, P., and Bitz, C.: Global Climate Impacts of Fixing the Southern Ocean Shortwave Radiation Bias in the Community Earth System Model (CESM), Journal of Climate, 29, 4617–4636, doi:10.1175/JCLI-D-15-0358.1, 2016.

Keith, D. W. and Dowlatabadi, H.: A serious look at geoengineering, Eos, Transactions American Geophysical Union, 73, 289–293, doi:10.1029/91EO00231, 1992.

Kravitz, B., Robock, A., Boucher, O., Schmidt, H., Taylor, K. E., Stenchikov, G., and Schulz, M.: The Geoengineering Model Intercomparison Project (GeoMIP), Atmospheric Science Letters, 12, 162–167, doi:10.1002/asl.316, 2011.

Kravitz, B., Caldeira, K., Boucher, O., Robock, A., Rasch, P. J., Alterskjær, K., Karam, D. B., Cole, J. N. S., Curry, C. L., Haywood, J. M., Irvine, P. J., Ji, D., Jones, A., Kristjánsson, J. E., Lunt, D. J., Moore, J. C., Niemeier, U., Schmidt, H., Schulz, M., Singh, B., Tilmes, S., Watanabe, S., Yang, S., and Yoon, J.-H.: Climate model response from the Geoengineering Model Intercomparison Project (GeoMIP), Journal of Geophysical Research: Atmospheres, 118, 8320–8332, doi:10.1002/jgrd.50646, 2013a.

Kravitz, B., Rasch, P. J., Forster, P. M., Andrews, T., Cole, J. N. S., Irvine, P. J., Ji, D., Kristjánsson, J. E., Moore, J. C., Muri, H., Niemeier, U., Robock, A., Singh, B., Tilmes, S., Watanabe, S., and Yoon, J.-H.: An energetic perspective on hydrological cycle changes in the Geoengineering Model Intercomparison Project, Journal of Geophysical Research: Atmospheres, 118, 13,087–13,102, doi:10.1002/2013JD020502, 2013b.

Kravitz, B., MacMartin, D., Wang, H., and Rasch, P.: Geoengineering as a design problem, Earth System Dynamics, 7, 469–497, doi:10.5194/esd-7-469-2016, 2016.

Laguë, M. M. and Swann, A. L. S.: Progressive Midlatitude Afforestation: Impacts on Clouds, Global Energy Transport, and Precipitation, Journal of Climate, 29, 5561–5573, doi:10.1175/JCLI-D-15-0748.1, 2016.

Merlis, T. M.: Interacting components of the top-of-atmosphere energy balance affect changes in regional surface temperature, Geophysical Research Letters, 41, 7291–7297, doi:10.1002/2014GL061700, http://dx.doi.org/10.1002/2014GL061700, 2014.

Merlis, T. M.: Direct weakening of tropical circulations from masked CO2 radiative forcing, Proceedings of the National Academy of Sciences, 112, 13 167–13 171, doi:10.1073/pnas.1508268112, http://www.pnas.org/content/112/43/13167.abstract, 2015.

Niemeier, U., Schmidt, H., Alterskjær, K., and Kristjánsson, J. E.: Solar irradiance reduction via climate engineering: Impact of different techniques on the energy balance and the hydrological cycle, Journal of Geophysical Research: Atmospheres, 118, 11,905–11,917, doi:10.1002/2013JD020445, 2013.

North, G. R.: Theory of Energy-Balance Climate Models, Journal of the Atmospheric Sciences, 32, 2033–2043, 1975.

Pendergrass, A. G. and Hartmann, D. L.: The Atmospheric Energy Constraint on Global-Mean Precipitaton Change, Journal of Climate, 27, 757–768, 2014.

Phipps, S. J., Rotstayn, L. D., Gordon, H. B., Roberts, J. L., Hirst, A. C., and Budd, W. F.: The CSIRO Mk3L climate system model version 1.0 – Part 1: Description and evaluation, Geoscientific Model Development, 4, 483–509, doi:10.5194/gmd-4-483-2011, 2011.

Pithan, F. and Mauritsen, T.: Arctic amplification dominated by temperature feedbacks in contemporary climate models, Nature Geoscience, 7, 181–184, doi:10.1038/ngeo2071, 2014.

Rose, B. E. J. and Rayborn, L.: The Effects of Ocean Heat Uptake on Transient Climate Sensitivity, Current Climate Change Reports, 2, 190–201, doi:10.1007/s40641-016-0048-4, 2016.

Rose, B. E. J., Armour, K. C., Battisti, D. S., Feldl, N., and Koll, D. D. B.: The dependence of transient climate sensitivity and radiative feedbacks on the spatial pattern of ocean heat uptake, Geophysical Research Letters, 41, 1071–1078, doi:10.1002/2013GL058955, http://dx.doi.org/10.1002/2013GL058955, 2014.

Schaller, N., Sedláček, J., and Knutti, R.: The asymmetry of the climate system's response to solar forcing changes and its implications for geoengineering scenarios, Journal of Geophysical Research: Atmospheres, 119, 5171–5184, doi:10.1002/2013JD021258, 2014.

Schmidt, G. A., Kelley, M., Nazarenko, L., Ruedy, R., Russell, G. L., Aleinov, I., Bauer, M., Bauer, S. E., Bhat, M. K., Bleck, R., Canuto, V., Chen, Y.-H., Cheng, Y., Clune, T. L., Del Genio, A., de Fainchtein, R., Faluvegi, G., Hansen, J. E., Healy, R. J., Kiang, N. Y., Koch, D., Lacis, A. A., LeGrande, A. N., Lerner, J., Lo, K. K., Matthews, E. E., Menon, S., Miller, R. L., Oinas, V., Oloso, A. O., Perlwitz, J. P., Puma, M. J., Putman, W. M., Rind, D., Romanou, A., Sato, M., Shindell, D. T., Sun, S., Syed, R. A., Tausnev, N., Tsigaridis, K., Unger, N., Voulgarakis, A., Yao, M.-S., and Zhang, J.: Configuration and assessment of the GISS ModelE2 contributions to the CMIP5 archive, Journal of Advances in Modeling Earth Systems, 6, 141–184, doi:10.1002/2013MS000265, 2014.

Schmidt, H., Alterskjær, K., Bou Karam, D., Boucher, O., Jones, A., Kristjánsson, J. E., Niemeier, U., Schulz, M., Aaheim, A., Benduhn, F., Lawrence, M., and Timmreck, C.: Solar irradiance reduction to counteract radiative forcing from a quadrupling of CO_2: climate responses simulated by four earth system models, Earth System Dynamics, 3, 63–78, doi:10.5194/esd-3-63-2012, 2012.

Seo, J., Kang, S. M., and Merlis, T. M.: A model intercomparison of the tropical precipitation response to a CO2 doubling in aquaplanet simulations, Geophysical Research Letters, 44, 993–1000, doi:10.1002/2016GL072347, 2016GL072347, 2017.

Smyth, J. E., Russotto, R. D., and Storelvmo, T.: Thermodynamic and dynamic responses of the hydrological cycle to solar dimming, Atmospheric Chemistry and Physics, pp. 1–17, doi:10.5194/acp-2016-886, http://www.atmos-chem-phys-discuss.net/acp-2016-886/, accepted article, 2017.

Swann, A. L. S., Fung, I. Y., and Chiang, J. C. H.: Mid-latitude afforestation shifts general circulation and tropical precipitation, Proceedings of the National Academy of Sciences, 109, 712–716, doi:10.1073/pnas.1116706108, 2012.

Taylor, K. E., Crucifix, M., Braconnot, P., Hewitt, C. D., Doutriaux, C., Broccoli, A. J., Mitchell, J. F. B., and Webb, M. J.: Estimating Shortwave Radiative Forcing and Response in Climate Models, Journal of Climate, 20, 2530–2543, doi:10.1175/JCLI4143.1, 2007.

Tilmes, S., Fasullo, J., Lamarque, J.-F., Marsh, D. R., Mills, M., Alterskjær, K., Muri, H., Kristjánsson, J. E., Boucher, O., Schulz, M., Cole, J. N. S., Curry, C. L., Jones, A., Haywood, J., Irvine, P. J., Ji, D., Moore, J. C., Karam, D. B., Kravitz, B., Rasch, P. J., Singh, B., Yoon, J.-H., Niemeier, U., Schmidt, H., Robock, A., Yang, S., and Watanabe, S.: The hydrological impact of geoengineering in the Geoengineering Model Intercomparison Project (GeoMIP), Journal of Geophysical Research: Atmospheres, 118, 11,036–11,058, doi:10.1002/jgrd.50868, 2013.

Viale, F. and Merlis, T. M.: Variations in tropical cyclone frequency response to solar and CO2 forcing in aquaplanet simulations, Journal of Advances in Modeling Earth Systems, 9, 4–18, doi:10.1002/2016MS000785, http://dx.doi.org/10.1002/2016MS000785, 2017.

Watanabe, S., Hajima, T., Sudo, K., Nagashima, T., Takemura, T., Okajima, H., Nozawa, T., Kawase, H., Abe, M., Yokohata, T., Ise, T., Sato, H., Kato, E., Takata, K., Emori, S., and Kawamiya, M.: MIROC-ESM 2010: model description and basic results of CMIP5-20C3M experiments, Geoscientific Model Development, 4, 845–872, doi:10.5194/gmd-4-845-2011, 2011.

Yoshimori, M. and Broccoli, A. J.: Equilibrium Response of an Atmosphere–Mixed Layer Ocean Model to Different Radiative Forcing Agents: Global and Zonal Mean Response, Journal of Climate, 21, 4399–4423, doi:10.1175/2008JCLI2172.1, 2008.

Zelinka, M. D., Klein, S. A., and Hartmann, D. L.: Computing and Partitioning Cloud Feedbacks Using Cloud Property Histograms. Part II: Attribution to Changes in Cloud Amount, Altitude, and Optical Depth, J. Climate, 25, 3736–3754, doi:10.1175/JCLI-D-11-00249.1, 2012.